RHEOLOGICAL STUDY OF KAOLIN CLAY SLURRIES

A Thesis Submitted to the College of

Graduate studies and Research

in Partial Fulfilment of the Requirements

for a Degree of Masters of Science

in the Department of Chemical Engineering

University of Saskatchewan

Saskatoon

PERMISSION TO USE

In presenting this thesis in partial fulfilment of the requirements for a Postgraduate degree from the University of Saskatchewan, I agree that the Libraries of this University may make it freely available for inspection. I further agree that permission for copying of this thesis in any manner, in whole or in part, for scholarly purposes may be granted by the professor or professors who supervised my thesis work or, in their absence, by the Head of the Department or the Dean of the College in which my thesis work was done. It is understood that any copying or publication or use of this thesis or parts thereof for financial gain shall not be allowed without my written permission. It is also understood that due recognition shall be given to me and to the University of Saskatchewan in any scholarly use which may be made of any material in my thesis.

Requests for permission to copy or to make other use of material in this thesis in whole or part should be addressed to:

Head of the Department of Chemical Engineering

University of Saskatchewan

Saskatoon, Saskatchewan S7N 5A9

ABSTRACT

Concentrated kaolin clay slurries are found in a number of industrial operations including mine tailings surface disposal, underground paste backfill, and riverbed dredging. An understanding of the impact of solids concentration and addition of chemical species on slurry rheology is of importance to designers of pipeline transport and waste disposal systems. A project to determine the rheology of an idealized industrial kaolin clay slurry using a concentric cylinder viscometer and an experimental pipeline loop was undertaken. Additional laboratory test work including particle size analysis, slurry pH, calcium ion concentration in the slurry supernatant and particle electrophoretic mobility measurements were completed to aid in the understanding of their effects on the slurry rheology.

The slurries were prepared in varying kaolin clay solids concentrations with reverse osmosis water. A flocculant, dihydrated calcium chloride ($CaCl_2 \bullet 2H_2O$), was added to the reverse osmosis water in concentrations equivalent to those found in typical industrial hard water supply. A dispersant, tetra-sodium pyrophosphate (TSPP, $Na_4P_2O_7$) was used to disperse the clay particles for selected slurries.

It was found that the kaolin clay slurries, in the absence of TSPP, exhibited yield stresses and could be characterized with either the two-parameter Bingham or Casson continuum flow models. Increasing the clay concentration in the slurry, while keeping the mass ratio of flocculant to kaolin constant, increased both the yield and plastic viscosity parameters. There was generally good agreement between the rheological parameters obtained in the Couette flow viscometer and that in the pipeline loop.

In slurries for which it was possible to obtain turbulent flow, the transition to turbulent flow was predicted accurately by the Wilson & Thomas method for both Bingham and Casson models.

It was possible to eliminate the yield stress of a slurry with the addition of the dispersing agent TSPP. The calcium ion content of the supernatant extracted from the slurries proved to be a indicator of the degree of flocculation.

When exposed to extended periods of high shear conditions in the pipeline loop, slurries with clay concentrations of 17% by volume solids or greater exhibited an irreversible increase in apparent viscosity with time. An attempt was made to investigate this irreversible thickening characteristic. Laboratory tests did not reveal any appreciable differences in particle size, electrophoretic mobility, calcium ion concentration or pH with this irreversible change. The shear duration test shows the importance of using the appropriate shear environment when testing high solids concentration kaolin clay slurries.

ACKNOWLEDGMENTS

I wish to express my sincere gratitude and appreciation to Dr. R. J. Sumner, my supervisor, for introducing me to the field of research. Without his guidance this thesis could not have been completed. I would also like to express my appreciation to Dr. C. A. Shook and Dr. R. S. Sanders for their assistance in the final preparation of my thesis.

Thanks to the Saskatchewan Research Councils Pipe Flow Technology Centre for the use of their research facility. I wish to express my deepest gratitude to the staff for their contributions in developing and sustaining a research division that is recognized around the world. I consider myself lucky to have been able to discuss ideas with more experienced researchers especially Dr. R.G. Gillies, Dr. M.J. McKibben, Mr. R. Sun, and Mr. J.J. Schaan.

I would like to acknowledge the work of the late Miss E. Reichert who helped me interpret a difficult scientific paper. A special thanks to the students that have contributed to this research program. Specifically, Mr. T. Barnstable and Mr. R. Spelay with whom I conducted the experimental test work and benefited from their assistance and invaluable input.

Finally, I thank my parents and family for instilling in me confidence and a drive for pursuing my education and for the support that they have provided me through my entire life.

DEDICATION

To my wife, Krista, without her love and support I doubt that the completion of this thesis would have ever been possible.

TABLE OF CONTENTS

LIST OF TABLES

LIST OF FIGURES

LIST OF SYMBOLS

A	Cross-section area
A	Constant, Eq 2.9
B	Constant, Eq 2.10
Cv	Concentration of solids by volume
D	Pipe internal diameter
D_p	Diameter of spherical particle
E	Applied field strength
f	Fanning friction factor
g	Acceleration due to gravity
h	Height
k	Pipe wall equivalent roughness
L	Length of pipe section
P	Pressure
Q	Volumetric flow rate
r	Radial coordinate position
R	Radius of particle of cylinder
R_1	Inner cylinder radius (concentric cylinder viscometer)
R_2	Outer cylinder radius (concentric cylinder viscometer)
Re	Reynolds number for pipe flow
R_ω	Taylor vortices transition criterion (concentric cylinder viscometer)
S	Separation distance
T	Torque

t	time
t_{RD}	Time of centrifuge deceleration, Eq. 3.2
t_{RU}	Time of centrifuge acceleration, Eq. 3.2
t_{RUN}	Time of centrifuge operation, Eq. 3.2
u^*	Friction velocity
v	Local velocity
V	Bulk velocity of pipe flow
V_N	Newtonian fluid velocity at specified condition, Eq. 2.29, 2.30
y	Cartesian coordinate position
z	Cartesian coordinate position

GREEK SYMBOLS

γ	Shear strain
$\dot{\gamma}$	Time rate of shear strain
μ	Viscosity
μ_{app}	Apparent viscosity
μ_p	Bingham Plastic Viscosity
μ_∞	Casson Viscosity
ν	Particle velocity, Eq. 2.33
θ	Angular coordinate position
ρ	Density
ρ_1	Density of particles, Eq. 3.1

ρ_2	Density of suspending medium, Eq. 3.1
τ	Shear stress
τ_c	Yield stress (Casson Fluid Model)
τ_y	Yield stress (Bingham Fluid Model)
υ	Electrophoretic mobility
ω_c	Angular velocity of the centrifuge, Eq. 3.2
ω	Angular Velocity
ξ	Stress ratio

1. INTRODUCTION

The study of pipeline transportation of solid-liquid mixtures has undergone considerable advances in the past half century. However, there is still an incomplete understanding of some aspects governing the flow characteristics of these systems. Proper slurry pipeline design and operation requires an understanding of the frictional pressure loss caused by delivering a specific solids concentration under laminar or turbulent flow conditions. This information is used to select the optimum pipeline diameter and pump horsepower required to provide the flow rate and discharge pressure necessary to avoid particle deposition and overcome the frictional resistance of the pipeline.

Two simplistic categories have been used to classify solid-liquid mixtures: settling and non-settling slurries (Shook et al., 2002). Settling slurries contain larger particles which have high settling velocities. A stationary bed will develop at low velocities and to avoid particle deposition, pipeline operation usually occurs under turbulent flow conditions. Non-settling slurries are composed of fine particles which, when flowing, have a uniform distribution across the pipeline cross section and produce a symmetrical velocity distribution. In fact it could be said that the term non-settling is not strictly accurate since many industrial slurries exhibit characteristics of both categories (Shook et al., 2002).

It is the focus of this thesis to further investigate factors affecting the rheological nature of an idealized kaolin clay industrial non-settling slurry. Non-settling slurries often exhibit non-Newtonian behaviour due to particle-particle

interactions. It is difficult to define a particle size at which the transition between the settling and non-settling slurry classifications occurs.

It is important to predict flow regime transition from laminar to turbulent flow of a non-settling slurry. Laminar flow pressure drops can be predicted for a variety of non-Newtonian model slurries. Wilson & Thomas (1985, 1987) have proposed a method for turbulent flows that is based on a model for the flow in the viscous sublayer. This method has produced accurate predictions.

In many industrial slurries it is clay particles that makes the most significant solids component of the non-settling carrier fluid. The rheological behaviour of slurries containing clay particles is important to industries as diverse as paint manufacturing, petroleum drilling, and mining waste disposal.

The mining industry is investigating alternative methods to dispose of mine wastes which contain a significant fraction of clays. By increasing the solids content of the slurry through the removal of water, mining companies are able to achieve two benefits. The footprint or area required to deposit the mine waste is significantly reduced from a large tailings pond to small land based deposit. There is also a reduction in demand for fresh water resulting from recycling of the process water, making this approach environmentally attractive.

A fine kaolin clay slurry may be described as a colloidal system in which the solids are dispersed through the liquid. Because of the high surface charge to mass ratio of clays, van der Waals attractive forces and electrostatic repulsive forces dominate particle interactions. It is the sum of these two forces between particles that determine the nature of the slurry rheology.

The net particle interactions can be strongly repulsive, where the particles remain dispersed, so that the fluid exhibits Newtonian characteristics. Alternatively, the net interaction between particles can be strongly attractive so that a floc structure is created. Flocs can form networks which cause the slurry to exhibit non-Newtonian characteristics. This structure can resist shear distortion giving the fluid a yield stress. Two non-Newtonian models which use a yield stress term are the Bingham and Casson models.

The rheological characteristics of fine particle clay slurries can be manipulated by altering the concentration of solids and by controlling the electrostatic repulsive forces between particles. The electrostatic repulsive forces can be increased or decreased by manipulating the pH and the ionic content in the suspending medium. Increasing the repulsive forces with the addition of a dispersing agent may break down the structure and reduce or eliminate non-Newtonian behaviour. Conversely by decreasing the repulsive forces and allowing the net interaction of particles to be dominated by attractive forces, the non-Newtonian behaviour can be increased.

To extend the current state of knowledge of fine particle clay slurries, the effects of solids concentration and chemical addition on the rheology of kaolin clay slurries have been studied. The rheology of kaolin clay slurries has been studied using a vertical pipe flow loop and a Couette viscometer. The experimental data have been interpreted using the Bingham and Casson models. All slurries were prepared with a constant mass ratio of calcium ion to clay to represent the ion content in a typical industrial fresh water supply. To understand the effects of chemical species in the suspending medium on the rheology of these fine particle slurries, the viscosity

was modified with the addition of tetra sodium pyrophosphate (TSPP) and the calcium ion content in the resulting supernatant was monitored.

To further understand the nature of viscosity modification additional experiments were conducted. For selected slurries the pH, particle size, electrophoretic mobility, and calcium ion content were monitored before and after the slurries had been exposed to a high shear environment.

2. LITERATURE REVIEW

2.1. Determination of Flow Properties

Rheology is the study of deformation of matter. When a shear stress (τ) is applied to a fluid it causes successive layers of that fluid to be displaced by different amounts. The displacement (S) of two parallel layers relative to each other divided by their separation distance (y) is the shear strain ($\gamma = S/y$). For liquids, the time derivative of the relative displacement yields the velocity component and if this displacement is divided by the separation distance one obtains the time rate of shear strain ($\dot{\gamma}$). This quantity is also known as the shear rate. Viscosity is a measure of the ability of a fluid to resist flow by means of internal friction. The magnitude of the shear stress that is developed during flow depends on the product of viscosity and the rate of deformation. The graphical representation of the shear stress versus the shear rate is known as a rheogram. Figure 2.1 details the shear stress as a function of shear rate for various fluids.

1. **Newtonian**
2. **Dilatant (Shear Thickening)**
3. **Pseudoplastic (Shear Thinning)**
4. **Hershel-Bulkley**
5. **Bingham**
6. **Casson**

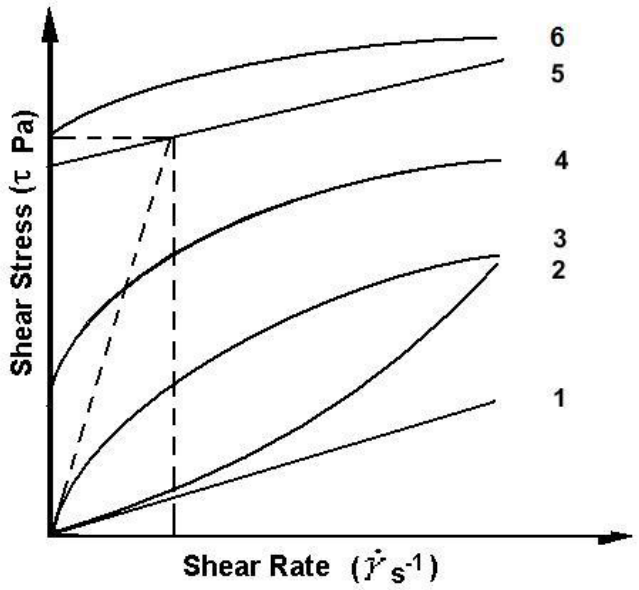

Figure 2.1: Rheograms of various continuum fluid models.

If the shear stress is linear with respect to shear rate and the rheogram passes through the origin, the fluid is considered to be Newtonian. The slope of the rheogram is the viscosity as shown in Equation 2.0.

$$\tau = -\mu \dot{\gamma} \qquad (2.0)$$

Although fine particle slurries are composed of two distinct phases, when flowing they are usually dispersed homogeneously so that the flow can be analysed with a continuum model. The Bingham and Casson fluid models are time-independent, two parameter rheological models. They are often used to characterize non-settling fine particle slurries. These slurries are considered to be viscoplastic, which means that they behave like solids below a critical stress (the yield stress). These slurries exhibit fluid behaviour when the applied shear stress exceeds the yield stress. This is illustrated by the curves in Figure 2.1 which represent the various fluid models.

There are other non-Newtonian rheological models which incorporate a yield stress term, but the Bingham and Casson models have been chosen to analyze the experimental data in this program because of their robust two parameter functional relationship. The Bingham model is presented in Equation 2.1 where τ_y is the Bingham model yield parameter and μ_p is the Bingham viscosity term. The Casson model is presented in Equation 2.2 where τ_c is the Casson yield parameter and μ_∞ is the Casson viscosity.

$$\tau = -\mu_p \dot{\gamma} + \tau_y \qquad (2.1)$$

$$\tau^{1/2} = -(\mu_\infty \dot{\gamma})^{1/2} + \tau_c^{1/2} \qquad (2.2)$$

In 1957 Casson arrived at this equation theoretically by considering the magnitude of interparticle forces such as those found in pigment-oil suspensions of the printing ink type.

The total resistance to shear for a two parameter model may be expressed using an apparent viscosity. For any fluid one can draw a secant line from the origin of Figure 2.1, as shown for the curve of a Bingham fluid by the dashed line, to a particular shear stress. The slope that this line reveals is the apparent Newtonian viscosity at that shear rate. The Bingham and Casson apparent viscosities are shown in Equations 2.3 and 2.4.

$$\mu_{app} = \frac{\mu_p}{1 - \frac{\tau_y}{\tau}} \tag{2.3}$$

$$\mu_{app} = \frac{\mu_\infty}{\left(1 - \sqrt{\frac{\tau_c}{\tau}}\right)^2} \tag{2.4}$$

These equations illustrate that the yield stress of the fluid will dominate the fluid behaviour if a shear stress slightly greater than the yield stress is applied. In this situation a high apparent viscosity is observed. As the shear rate increases, the apparent viscosity term approaches the Bingham or Casson viscosity.

In concentrated clay slurries, particle interactions produce a structure with some rigidity which is the source of the yield stress. If a shear stress is applied below the yield stress this network or structure prevents flow. At high particle concentrations, this structure would be present throughout the suspending water medium. For shear stresses above the critical yield stress flow causes the structure to break up into smaller and smaller elements composed of flocculated particles

(Michaels and Bolger 1962). The apparent viscosity may also decreases with increasing shear rate as particle or aggregate orientation becomes more ordered (Carty, 2001).

Rheological parameters for non-Newtonian slurries are determined experimentally using a viscometer. In the present study a pipeline loop (tube viscometer) and a concentric cylinder viscometer have been employed.

2.2. Principles of Pipeline Flow

For the specific case of steady state operation of a vertical pipeline of constant cross-section, transporting a constant density fluid, a force balance over a pipe element, shown in Figure 2.2, provides the following relationship between pressure gradient and wall shear stress:

$$\frac{4\tau_w}{D} = -\frac{dP}{dz} - \rho g \frac{dh}{dz} \qquad (2.5)$$

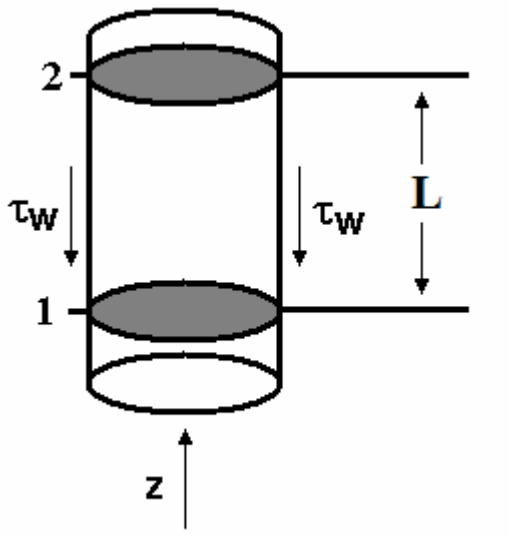

Figure 2.2: Flow in a vertical pipeline.

The left hand side of Equation 2.5 is the frictional resistance to flow where τ_w is the wall shear stress and D the diameter of the pipe. For a horizontally orientated pipe (dh/dz = 0), Equation 2.5 shows that τ_w can be obtained experimentally by measuring the difference in the static pressures between planes 1 and 2 and dividing by the length (L) of the pipeline section.

For a vertical pipeline loop with upward and downward flow test sections the average pressure gradient between the sections can be used to calculate the wall shear stress because the gravitational term in Equation 2.5 is eliminated.

For a Newtonian fluid it is possible to express the frictional energy loss in terms of the Fanning friction factor f defined in Equation 2.6:

$$f = \frac{2\tau_w}{\rho V^2} \tag{2.6}$$

The friction factor for a Newtonian fluid can be estimated using Churchill's equation (Churchill, 1977) using the bulk velocity (V), viscosity (μ), and density (ρ) of the fluid, in a pipeline of known diameter and wall roughness (k).

$$f = 2\left[\left(\frac{8}{Re}\right)^{12} + (A+B)^{-1.5}\right]^{\frac{1}{12}} \tag{2.7}$$

$$A = \left\{-2.457 \ln\left[\left(\frac{7}{Re}\right)^{0.9} + \frac{0.27k}{D}\right]\right\}^{16} \tag{2.8}$$

$$B = \left(\frac{37530}{Re} \right)^{16} \tag{2.9}$$

$$Re = \frac{DV\rho}{\mu} \tag{2.10}$$

To obtain the fluid viscosity from pipe flow data, it is necessary to integrate the relationship between shear stress and shear rate as a function of radial position. The shear stresses for steady laminar pipe flow of Newtonian, Bingham, and Casson fluids are shown in Equations (2.11 to 2.13)

$$\tau_{rx} = -\mu \frac{dv_x}{dr} \tag{2.11}$$

$$\tau_{rx} = -\mu_p \frac{dv_x}{dr} + \tau_y \tag{2.12}$$

$$\tau_{rx} = -\mu_\infty \frac{dv_x}{dr} + \tau_c \tag{2.13}$$

The shear stress decay law provides a relationship for the radial variation of shear stress with respect to the wall shear stress.

$$\frac{\tau_{rx}}{\tau_w} = \frac{2r}{D} \tag{2.14}$$

Combining the shear stress decay law with the pipe flow rheological equations of state (Equations 2.11, 2.12, or 2.13) and integrating, the velocity profile can be obtained by assuming a “no slip” condition at the pipe wall ($v_x = 0$ at $r = ½ D$). The velocity profile for a Newtonian fluid in laminar flow is given in Equation 2.15.

$$u_z = \frac{\tau_w D}{4\mu}\left(1 - \frac{4r^2}{D^2}\right) \tag{2.15}$$

A second integration over the pipe cross-section provides a relationship between bulk velocity and wall shear stress in pipe flow. These laminar pipe flow equations for Newtonian, Bingham, and Casson fluids are shown in Equations 2.16, 2.17 and 2.18.

Laminar Pipe Flow of Newtonian fluid (Poiseuille flow):

$$\frac{8V}{D} = \frac{\tau_w}{\mu} \tag{2.16}$$

Bingham fluid (Buckingham equation):

$$\frac{8V}{D} = \left(\frac{\tau_w}{\mu_p}\right)\left[1 - \frac{4\tau_y}{3\tau_w} + \frac{\tau_y^4}{3\tau_w^4}\right] \tag{2.17}$$

Casson Fluid:

$$\frac{8V}{D} = \left(\frac{\tau_w}{\mu_\infty}\right)\left[1 - \left(\frac{16}{7}\right)\left(\frac{\tau_c}{\tau_w}\right)^{\frac{1}{2}} + \left(\frac{4}{3}\right)\frac{\tau_c}{\tau_w} - \left(\frac{1}{21}\right)\left(\frac{\tau_c}{\tau_w}\right)^4\right] \tag{2.18}$$

The left hand sides of these equations can be determined experimentally by dividing the measured volumetric flow rate by the cross sectional area to obtain the bulk velocity.

$$V = Q/A \tag{2.19}$$

Experimental measurement of pressure drop (P_1-P_2) over a pipe section of length L provides a direct measure of wall shear stress τ_w as shown in Equation 2.5.

Results obtained from laminar flow experiments are plotted to show the variation of wall shear stress with bulk velocity. The "best fit" model parameters may be obtained using an iterative computer program. The slope and intercept of the pressure gradient versus velocity experimental data are calculated. Velocities are calculated using the laminar pipe flow Equations (2.16, 2.17, or 2.18) for the set of experimental pressure gradient data given an initially low guess of yield stress and viscosity. The slope and intercept of this modelled data is compared to the experimental slope and intercept. A bisection method is used to converge on a yield stress and plastic viscosity which satisfies the condition that the slope and intercept differences are less then a specified value.

2.3. Principles of Couette Flow

It is possible to measure the rheology of a fluid by shearing the fluid in the annular space between two concentric cylinders. This type of viscometer is advantageous compared to a pipeline loop in that it only requires a small sample. However, because of the differing geometries, the shear stress distribution is different for a pipe and concentric cylinder viscometer. When comparing test results for these two types of flow it is important to ensure that the shear rates are similar. (Hill and Shook 1998).

In a Couette viscometer, fluid is placed in the annular space between the outer cylinder and the inner cylinder and sheared by rotating the outer or inner cylinder and keeping the other stationary. The device used during this experimental program measured the torque required to rotate the inner cylinder of radius R_1 and height L at an angular velocity ω while the outer cylinder remained stationary as illustrated in Figure 2.3.

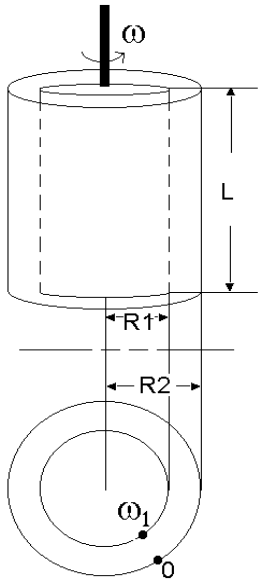

Figure 2.3: Concentric cylinder viscometer

Once again, the constitutive equation for each fluid model can be written for this particular geometry. The shearing process for Couette flow of a Newtonian, Bingham, and Casson fluid is described by Equation 2.20, 2.21, or 2.22.

$$\tau_{r\theta} = -\mu r\left(\frac{d\left(v_\theta / r\right)}{dr}\right) \tag{2.20}$$

$$\tau_{r\theta} = -\mu_p r\left(\frac{d\left(v_\theta / r\right)}{dr}\right) + \tau_y \tag{2.21}$$

$$\tau_{r\theta} = -\mu_{\infty} r\left(\frac{d\left(v_{\theta}/r\right)}{dr}\right) + \tau_{c} \qquad (2.22)$$

In these equations the subscript θ represents the tangential direction. We assume that the only velocity component is tangential.

The relationship between the shear stress and measured torque is obtained by performing a force balance on a cylindrical shaped elemental volume of length L and thickness dr for any surface of a fluid between the cup (R_2) and spindle (R_1) at radius r and the torque:

$$T = \left(2\pi L r \tau_{r\theta}\right) r \qquad (2.23)$$

The boundary condition at $r=R_1$ is given by Equation 2.24.

$$v_{\theta}(r=R_1) = R_1\omega \qquad (2.24)$$

One can determine the relationship between the torque T applied to the spindle and the angular velocity ω by substituting Equation 2.23 into the Newtonian, Bingham, or Casson Couette flow expressions Equations (2.20, 2.21, or 2.22) and then integrating. The corresponding relationships for these fluids are presented as Equations 2.25, 2.26 and 2.27.

Newtonian:

$$\omega = \left(\frac{T}{4\pi\mu}\right)\left(\frac{1}{R_1^2} - \frac{1}{R_2^2}\right) \qquad (2.25)$$

Bingham:

$$\omega = \left(\frac{T}{4\pi\mu_p}\right)\left(\frac{1}{R_1^2}-\frac{1}{R_2^2}\right)-\left(\frac{\tau_y}{\mu_p}\right)\ln\left(\frac{R_2}{R_1}\right) \qquad (2.26)$$

Casson:

$$\omega = \left\{\left(\frac{T}{2\pi}\right)\left(\frac{1}{R_1^2}-\frac{1}{R_2^2}\right)-4\tau_c^{\frac{1}{2}}\left(\frac{T}{2\pi}\right)^{\frac{1}{2}}\left[\left(\frac{1}{R_1}\right)-\left(\frac{1}{R_2}\right)\right]+\tau_c \ln\left(\frac{R_2^2}{R_1^2}\right)\right\}/2\mu_\infty \qquad (2.27)$$

Using the dimensions of the cup and spindle one can obtain model parameters by "fitting" the appropriate equations to a set of (T,ω) data. The Bingham Couette flow Equation 2.26 is linear with respect to T,ω so that one can calculate the plastic viscosity and yield stress directly from the slope and intercept of the (T,ω) data. However, the Casson Couette flow Equation 2.27 is non linear with respect to torque therefore an iterative method must be used. The method used is analogous to that used in obtaining model parameters from pipe flow data.

In steady flow the torque is constant with radial position within the annular gap for concentric radial surfaces and the quantity $r^2\tau_{r\theta}$ in Equation 2.23 is constant. Therefore, the shear stress decreases with increasing radial distance from the spindle with this viscometer. In fluids with yield stresses it is important to ensure that the shear stress in the gap between the spindle and cup does not fall below the yield stress of the fluid.

It is also important to ensure that data are obtained in a region where only the tangential velocity component contributes to flow. Instability occurs when a velocity component other than v_θ contributes to the shear stress. At higher angular velocities,

the fluid experiences a significant centrifugal force and Taylor vortices may be generated as shown in Figure 2.4. At the onset of Taylor vortices the flow is no longer one dimensional and the relationship between torque and angular velocity becomes non-linear, curving upward. Data obtained with angular velocities above the onset of Taylor vortices must be rejected.

For a rotating spindle, Shook and Roco (1991) suggest that vortices occur at:

$$R_\omega \le 45 \left(\frac{R_m}{(R_2 - R_1)} \right)^{\frac{1}{2}} \qquad (2.28)$$

where

$$R_\omega = \frac{R_m \omega (R_2 - R_1) \rho}{\mu} \quad ; \quad R_m = \frac{1}{2}(R_2 + R_1)$$

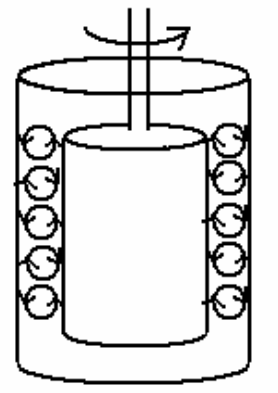

Figure 2.4: Taylor Vortices, a secondary flow pattern at high rotation rates in a concentric cylinder viscometer.

Once model parameters have been determined from laminar pipeline tube or viscometer Couette flow, turbulent flow predictions of wall shear stress and the laminar-turbulent transition velocity can be made.

2.4. Wilson & Thomas Turbulent Flow Prediction

The Wilson & Thomas model (1985, 1987) has often been employed for turbulent flow predictions of fine particle slurries which exhibit yield stresses. Turbulent flow of a Newtonian fluid in a pipeline has been separated conceptually into two flow regions. In the thin sub-layer near the wall of the pipeline, viscous effects dominate and in the turbulent core momentum transfer occurs by inertial turbulent mixing. The Wilson & Thomas model proposes that for a non-Newtonian fluid the thickness of the viscous sub-layer increases. When their model is applied to a fluid with a yield stress there is also a flattening of the velocity profile near the centre of the pipeline where the shear stress is less than the yield stress.

For Bingham and Casson fluids the Wilson & Thomas model for bulk velocity V is written in terms of the friction velocity $u^* = (\tau_w/\rho)^{1/2}$ as shown in Equations 2.29 and 2.30.

Bingham:

$$V = V_N + 2.5\left[u^* \ln\left(\frac{1-\xi}{1+\xi}\right) + \xi\left(14.1+1.25\xi\right)\right]; \qquad \xi=\tau_y/\tau_w \qquad (2.29)$$

Casson:

$$V = V_N + 2.5u^* \ln\left(\frac{1-\xi}{1+\frac{2\xi^{1/2}}{3}+\frac{\xi}{3}}\right)$$
$$+u^*\left[\xi\left(2.5+1.25\xi\right)+11.6\left(2\xi^{1/2}+\frac{\xi}{3}\right)\right]; \qquad \xi=\tau_c/\tau_w \qquad (2.30)$$

Equation 2.30 is given by Shook et al. (2002). In these equations V_N is the bulk velocity calculated using the Newtonian frictional energy loss approach of

Equation 2.7. In the evaluation of the friction factor the apparent viscosity and mixture density are used to calculate the Reynolds number:

Bingham:

$$\mathrm{Re} = \frac{D V_N \rho_m \left(1-\xi\right)}{\mu_p} \tag{2.31}$$

Casson:

$$\mathrm{Re} = \frac{D V_N \rho_m \left(1-\xi^{1/2}\right)^2}{\mu_\infty} \tag{2.32}$$

Iteration is necessary when the velocity is calculated using Equation 2.31 or 2.32.

The transition from laminar to turbulent flow for a fluid with a yield stress is defined by the intersection of the laminar wall shear stress locus with the turbulent wall shear stress locus.

2.5. Factors Affecting Clay Rheology

Fine clay particle slurries may be described as colloidal systems in which the solids are dispersed through the liquid. In these systems the clay particle-particle interactions strongly affect slurry rheology. Particles falling into the colloidal size range have a high surface area to mass ratio. This high surface to mass ratio allows van der Waals attractive forces and electrostatic repulsive forces to dominate particle-particle interactions. The rheological characteristics of fine particle slurries can be manipulated by altering the ionic content in the suspending medium through addition of flocculating and dispersing agents.

Clay particles carry a net negative charge and when placed in water, inter-particle attractive and repulsive forces become evident. The interaction forces can be

strongly attractive so that the particles form a coherent structure in the suspending medium. Alternatively, if the forces are strongly repulsive the particles remain isolated and dispersed. Strong attraction and strong repulsion forces between particles represent the extreme forms of clay slurry particle interactions and the typical situation lies between these limits.

A highly concentrated kaolin clay slurry exhibits non-Newtonian rheological characteristics if particle attraction forces are significant. In order for flow to occur a critical stress must be overcome and above this yield stress the slurry will deform continuously. The relationship between shear stress and shear rate for these slurries can be characterized with the two parameter Bingham and Casson rheological models as described in Equations 2.1 and 2.2. If the particle-particle interactions are highly repulsive such that no structure forms, the resulting slurry often exhibits Newtonian behaviour.

To understand how clay particle-particle interactions affect slurry rheological characteristics it is necessary to understand particle repulsion and attraction. The subsequent sections are devoted to a review of clay particle charge mechanisms and the influence of particle charge and particle-particle interactions on clay slurry rheology.

2.5.1. Structure of Kaolin Clay and Associated Surface Charges

Kaolin clay is composed of two layer-lattice sheets making up a platelet or unit layer. Unit layers stack face to face to form a crystal lattice. Approximately 100 unit layers make up one kaolin clay particle. The unit layer is composed of dioctahedral and tetrahedral sheets. In the dioctahedral sheet oxygen atoms and

hydroxyl groups are arranged octahedrally around a central aluminium atom. In the tetrahedral sheet the oxygen atoms surround a primary silicon atom. These sheets are covalently bonded by sharing common oxygen atoms as shown in Figure 2.5. The unit layers are held together by fundamental attractive forces between molecules known as van der Waals attractive forces.

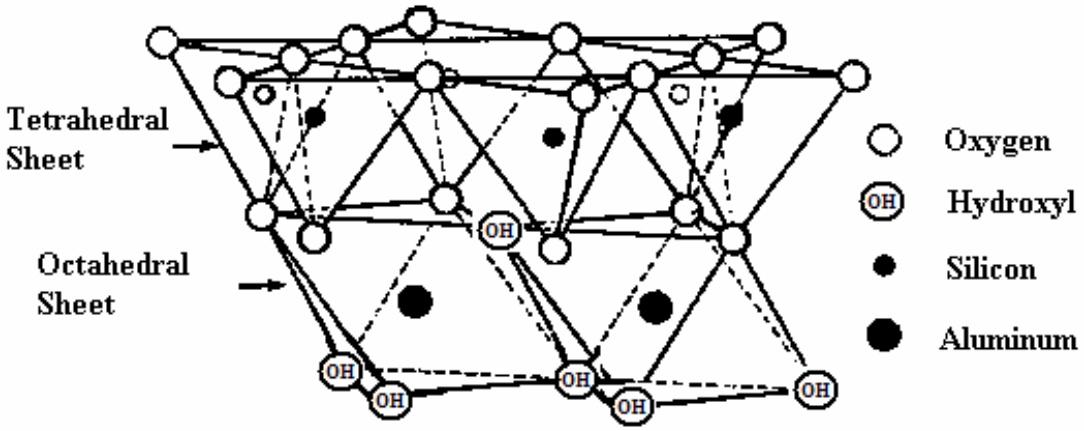

Figure 2.5: Atomic Structure of Kaolin Clay, Holtz and Kovacs (1981)

Kaolin clay minerals are plate-like in structure and carry a net negative potential. Van Olphen (1977) suggested that both basal surfaces carry a negative charge because of isomorphous substitutions of central atoms in the mineral structure by atoms of a lower valence (i.e. Al^{3+} for Si^{4+}, or Mg^{2+} for Al^{3+}). The atoms which are substituted in the crystal structure are not exactly the same size however they are called isomorphous because they do not disrupt the mineral structure. This creates negative basal surfaces on the clay particle as illustrated in Figure 2.6.

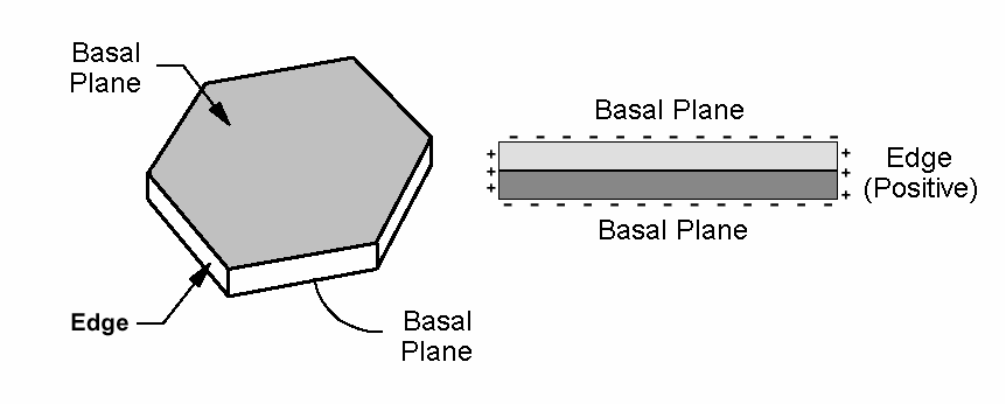

Figure 2.6: Van Olphen idealized kaolin clay particle charge distribution. (Carty 2002)

More recently Carty (1999) has suggested that the basal surfaces of kaolin clay are of opposite charge in a fluid having a pH ranging from 3.0 - 8.5. The pH at which the particle exhibits a reversal of charge is known as the isoelectric point (i.e.p.). Carty states that alumina sols (dilute slurries) have an i.e.p. at a pH of approximately 2.0 - 3.0 whereas the silica sols have an i.e.p. at a pH of 8.5 - 10.0. This indicates that kaolin particles in a slurry having a pH between 3.0 - 8.5 should have oppositely charged basal surfaces with the tetrahedral silica-like sheet carrying a positive potential and the dioctahedral alumina-like sheet carrying a negative potential as illustrated in Figure 2.7.

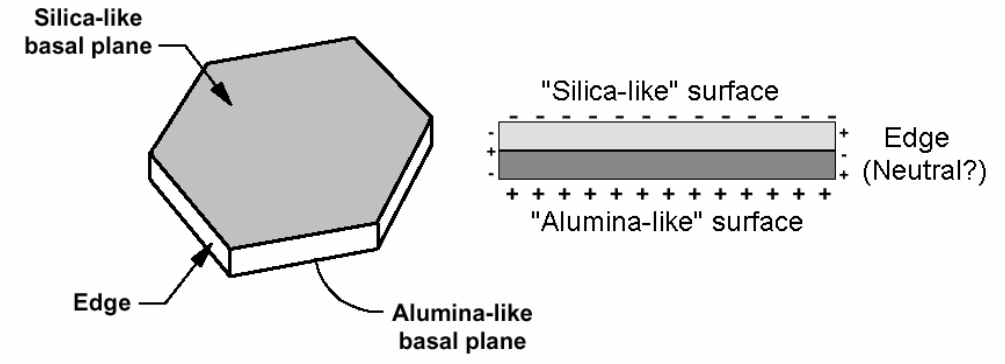

Figure 2.7: Carty idealized kaolin particle charge distribution. (Carty 2002).

The clay particle cannot extend in the lateral direction indefinitely. The interruption of the crystal structure results in exposed atoms with positive valences so that at these edges a slight positive charge is apparent. Thiessen (1942) mixed kaolin sols (dilute slurries) and negatively charged gold sols and prepared electron-microscopic pictures of the suspensions. Van Olphen (1977) interpreted Thiessen's photograph, shown in Figure 2.8, as a mutual attraction of the negatively charged gold particles (which appear as the fine black dots) to the kaolin. This suggests that the kaolin has positively charged edges.

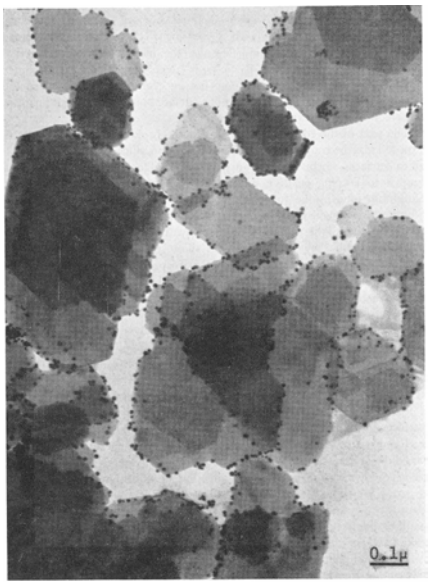

Figure 2.8: Electron micrograph of a kaolinite and gold sol. Van Olphen (1977).

2.5.2. Charged Atmosphere Surrounding a Particle

It is possible to manipulate clay particle-particle interactions by altering the ionic environment of the suspending liquid which can alter the rheological properties of the slurry significantly. Manipulating the chemical species in the suspending fluid affects the balance of electrostatic repulsion and van der Waals attraction forces between particles. When a charged particle is suspended in liquid, the ionic

environment surrounding the particle develops in such a way to balance the charge difference between the particle and the bulk liquid medium. This charged atmosphere is known as the electrical double layer and is illustrated in Figure 2.9 for an idealized sphere having a negative charge.

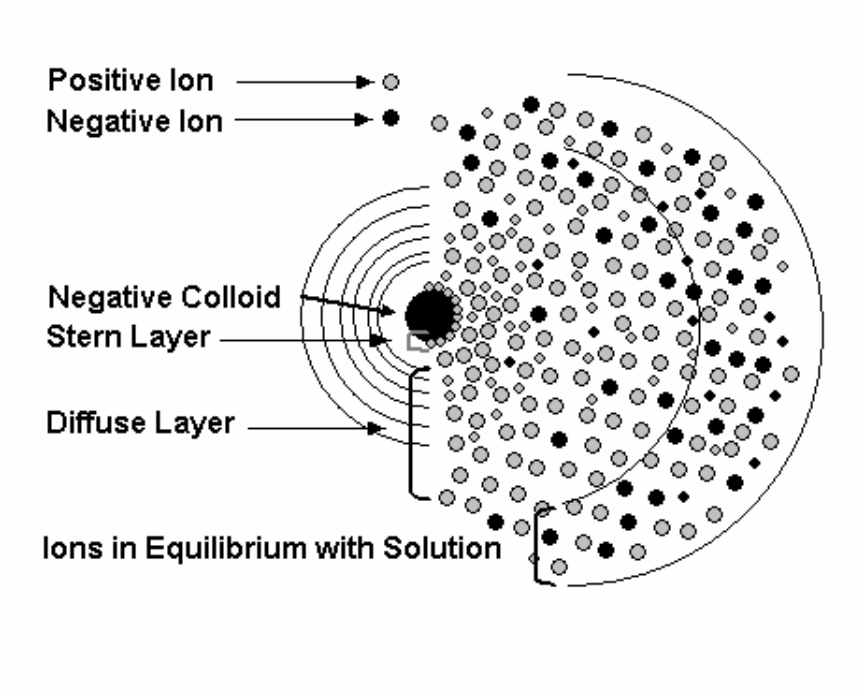

Figure 2.9: The electric double layer used to visualize the ionic environment surrounding a charged particle.

Clay particles which have two oppositely charged surfaces develop two separate electrical double layers. The negatively charged basal surface of a clay particle is balanced by positive cations in solution creating one double layer. Conversely the positively charged edge surface is balanced by anions in solution creating a double layer of opposite charge. These charge balancing ions are considered exchangeable because they can be readily substituted by other ions in solution.

In the double layer model, the layer of ions adsorbing around the surface of the clay particle is termed the Stern layer. Additional positive ions in solution are now repelled by the positive ions in the attached Stern layer and create a dynamic equilibrium of ions between this layer and the bulk fluid. This secondary ion layer called the diffuse layer. The Stern and diffuse layers make up the double layer.

Figure 2.10 illustrates the electrical potential surrounding a negatively charged particle where a maximum electrical potential exists at the surface of the clay and decreases to zero in the bulk solution. The thickness of the electric double layer is referred to as the Debye length (κ^{-1}). For a clay particle suspended in water containing ions the Debye length is a function of the particle charge, the valence of the ions in solution, and the ionic concentration in the bulk solution.

When a dilute clay slurry is subjected to an electric field, particles and adsorbed ions in the Stern layer (electro-kinetic unit) will move in the direction of the oppositely charged electrode through the solution. The movement of particles under the action of an electromotive force is called electrophoresis. Drag forces acting upon the moving electro-kinetic unit oppose the motion induced by the electromotive attractive force. The particles reach a constant velocity when the forces are balanced. The potential at the surface of shear, as illustrated in Figure 2.10, is known as the zeta potential and can be determined by measuring the electrophoretic mobility (υ) of the particles.

$$\upsilon = \nu / E \qquad 2.33$$

where ν is the particle velocity and E is the applied field strength (V/L) where V is the voltage and L is the effective inter-electrode distance. Changes in mobility or

zeta potential represent changes in electrical repulsive forces between particles. Monitoring the electrophoretic mobility aids in understanding the effect of chemical species on particle-particle interactions

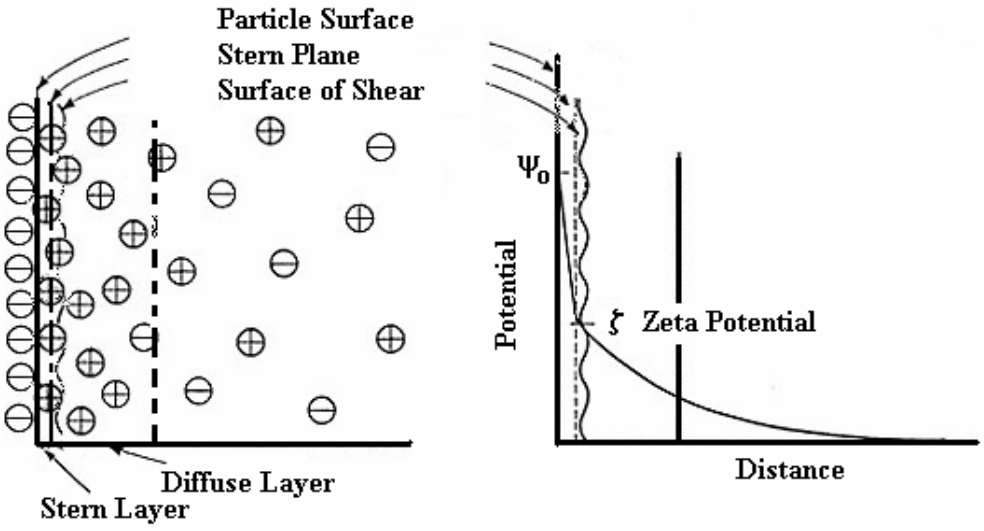

Figure 2.10: The electrical potential in the atmosphere surrounding a negative surface of a particle. (adapted from Masliyah, 1994)

If the electrophoretic mobility of a particle in the suspending medium is known, the particle zeta potential can be determined by evaluating the forces acting on the particle. After an electric field is supplied and the particle has reached a constant velocity there is an electrical force on the charged particle which is balanced by the hydrodynamic frictional forces on the particle by the liquid. There are additional forces caused by the movement of water and counter ions which move in the opposite direction of the particle. When calculating the zeta potential for clays complications arise due to their nonspherical geometry and the presence of two different double layers. Van Olphen (1977) suggests that it is advisable to report

electrophoretic mobility results (i.e. in cm/s per volt/cm) instead of zeta potential as calculated from simpler formulas.

The net interaction of particles results from the balance of opposing repulsion and attraction forces. The Derjaguin, Landau, Verwey and Overbeek (DLVO) theory explains why some particles will flocculate while others remain dispersed. Electrostatic repulsion occurs between the electric double layers of charged particles when they have the same charge. As the particles approach, and double layers begin to overlap, the level of energy required to overcome this repulsion increases. There is also an attraction between the particles. The intermolecular van der Waals attractive forces become large with particles in colloidal systems as the distance between the particles decreases.

The net interaction energy can be illustrated on a graph with attractive or repulsive energy on the ordinate and the distance between colloid surfaces on the abscissa as shown in Figure 2.11. This diagram shows the net interaction of two charged particles. The solid line N1 on Figure 2.11 shows the net energy of interaction for a given system by summing the van der Waals attraction energy curve and the electrical repulsion curve R1. The peak of curve N1 represents an energy barrier between particles and indicates how resistant the system is to flocculation.

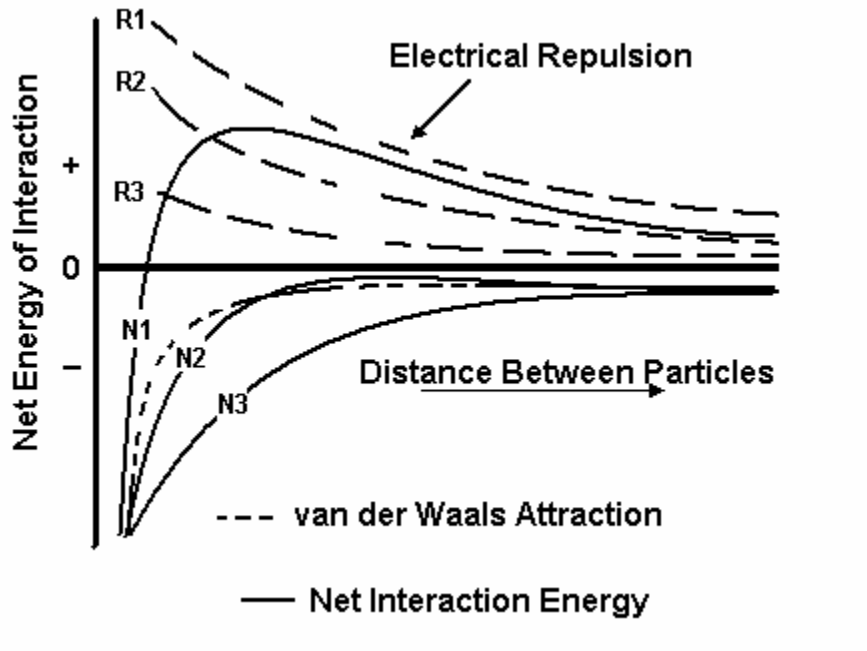

Figure 2.11: Net Energy Interaction Curve (adapted from Masliyah, 1994)

Flocculation can occur if the particles have sufficient kinetic energy to overcome the energy barrier and come into close enough contact that van der Waals forces will dominate. By manipulating the ionic content in the suspending medium the thickness of the electric double layer can be reduced. A lower energy barrier is then produced and flocculation can occur.

2.5.3. Factors Affecting Flocculation

As mentioned earlier clay particles carry a net negative charge. As a result of their like charge, clay particles suspended in deionized water (free from ions) will remain dispersed and will not flocculate. These particles have a large diffuse layer and the electrical repulsion energy remains large as illustrated by the R1 curve in Figure 2.11. However, if the charge on the particle is balanced with the addition of

counterions (ions of opposite charge to the clay surface) such as Ca^{2+} a reduction of the electric double layer thickness occurs. Figure 2.11 illustrates an electric repulsion energy decrease between particles associated with a double layer reduction (curves R2 and R3). The net interaction energy, curves N2 and N3, will fall into a region where particle association is dominated by van der Waals forces and flocculation will occur.

The concentration of ions at which flocculation occurs is known as the flocculation value. This value is dependent upon a combination of the clay mineral being flocculated and the ion used to flocculate. There is a difference in flocculation value between ions. In 1882 Schulze studied the effects of cation valence on the flocculation of negative sols. At the same time Hardy was studying the effects of anion valence on the flocculation of positive sols. In 1900 the Schulze-Hardy rule was formulated. "The coagulative power of a salt is determined by the valency of one of its ions. This proponent ion is either the negative or the positive ion, according to whether the colloidal particles move down or up the potential gradient. The coagulating ion is always of the opposite electrical sign to the particle." Van Olphen (1977). For cations this flocculation power is shown below. This series is known as the Hofmeister series.

$$H^{+} > Ba^{2+} > Sr^{2+} > Ca^{2+} > Cs^{+} > Rb^{+} > NH_4^{+} > K^{+} > Na^{+} > Li^{+}$$

Note that hydrogen is strongly adsorbed, so that pH has a large influence on particle-particle interactions. It is possible to achieve a particle with zero charge by reducing

the pH. Remembering that the source of the negative basal charge on the clay is due to isomorphous substitutions i.e. (Al^{3+} for Si^{4+}), the added H^{+} ions can combine with the oxygen atoms on the tetrahedral surface to form hydroxyl groups (Masliyah 1994).

Clay particles may orient themselves in a flocculated structure in different ways. The mode of particle association is governed by the interaction of the two double layers on each clay particle. The flat plate like structure can lead to edge-to-edge (EE), edge-to-face (EF), and face-to-face (FF) particle associations as illustrated in Figure 2.12 (Van Olphen 1977).

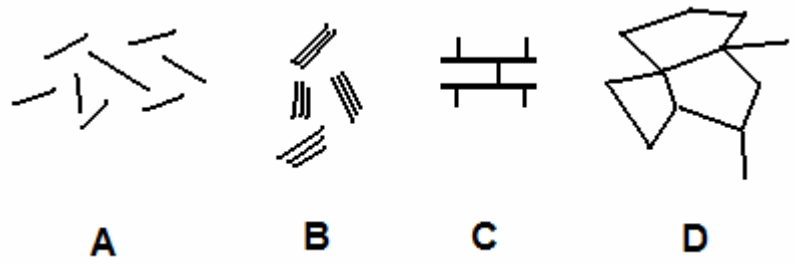

Figure 2.12: Modes of particle association. (A) Dispersed, (B) Face-to-Face, (C) Edge to Face, (D) Edge to Edge.

A flocculated structure is created by EE and EF particle associations. These associations immobilize free water and strongly affect the nature of the suspensions created by these associations. The FF associations create an effectively thicker particle with a minimal immobilization of water. When the concentration of the clay in the suspending fluid is high enough and the ionic environment promotes flocculation, a continuous structure known as a gel will form. If fluid ionic conditions favour charged particles having negative basal surfaces and positive edges there will preferentially be edge to face particle associations in the flocculated gel.

The EF orientations of particles are sometimes referred to as the "card house" structure.

2.5.4. Factors Affecting Deflocculation

With the addition of small amounts of specific chemicals it is possible to manipulate particle-particle interactions between clay particles in a slurry. Variations in flow behaviour including elimination of yield stress are associated with these changes. Flocculation of clay particles may be prevented or reversed by manipulating the ionic environment surrounding the clay particles. It can also be prevented by changing the surface charge of the particle causing electrostatic repulsive forces to dominate over attractive van der Waals. Tetrasodium pyrophosphate (TSPP), which was used in this experimental program, can complex with metal ions such as aluminium, magnesium, and calcium. Complexing with calcium in solution will shift the ionic equilibrium between the clay surface and the bulk solution thereby increasing the electrical repulsion energy between particles. There is also strong evidence to indicate that chemisorption of the phosphate group occurs on the edge surfaces of the clay particle as shown in Figure 2.13 (Van Olphen 1977).

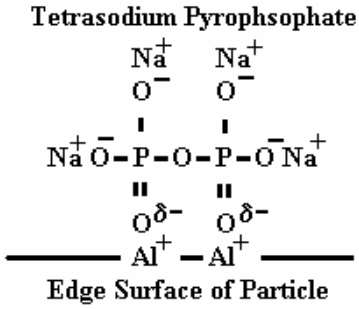

Figure 2.13: Chemisorption of tetrasodium pyrophosphate on a positively charged edge surface of a clay particle. (adapted from Van Olphen, 1977).

Tetrasodium pyrophosphate is known to form insoluble salts, or complexes, with aluminium, whose atoms are exposed at the edge of the clay particle indicating chemisorption. Dissociation of the sodium ions will produce a negative edge surface and one double layer will surround the charged particle. As a result, electrostatic repulsive forces dominate between clay particles and the EE and EF associations will be reduced or eliminated. The floc structure will weaken and the yield stress of the slurry may be also reduced or eliminated. A reduction in apparent viscosity will be associated with this dispersed slurry. Higher concentrations of multivalent cations will now be required to reduce repulsive forces and reverse this affect. In other words, adding a small amount of TSPP to a clay slurry increases its flocculation value.

2.6. Clay Rheology

Many researchers have investigated the rheological behaviour of kaolin clay slurries. In a classical study Michaels and Bolger (1962) investigated the flow behaviour of kaolin suspensions. They proposed a physical model of the floc structure which produced the yield stress in clay slurries. The floc was considered to be the basic flow unit of a small cluster of particles plus the immobilized water that they contained. These units could grow by collision or would be broken down by shear forces. They could also extend into networks giving the slurry a yield stress. In 1963 D. G. Thomas published a study of factors affecting Bingham rheological parameters of fine particle slurries. He reported that in the case where slurry particles

approach colloidal size, such as kaolin clay in water, the yield stress and plastic viscosity vary with concentration. He found that the plastic viscosity varied exponentially with volumetric concentration and the yield stress varied with volumetric solids concentration to the third power.

Xu et al. (1993) reported the experimental results of laminar and turbulent flow of kaolin clay slurries. The slurries characterized with the Bingham model showed good agreement between yield stress values obtained from laminar pipe flow experiments and concentric cylinder viscometry. However, the plastic viscosities obtained from pipe flow measurements were found to be approximately 50% higher than those obtained with concentric cylinder viscometry.

Xu et al. also found that the transition velocity from laminar to turbulent flow as predicted by the intersection of the pressure gradient predicted by the Buckingham Equation (2.17) and that predicted for turbulent flow by the Wilson & Thomas Equation (2.29) agreed well with experimental observation. However the theoretical pressure gradient calculated for a Bingham fluid, using Equation (2.29), was found to over predict that found experimentally. It was suggested that the deflocculation mechanism proposed by D. G. Thomas (1964) caused lower experimental frictional resistance which is not considered in the Wilson & Thomas model. D.G. Thomas stated that the break up of the floc is promoted by an increase in the energy dissipation per unit mass of the fluid. Because this energy dissipation is a maximum near the pipe wall, the floc size is at a minimum in this region.

The effect of modifying clay particle-particle interaction, and consequently the slurry rheology, by manipulation of continuous phase ion composition has been

experimentally studied by researchers in the ceramic industry. O'Connor and Carty (1998) evaluated viscosity modification of clay systems by adding six salts (NaCl, Na_2SO_4, $CaCl_2$, $CaSO_4$, $MgCl_2$ and $MgSO_4$) over a broad concentration range for a slurry composed of 30% solids by volume porcelain batch clay in distilled water. The batch composition of their typical whiteware suspension consisted of kaolin 29%, ball clay 7%, alumina 12.5%, quartz 29.5% and Nepheline syenite 22.0% all based on dry weight percent of solids.

The dispersant sodium polyacrylic acid (Na-PAA) was added and it was found that an increased amount of salt was necessary to induce flocculation. Figure 2.14 illustrates that the flocculation value for Ca^{2+} and Mg^{2+} are almost identical where as it is necessary to add approximately eight times the amount of the monovalent Na^{+} ion to achieve flocculation with the associated dramatic increase in apparent viscosity.

O'Connor and Carty found that once enough counter-ion (Na^{+}, Ca^{2+}, Mg^{2+}) was added to reach the flocculation value of the clay the apparent viscosity of the suspension increased dramatically. It was also evident that above a certain ionic concentration the apparent viscosity reached a stable plateau where any further addition of counter-ion did not increase the apparent viscosity. These results are shown in Figure 2.14.

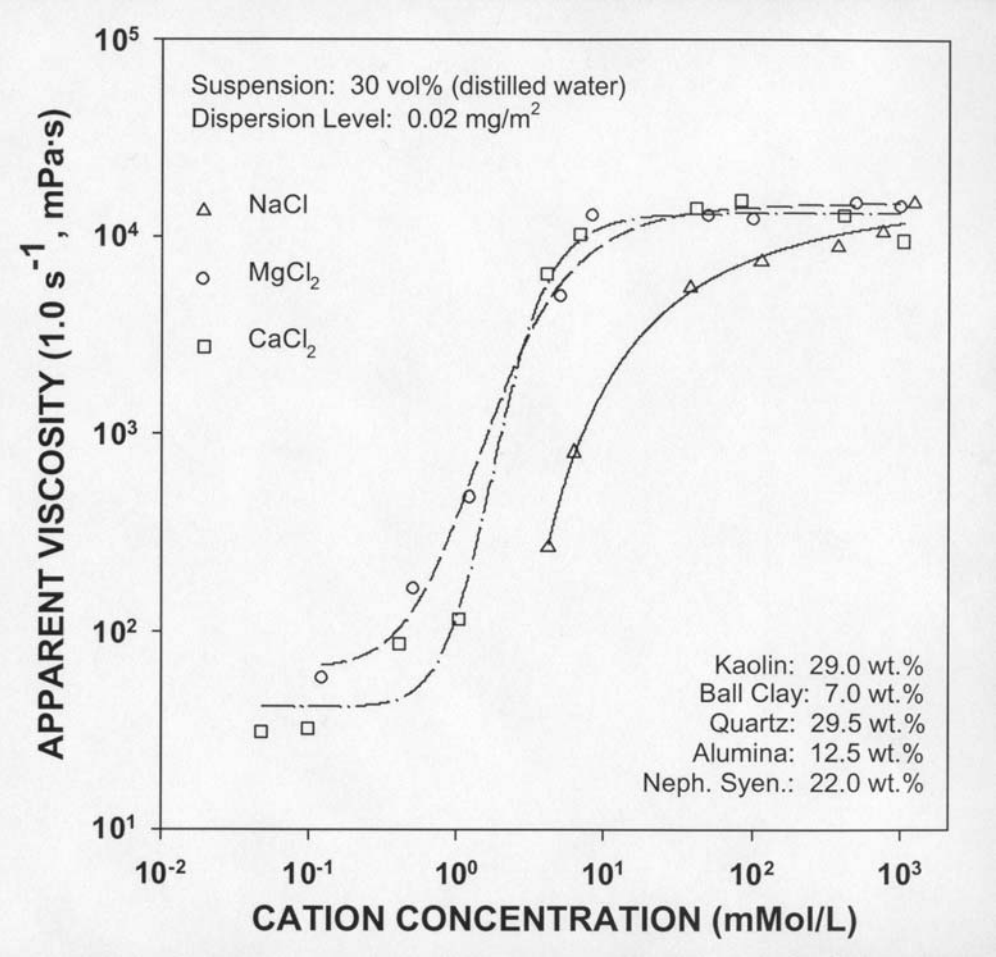

Figure 2.14: Effect of counter ions on the viscosity of porcelain batch suspensions (O'Connor and Carty 1998).

Rossington et al. (1999) studied the effects of six dispersants commonly used in the ceramics industry on the rheological properties of highly concentrated (Cv ≈ 30% solids) kaolin clay slurries. The slurries were prepared with distilled water in the absence of dispersant. Stepwise dispersant additions were used to create a dispersion demand curve. Sodium hexametaphosphate (Na-HMP), which has an identical dispersing mechanism to TSPP, was one of the dispersants tested. The apparent viscosity at a time rate of shear strain = 1.0 s^{-1} and the pH were reported for all the dispersed slurries. Effectiveness was measured by the amount of phosphate

group needed to reduce the apparent viscosity. Na-HMP was found to reduce the apparent viscosity of the slurries by a factor of 1000. The concentrations of dispersant addition are reported in mass of dispersant per surface area of clay particle (mg/m^2). The pH value remained relatively constant (7.3-7.8) when compared to the slurries prepared without the phosphate group.

Carty (2001) also states that thixotropy has been observed in which the viscosity decreases with time at a constant shear rate and, when the shear is removed, the viscosity increases slowly with time. When shear is removed the particles begin to slowly rearrange by Brownian motion to develop a structure similar to that which was present prior to shearing. The time required to return to the pre-sheared viscosity may be several days.

Work performed by P. Larsen et al. (1994) reported rheopectic behaviour in kaolin clay suspensions at a concentration of 32% by volume. Rheopexy is observed when the viscosity increases with time at a constant shear rate. Like thixotropic behaviour when shear is removed the particles will rearrange to develop a structure similar to the one present prior to shear. They found that at low clay concentrations or if the shear rate was lower than a threshold value, the shear stress did not increase. Larsen proposed that an explanation of the phenomenon could be that "a considerable part of the flat clay particles overlapped each other in the suspensions, they were separated by the high shear rate, and therefore, more and thinner particles built stronger flocculant structure." The kaolin clay slurry initially exhibited a yield stress of 30 Pa but after being exposed to a high shear rate the yield stress increased to 300 Pa.

2.7. Key Elements of This Investigation

The present work investigated vertical pipe flow and Couette viscometer flow of kaolin clay slurries. The intent of the work was to advance the present state of knowledge regarding factors affecting fine particle slurry rheology. Specifically, the study investigates which constitutive model describes fine kaolin clay particle rheology, and to determine if the rheological parameters inferred from pipe flow and Couette viscometry agree. The experimental matrix was designed to examine the nature of the effects of clay concentration and chemical species on the rheology of kaolin clay slurries. The dispersant TSPP was added to various concentrated kaolin clay slurries containing calcium ions in the suspending water medium. The calcium ion concentration was monitored in an attempt to understand particle-particle interactions and their effect on slurry rheology.

3. MATERIALS APPARATUS AND PROCEDURE

3.1. Materials

The Pioneer clay used in this experimental program was obtained from Dry Branch Kaolin Clay Company, located in Dry Branch, GA, USA. Mr. B. Blossom (2002) of IMERYS research laboratory located in Roswell, GA, revealed that this clay originated from the in-situ degradation of igneous rock. The clay ore body is mined and sent through a primary crushing mill and then to a secondary roller mill to achieve a specific bulk density. In this dry air separation process there is no chance for ions to be exchanged from the surface of the kaolin. Exchangeable ions such as Ca^{2+}, Mg^{2+} and Na^{+} may be present on the surface of the clay because the kaolin deposit may have undergone a weathering process in which the minerals came into contact with a hard water supply.

Calcium ions may also be present in small amounts from residual calcite (calcium carbonate) or dolomite (calcium magnesium carbonate) that remains with the clay even after beneficiation. It is therefore necessary to determine the prevalent ion on the surface of the clay by washing with pure water. The results of a mass spectrometer analysis of supernatant obtained from a 14 volume percent solids slurry prepared with Pioneer clay and reverse osmosis (R/O) water are presented in Appendix B, Table B.5. The most concentrated ions found in the supernatant are calcium (24 ppm) and sodium (5ppm). A microphotograph of a sample of Georgia kaolin is illustrated in Figure 3.1.

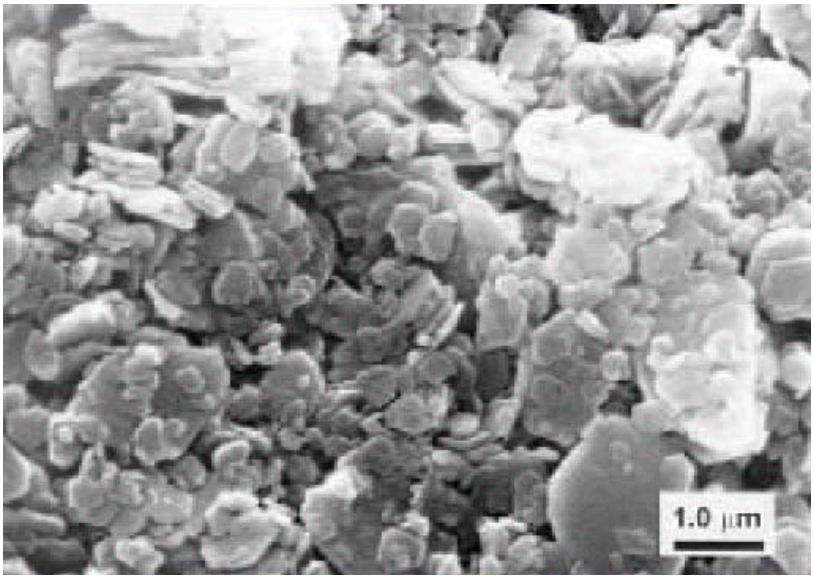

Figure 3.1: Electron scanning microscope image of well crystallized Georgia kaolin. (Carty 2002)

3.2. Particle Properties

3.2.1. Particle Size Analysis

The method with which particle size is analysed is dependent on the size of the particles. For coarse granular particles sieve analysis may be performed in which a sample is shaken mechanically through a series of wire mesh sieves with successively smaller openings. Sub-sieve size particles are considered to be fine grained. The particle size of fines can be determined using sedimentation of the particles in a viscous fluid. Gravity sedimentation with an Andreasen pipette may be used for particles in this sub sieve size range down to 0.6 μm. Below 0.6 μm gravitational techniques (Andreasen pipette) are inappropriate because settling rates start to become affected significantly by Brownian motion.

Brownian motion is the diffusional broadening of the path of a settling particle and is a topic of much debate Allen (1997). By diffusion, it is meant that the particles no longer travel only in the settling direction (downward for gravity or outward for centrifuges) but have a velocity component in a random direction determined by the molecules of the carrier fluid. This diffusional phenomenon is due to bombardment of the solid fine particles by the fluid molecules. This causes the particles to move about in a random matter rather than solely in a settling manner.

Loomis (1938) has shown that a centrifuge can be used to increase the sedimentation rate particles below 0.6 μm. A centrifuge employs a spinning apparatus and a centrifugal driving force rather than a gravitational driving force. This speeds up sedimentation rates significantly and allows for the determination of the particle size distribution at the fine end. It is for this reason that centrifugal sedimentation is known as a sub-micron technique. In this experiment the particle size distribution for particles below 0.6 μm were obtained using centrifugal sedimentation.

The equivalent spherical diameter of a particle settling in Stokes Region under gravity sedimentation can be found using Equation 3.1.

$$D_p = \sqrt{\frac{18h\mu}{2(\rho_1 - \rho_2)gt}} \qquad 3.1$$

where D_p = diameter of spherical particle

μ = viscosity of suspending medium

h = distance between liquid surface and pipette tip when sample is drawn

ρ_1 = specific gravity of particles

ρ_2 = specific gravity of suspending medium

g = gravitational acceleration

t = time from start of test

It is assumed that the particles are so fine that they immediately reach their terminal settling velocity. The concentration of particles is also assumed to be low so that there is no hindered settling. Particle-wall effects are also assumed to be negligible because the settling vessel diameter is several orders of magnitude larger than the particle diameter. The assumption of a single particle settling at infinite dilution is used in Stokes' Law and is assumed to apply to both sedimentation techniques but it may not be applicable if the system contains flocculated particles. Bolger and Michaels (1962) have shown that significant variations in the settling rate and the rheological behaviour can occur when particles are flocculated. To eliminate flocs, the dispersant tetrasodium pyrophosphate (TSPP) is added to the slurry. As well, low concentration slurries are used to limit the interparticle interactions as much as possible.

The centrifugal sedimentation method was used to achieve separation of particles below 0.6 μm in diameter. By using a centrifuge, the driving force for sedimentation of the particles can be increased from gravity (1.0 g) to much higher centrifugal forces (g-forces) which arise through the angular velocity of the particle in the centrifuge. The g force is $\omega^2 r$ where ω is the angular velocity in rad/s and r is the radial distance of the particle from the axis of rotation. One can see that if angular

velocities of 2000 rpm (209 rad/s) are used at a radial distance of 10 cm the angular acceleration is 4386 m/s^2, or 447 g.

When working with a centrifuge the desired angular velocity is not achieved instantaneously but rather it takes a finite period of time to be reached. This is also true when the centrifuge decelerates. These acceleration and de-acceleration times must be accounted for in the derivation of the particle sedimentation under centrifugal forces.

The equivalent spherical diameter of a particle settling during centrifugal forced sedimentation including ramping (accelerating and decelerating) times can be found using Equations 3.2. The derivation can be found in the Appendix D.

$$D_P = \left[\frac{\mu \ln\left(\frac{R}{S}\right)}{\omega_C{}^2 (\rho_s - \rho_f)\left(\frac{t_{RU}}{54} + \frac{t_{RUN}}{18} + \frac{t_{RD}}{54}\right)} \right]^{1/2} \qquad 3.2$$

where

R = the final radial displacement of a particle with D_P

S = the initial radial displacement of a particle with D_P

ω_c = the angular velocity of the centrifuge

ρ_s = density of the solid

ρ_f = density of the fluid

t_{RUN} = time of centrifuge operation at specified angular velocity

t_{RU} = time required to accelerate centrifuge to specified angular velocity

t_{RD} = time required to decelerate centrifuge to specified angular velocity

μ = viscosity of the fluid

D_p = equivalent spherical particle diameter

In both Andreasen sedimentation pipette tests (gravity and centrifugal), once the samples have been dried and weighed and the particle diameters have been calculated for the various samples, one must associate a fraction of the total weight percent of the sample with them. This is commonly expressed as a "percent finer than" term. If samples are drawn at both the initial state and at some later time it can be assumed that the larger particles have been allowed to settle to the bottom of the sampling zone. In this way the fraction or percentage of particles finer than the given particle size can be calculated.

Andreasen Sedimentation Pipette (Gravity Settling)

The Andreasen sedimentation pipette was used to determine the particle size distribution of kaolin clay having particles larger than 0.6 μm. An illustration of the pipette is detailed in Figure 3.2. The stem of the pipette is inserted into a glass cylinder with a capacity of 550 ml. The bottom of the stem extends 20 cm below the surface of the fluid and is elevated ≈ 4 cm off the bottom of the cylinder. At the top of the pipette there is a three way stopcock and spout for drainage of an aspirated sample into a weighed evaporation dish.

Figure 3.2: Illustration of an Andreasen pipette used in for gravity sedimentation.

The following procedure is a replication of work by Loomis (1938) for determining grain sizes of white ware clays.

Procedure:

1. Weigh out sufficient solid material (clay) so that upon dilution a 1% by volume solid slurry will exist. One must make sure that a representative sample of clay is obtained from the source so that an accurate particle size distribution can be obtained.
2. For a separate sample, determine the moisture content to determine the true powder mass percent.
3. Prepare the suspension so that a high degree of dispersion is obtained. In all cases $Na_4P_2O_7$ was added at 0.002 g-mol/L and RO water was used as the medium (Loomis, 1938).
4. Transfer the dispersed sample to the Andreasen Pipette and add RO water up to the 20 cm mark.
5. Insert a stopper in the pipette and shake the apparatus vigorously until the slurry is well mixed. Allow the temperature of the apparatus to come to equilibrium with the room.
6. Once equilibrium is obtained with the room, the apparatus should once again be shaken for approximately 2 minutes.
7. Note the exact time when the shaking is stopped.
8. Take the first sample from the apparatus with the pipette bulb immediately by drawing 10 mL of slurry into the pipette. A reasonable sampling time would be 20 seconds. If the sample is drawn too fast one might create a disturbance within

the apparatus and thus the quiescent fluid assumption will not be valid. All results obtained after this sample will therefore be biased by the first sample.

9. Drain the sample into a pre-weighed crucible (weighing vessel) and immediately weigh the sample. Then place the sample in an oven and dry it until all moisture is eliminated from the slurry. Once again weigh the sample. One can now calculate the mass percent of solids in the slurry.
10. Withdraw samples from the Andreasen pipette at the appropriate intervals so that the desired particle sizes may be obtained as done in step (8).
11. Weigh and dry all samples.

Modified Andreasen Sedimentation Pipette (Centrifugal Settling)

Figure 3.3 shows the centrifuge tube and the associated syringe, which was used to draw the fluid samples during the modified Andreasen Centrifugal settling tests. This apparatus was used for the sub-micron particle size distributions in the centrifuge. It was designed and constructed for the specific centrifuge and the particular clay used in this experimental work. Only one sample may be withdrawn from this centrifuge tube therefore a predetermined time must be calculated to obtain a data point for a target particle diameter.

Figure 3.3. Picture of Modified Andreasen Sedimentation Pipette used in centrifuge sedimentation.

Procedure:

1. Turn on the centrifuge and turn dial on side to desired setting to warm up. This will minimize any fluctuation in set rotational velocity. Switch the cooling compressor motor on to maintain a constant temperature in the centrifuge. Once the centrifuge motor has been operated for 10 min shut down to load samples.
2. Preparation of the sample suspension is identical to that previously discussed for the gravity sedimentation trials.
3. Draw 10 mL of original sample with syringe and place in crucible.
4. Weigh the sample and record the mass.
5. Dry the sample and re-weigh to find the original powder weight.
6. Fill the centrifuge bottles with the sample. Put lids on the bottles and swirl vigorously.

7. Place samples in the centrifuge and set rotational velocity to desired value. Once complete start the timer.
8. Record the time (t_{RU}) at which the centrifuge reaches steady state operation.
9. Continue to time the run. Monitor the RPM value periodically to verify it is holding constant.
10. Record both the set point temperature and room temperature.
11. At the end of the run when the desired time is reached, switch the centrifuge motor off. Let the centrifuge come to a stop and record the time the centrifuge took to decelerate t_{RD}.
12. Draw out 10 cc samples from each bottle using the corresponding syringe. Each draw should take approximately 30 seconds. Ensure that the bottle is vertical when performing the withdrawal.
13. Place each withdrawn sample into a pre-weighed crucible and weigh quickly. The mass will begin to change immediately because of evaporation. Record the mass of the (slurry + crucible).
14. Place the crucibles in the oven to dry.
15. Weigh again after the samples are dried in the oven. Put samples back in the oven and allow them to dry for a few more hours (2 or 3). Continue to repeat this procedure until the mass of the dry clay and crucible are constant.

3.2.2. Particle Density

The density of the Dry Branch Pioneer kaolin clay used in these experiments was determined experimentally by the Saskatchewan Research Council. Approximately 100 ml of premixed 40 wt% slurry of clay and water was placed in a 200 ml volumetric flask. The flask was then connected to a vacuum pump for 20 min to remove any air that may have been attached to the clay particles. After aspiration of the air was completed the resulting slurry volume was made up to the 200 ml mark on the flask and weighed. The slurry was then oven-dried and the mass of solids was recorded. This procedure was repeated four times by two different operators. The clay particle density could then be determined from the weight of solids w_S, the weight and density of liquid, $w_{L,}$ and $\rho_{L,}$ and the volume of the flask:

$$V_{Flask} = \frac{w_S}{\rho_S} + \frac{w_L}{\rho_L} \qquad 3.4$$

From this information an average density of 2693 kg/m^3 was determined for the Pioneer kaolin clay. The experimental data can be found in Table 4.7. This is within the acceptable limits of typical Georgia kaolin clay.

3.3. Electrophoretic Mobility

A Rank Brothers Ltd. Microeletrophoresis apparatus (MKII) was used to obtain electrophoretic mobility of various clay particles from previously characterized slurries. This information is used in the understanding of associated electrical repulsive forces between particles in those slurries. An illustration of the apparatus is shown in Figure 3.4. The unit consists of a microscope, lamp, collimator tube, cylindrical sample cell containing electrodes, and a water bath.

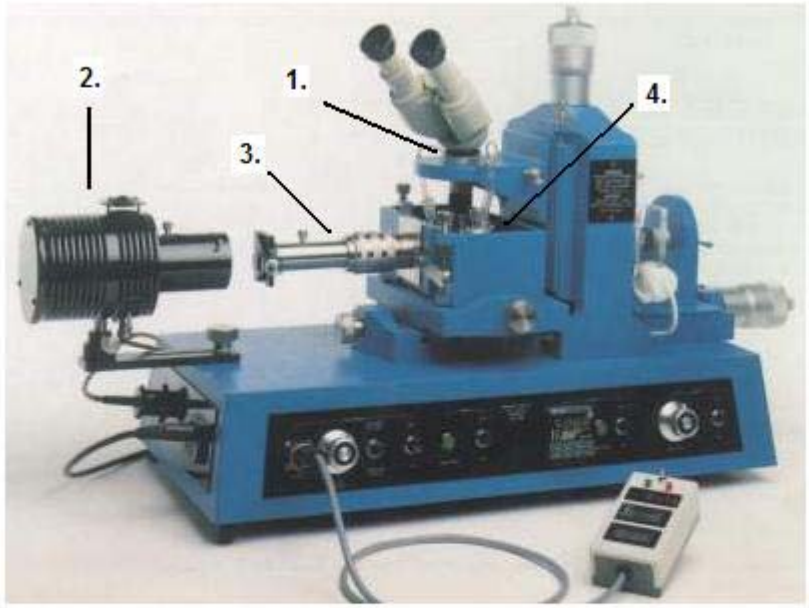

Figure 3.4: Rank Brothers micro electrophoresis apparatus Mk II with rectangular cell set-up (adapted from Rank Brothers operating instructions)

A dilute clay sample is placed in the sample cell and positioned under the microscope. An electric field is applied across the sample chamber. This causes

charged particles to move towards the oppositely charged electrode. The terminal velocity of the particle is measured by timing the motion of the particle across a grid in the microscopic eyepiece. The velocity and direction under the applied voltage are used in the calculation of electrophoretic mobility of the particle and adsorbed ions in the Stern layer.

To ensure that the Rank Brothers instrument was working properly styrene particles purchased from Interfacial Dynamics Corp. (IDC) of known electrophoretic mobility were tested. The particles are spherical and have a diameter of 0.83 μm. When place in a 25.0°C 0.01 M NaCl aqueous solution the particles should have a mobility of 3.00×10^{-8} m^2/sec/volt. The average of 15 trial runs confirmed the IDC stated mobility of the standard particles to be 2.96×10^{-8} m^2/sec/volt with a standard deviation of 1.07×10^{-9} m^2/sec/volt resulting in an error of 1.31%. The results are shown in Table 3.1.

Table 3.1 IDC standard particle electrophoretic mobility measurements.

Trial	Voltage (volts)	Divisions Traveled	Distance (μm)	Time (sec)	Velocity (μm/s)	Field Strength (volts/m)	Mobility (m^2/volt sec)
1	60.1	8	248	10.27	24.1	847	2.85E-08
2	-60.2	8	248	10.34	24.0	-848	2.83E-08
3	60.1	8	248	9.76	25.4	847	3.00E-08
4	-60.2	8	248	9.48	26.2	-848	3.08E-08
5	60.1	8	248	9.40	26.4	847	3.12E-08
6	-60.2	8	248	9.89	25.1	-848	2.96E-08
7	60.1	8	248	10.23	24.2	847	2.86E-08
8	-60.2	8	248	10.36	23.9	-848	2.82E-08
9	60.1	8	248	9.94	24.9	847	2.95E-08
10	-60.2	8	248	9.98	24.8	-848	2.93E-08
11	60.1	8	248	9.49	26.1	847	3.09E-08
12	-60.2	9	279	10.75	26.0	-848	3.06E-08
13	60.1	8	248	9.57	25.9	847	3.06E-08
14	-60.2	9	279	10.99	25.4	-848	2.99E-08
15	60.1	7	217	9.12	23.8	847	2.81E-08

The study of concentrated or flocculated clay samples in the cylindrical electrophoretic sample cell is not recommended (Goodwin, 2001). Flocs may fall out of the field of view not allowing the operator to get an accurate measurement of distance travelled. Goodwin suggested a procedure to minimize flocculated structures in the sample. A sample was prepared and the flocculated structures where allowed to settle. Once settled, a sample was drawn from the interface of clear supernatant and settled solids. This procedure was adopted for the clay experimental test work.

3.4. Supernatant Chemical Analysis

After samples had been withdrawn from the pipeline loop and rheological characterization had been completed using Couette viscometry, the solid particles were allowed to settle in the sample container to provide a volume of clear

supernatant. If the samples contained dispersant tetrasodium pyrophosphate, the clay remained dispersed and the sample remained cloudy. These cloudy samples were centrifuged at 2000 rpm for 20 min to obtain a clear supernatant. Approximately 30 ml of clear supernatant was then decanted from samples and analysed for calcium ion content using a Perkin Elmer Atomic Absorption Spectrophotometer. The spectrophotometer, located in the environmental engineering labs at the University of Saskatchewan, was calibrated with calcium ion standards and operated by Mr. D. Fisher.

Phosphate groups are known to form non-volatile complexes with calcium in the flame of an atomic absorption spectrophotometer. It is therefore necessary to add an ion which will preferentially complex with any phosphate present. Lanthanum, which has a higher positive valence, is preferentially complexed with TSPP over the lower valence calcium ion. The supernatants decanted from clay slurry samples containing TSPP were treated with a 10% by volume Lanthanum nitrate solution. To verify that calcium ion concentration data obtained with the atomic absorption spectrophotometer were not altered by phosphate interference, selected samples were analysed with a mass spectrometer. The mass spectrometer technique provides an accurate measurement of ion concentration and is not subject to complexing interference.

3.5. Pipeline Loop Operation

A vertical pipeline loop (I.D. = 25.8 mm) was used to collect experimental data. The loop is illustrated in Figure 3.5. The loop, which has a volume of 11.95 litres, consists of two vertical pipeline test sections, a progressive cavity pump

controlled by a variable speed drive, and a stand tank for loading the experimental slurry. The loop operates as a closed system whereby the slurry delivered at the pump outlet is fed through the pipeline test sections returning to the inlet of the pump.

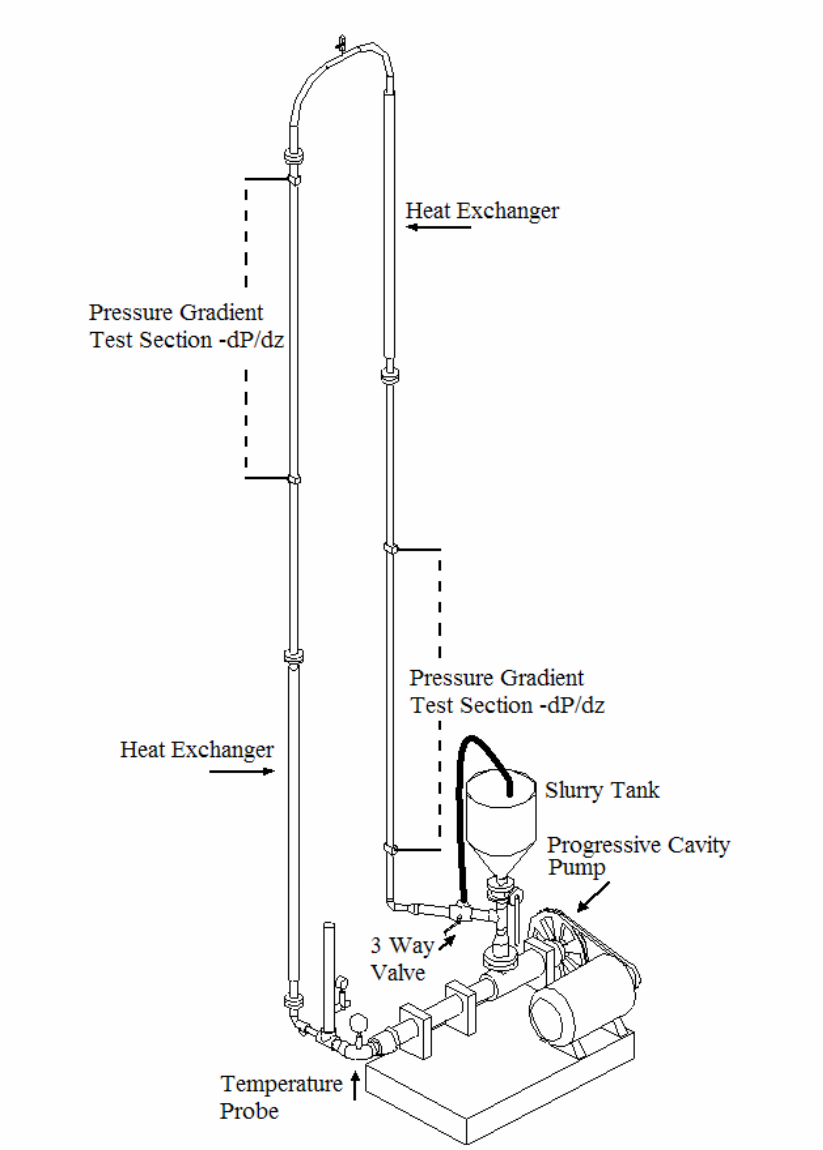

Figure 3.5: SRC's 25.8 mm vertical pipeline flow loop.

A progressive cavity pump (3 stage, L frame, Moyno, Inc.) was used to re-circulate slurry through the pipe loop. The stand tank and return line delivered slurry to a 75 mm suction port. The slurry was discharged through a 64 mm discharge port.

The pump shaft was coupled to a 1725 rpm 60 Hz Baldor 7.5 kW electric motor. The pulley ratio of the motor and pump shaft was set to achieve a maximum pump shaft rotational velocity of 550 rpm. The rotational velocity of the pump was varied using a Baldor variable frequency drive. A bucket and stopwatch water calibration was used to obtain the volumetric flow rate versus rotational velocity indicator voltage output relationship for the pump. Water was discharged into a bucket over a recorded time interval and its mass and temperature were recorded. The volumetric flow rate was then calculated. This calibration can be found in Appendix E.

The pressure gradient versus velocity data sets to characterize the fluids were recorded under isothermal operation of the pipe loop. The temperature was controlled to within ± 1°C of 20°C with the use of two double pipe heat exchangers. An ethylene glycol water mixture was recirculated counter currently through the heat exchangers to a refrigeration system which removed thermal energy created by pipeline friction energy losses.

Pressure gradient measurements were recorded with the use of Validyne Engineering variable reluctance differential pressure transducers which were calibrated against U-tube manometers. This calibration can be found in Appendix E. The pressure gradient is $(\Delta P) / L$ where the pressure difference between the pressure taps of a known length L (1.83m). Pressure gradients were recorded for both upstream and downstream vertical test sections. A 3.3 m (L/D = 127) approach of straight run pipeline, free of disturbances, was used upstream of the pressure gradient test sections to ensure fully developed flow. The test section diameters were determined to be 0.0258m by filling the section lengths with a known volume of

deaerated water. Stainless steel polished tubing was used for the test sections. A water run was completed prior to experimental slurry data collection to verify equipment calibration and to determine the pipe wall roughness. A physically reasonable wall roughness value of 2.5 μm was obtained.

Measurement outputs of rotational velocity, pressure, and temperature were electronically stored using a computerized data acquisition system which consisted of a Keithley Metrabyte Das-20 (Keithley Instruments, Inc.) analogue to digital converter installed in a Dell computer. Acquisition code for this system was developed by Dr. Randall Gillies of the Saskatchewan Research Council's Pipe Flow Technology Centre.

Each test consisted of the following steps:

1. 30 Litres of clay slurry, which represented approximately 3 pipe loop volumes, were prepared in a separate mixing vessel. The mixing vessel was placed on a Toledo scale, tarred, and appropriate amounts of dry clay were added. The required amount of reverse osmosis (R/O) water to achieve the experimental concentration of interest was then added to the dry clay, and the weight recorded. A pre-determined amount of calcium chloride $CaCl_2 \bullet 2H_2O$ crystalline powder was added to the unmixed slurry. The slurry was then blended with a Lightnin™ ¼ HP mixer with a maximum rated RPM of 1800. The mixing speed was increased to a maximum provided that air entrainment did not occur. If the experimental plan required, tetrasodium pyrophosphate

$Na_4P_2O_7$ was added during the first few minutes of mixing. Mixing continued for approximately 60 minutes to ensure that all of the clay had been homogeneously dispersed and ionic equilibrium had been developed.

2. The vertical pipe loop was filled with water and purged of all air. The water level in the stand tank was lowered to the valve at the base of the tank and the pipe loop recirculation was stopped. Pressure transducer lines were purged of air, isolated from the pipe loop, and zeroed. The valve was closed to avoid mixing prepared clay slurry with water in the line.
3. The slurry was loaded to the stand tank. The pump was started and valves were manipulated so that the contents of the stand tank were injected into the pipe loop. Water and some slurry were discharged during the recirculation to drain.
4. Recirculation was maintained at 1.0 m/s until a temperature of 20°C had been achieved. Steady state pressure gradient versus bulk velocity data were then collected. After the pump rotational speed had been manipulated to achieve a pre-determined low initial bulk velocity, one minute time-averaged measurements of pressure gradient were recorded. The velocity was then increased stepwise to the maximum pump speed and then decreased to the initial velocity.
5. 1.0 litre samples were collected prior to loading and after pipeline discharge to analyze density, supernatant water chemical properties, particle size distribution, electrophoretic mobility, and rheological viscometric properties.

These procedures can be assumed to apply to the results reported herein unless otherwise indicated.

3.6. Couette Viscometer Operation

A Haake Rotovisco 3 Concentric Cylinder Viscometer was used to determine the torque versus angular velocity relationship of each sample withdrawn during pipe loop operation. The complete viscometer system consisted of a drive, measuring head, sensor system, control console and a strip chart recorder. A cup of radius 21.00 mm and a spindle of radius 20.04 mm were attached to an interchangeable measuring head sensor system as shown in Figure 3.6.

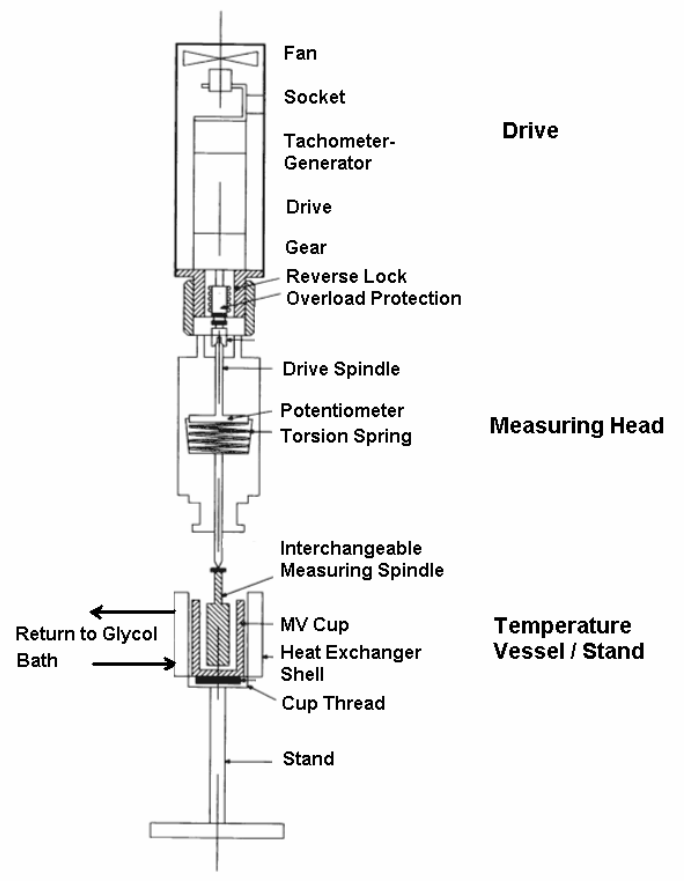

Figure 3.6: Haake Rotovisco 3 viscometer with interchangeable measuring head sensor system (adapted from Haake operating instructions).

A viscosity standard fluid, Cannon S200, was used to verify the MK50 and MK500 viscometer measuring heads operation. The data can be found in Appendix E. The viscosities obtained from the torque / length versus angular velocity data for both measuring heads were within one percent of the Cannon certified standard fluid.

Immediately after samples had been withdrawn from the pipe loop they were tested with viscometer using the appropriate measuring head. Rheological properties for the fluid were assessed by analysing the torque required to rotate the inner cylinder for a range of rotational speeds. For fluids displaying a yield stress it is possible that shear between the cup and spindle may fall below this yield stress, leaving a region of unsheared fluid. Data points were rejected if a measured torque value fell below the minimum torque as calculated with Equation 2.23 with $\tau_{r\theta}$ replaced by the model τ_y. Iteration was used since the yield stress is obtained implicitly within the calculation. Data points were also rejected if the flow was affected by the presence of Taylor vortices.

4. RESULTS AND DISCUSSION

4.1. Introduction

Satisfactory fine particle slurry pipeline design and operation requires a thorough understanding of the rheological nature of the slurry being transported. For these flows, experimental testing is necessary because of an incomplete understanding of some aspects governing the flow characteristics of these systems. Rheological characterization can be accomplished with a viscometer or pipeline loop to model the flow behaviour. The Bingham and Casson rheological models have been used in this research program to describe the behaviour of the slurries tested. Both models use two parameters, a yield term and a viscosity term, to characterize the non-Newtonian behaviour.

An experimental research program was conducted at the Saskatchewan Research Council Pipe Flow Technology Centre to determine the nature of the effects of solids concentration and chemical species on the rheology of kaolin clay slurries. Kaolin clay slurries were prepared in varying volumetric concentrations with reverse osmosis water and a constant mass ratio of calcium chloride dihydrate ($CaCl_2 \bullet 2H_2O$) to mass clay. The mass ratio of calcium chloride dihydrate was chosen to represent a typical industrial hard water source. Varying mass ratios of tetrasodium pyrophosphate ($Na_4P_2O_7$), a particle dispersant, to clay mass were added to selected slurries. A 25.8 mm vertical pipeline flow loop and a Haake Couette viscometer were used to determine the rheological characteristics of these slurries.

A summary of the operating conditions for each test can be found in Tables 4.1, 4.2, and 4.3. Tests were also conducted with the department of environmental engineering's atomic absorption spectrophotometer to determine the ionic concentration of calcium in the clay suspending medium of water. This analysis was performed to aid in the understanding of the nature of the kaolin clay particle-particle interactions and their effect on the slurries rheology.

The experimental frictional head loss data and associated Couette viscometer frictional resistance data can be found in tabular form in Appendix A. The calcium ion analysis performed on the slurry supernatant for each operating condition can be found in Appendix B. Appendix C presents the data obtained with pipe flow in graphical form. Curves representing the best fit Buckingham equation (laminar flow) and Wilson & Thomas equation (turbulent flow) have been included in these figures.

Table 4.1: Summary of slurry flow tests and inferred rheological parameters.

Run #	Cv	Mass Ratios		Pipe Line Loop Inferred Parameters				Couette Viscometry Inferred			
		$\frac{CaCl_2 \cdot 2H_2O}{Clay}$	$\frac{Na_4P_2O_7}{Clay}$	Bingham		Casson		Bingham		Casson	
				τ_y (Pa)	μ_p (Pa.s)	τ_c (Pa)	μ_∞ (Pa.s)	τ_y (Pa)	μ_p (Pa.s)	τ_c (Pa)	μ_∞ (Pa.s)
G2000106	0.10	0.10	--	2.6	0.0051	1.9	0.0016	3.3	0.0052	2.3	0.0018
G2000208	0.10	0.10	--	2.6	0.0055	1.9	0.0015	3.2	0.0048	2.3	0.0016
G2000212	0.10	0.10	0.27	--	0.0022*	--	0.0022*	--	0.0033*	--	0.0033*
G2000205	0.14	0.10	--	14.3	0.0057	12.0	0.0010	11.3	0.0094	9.2	0.0022
G2000105	0.14	0.10	0.10	5.9	0.0078	4.4	0.0021	7.1	0.0084	5.2	0.0025
G2000214	0.14	0.10	0.13	6.7	0.0072	5.2	0.0018	6.2	0.0077	4.5	0.0023
G2000215	0.14	0.10	0.27	--	0.0035*	--	0.0035*	--	0.0040	--	0.0040
G2000217	0.14	0.10	0.27	--	0.0032*	--	0.0032*	--	0.0043*	--	0.0043*
G2000217	0.14	0.10 + 5grams	0.27	--	0.0034*	--	0.0034*	--	0.0049*	--	0.0049*
G2000217c	0.14	0.10 +10grams	0.27	7.9	0.0092	6.1	0.0023	8.2	0.0097	6.0	0.0028
G2000217	0.14	0.10 + 15grams	0.27	15.9	0.0096	12.9	0.0020	15.6	0.0119	12.5	0.0025

***Viscosity values presented in table did not exhibit a yield stress and were inferred with a Newtonian fluid model.**

Table 4.2: Summary of slurry flow tests and inferred rheological parameters.

Run #	Shear Duration (Hr:min)	Cv	Mass Ratios $\frac{CaCl_2 \cdot 2H_2O}{Clay}$	Mass Ratios $\frac{Na_4P_2O_7}{Clay}$	Pipe Line Loop Inferred Parameters Bingham τ_y (Pa)	Bingham μ_p (Pa.s)	Casson τ_c (Pa)	Casson μ_∞ (Pa.s)	Couette Viscometry Inferred Bingham τ_y (Pa)	Bingham μ_p (Pa.s)	Casson τ_c (Pa)	Casson μ_∞ (Pa.s)
SLURRY G2000206 EXHIBITED AN IRREVERSIBLE INCREASE IN APPARENT VISCOSITY WITH DURATION OF SHEAR.												
G2000206	Before	0.17	0.10	--	--	--	--	--	24.8	0.0139	20.6	0.0025
Day 1	2:20	0.17	0.10	--	57.2	0.0134	49.1	0.0021	--	--	--	--
Day 2	8:40	0.17	0.10	--	93.9	0.0210	80.5	0.0033	--	--	--	--
Day 3	9:00	0.17	0.10	--	100.0	0.0222	86.3	0.0034	--	--	--	--
	After	0.17	0.10	--	--	--	--	--	104.8	0.0335	93.3	0.0039
SLURRY G2000210 EXHIBITED AN IRREVERSIBLE INCREASE IN APPARENT VISCOSITY WITH DURATION OF SHEAR.												
G2000210	Before	0.17	0.10	0.07	--	--	--	--	19.4	0.0133	15.8	0.0027
Day 1	3:25	0.17	0.10	0.07	40.8	0.0149	33.8	0.0029	--	--	--	--
Day2	10:45	0.17	0.10	0.07	71.1	0.0192	60.2	0.0033	--	--	--	--
Day3	17:00	0.17	0.10	0.07	93.8	0.0243	80.1	0.0040	--	--	--	--
	After	0.17	0.10	0.07	--	--	--	--	98.1	0.0345	86.3	0.0044
G2000209	--	0.17	0.10	0.13	12.0	0.0090	9.6	0.0020	11.1	0.0117	8.3	0.0032
	--	0.17	0.10	0.27	--	0.0047*	--	0.0047*	--	0.0047	--	0.0047

***Viscosity values presented in table did not exhibit a yield stress and were inferred with a Newtonian fluid model.**

Table 4.3: Summary of slurry flow tests and inferred rheological parameters.

Run #	Shear Duration (Hr:min)	Cv	Mass Ratios $\frac{CaCl_2 \cdot 2H_2O}{Clay}$	Mass Ratios $\frac{Na_4P_2O_7}{Clay}$	Pipe Line Loop Inferred Parameters Bingham τ_y (Pa)	Bingham μ_p (Pa.s)	Casson τ_c (Pa)	Casson μ_∞ (Pa.s)	Couette Viscometry Inferred Bingham τ_y (Pa)	Bingham μ_p (Pa.s)	Casson τ_c (Pa)	Casson μ_∞ (Pa.s)
SLURRY G2000201/G2000202 EXHIBITED AN IRREVERSIBLE INCREASE IN APPARENT VISCOSITY WITH DURATION OF SHEAR.												
G2000201	Before	0.19	0.10	--	--	--	--	--	51.9	0.0255	44.0	0.0042
Day 1	0:10	0.19	0.10	--	51.7	0.0108	44.0	0.0018	--	--	--	--
--	1:30	0.19	0.10	--	86.7	0.0198	74.5	0.0031	--	--	--	--
Day 2	1:40	0.19	0.10	--	90.4	0.0215	77.8	0.0034	--	--	--	--
--	4:00	0.19	0.10	--	126.3	0.0268	108.3	0.0042	--	--	--	--
--	5:45	0.19	0.10	--	147.8	0.0321	128.0	0.0048	--	--	--	--
	After	0.19	0.10	--	--	--	--	--	158.4	0.0353	138.9	0.0046
SLURRY G2000204 EXHIBITED AN IRREVERSIBLE INCREASE IN APPARENT VISCOSITY WITH DURATION OF SHEAR.												
G2000204	Before	0.19	0.10	0.13	--	--	--	--	31.0	0.0207	25.2	0.0041
Day 1	3:00	0.19	0.10	0.13	40.9	0.0205	32.5	0.0047	--	--	--	--
Day2	3:30	0.19	0.10	0.13	46.8	0.0266	37.2	0.0062	--	--	--	--
	After	0.19	0.10	0.13	--	--	--	--	51.4	0.0355	41.5	0.0073
SLURRY G2000203 EXHIBITED AN IRREVERSIBLE INCREASE IN APPARENT VISCOSITY WITH DURATION OF SHEAR.												
G2000203	Before	0.19	0.10	0.27	--	--	--	--	0.56	0.0065	0.13	0.0052
Day 1	3:00	0.19	0.10	0.27	--	0.0058*	--	0.058*	--	--	--	--
Day2	3:30	0.19	0.10	0.27	0.52	0.0070	0.21	0.0042	--	--	--	--
	After	0.19	0.10	0.27	--	--	--	--	1.05	0.0087	0.3	0.0064

***Viscosity values presented in table did not exhibit a yield stress and were inferred with a Newtonian fluid model.**

4.2. Particle Characterization

The Dry Branch Pioneer kaolin clay used in this experimental program is fine grained and therefore the particle size determination required the use of methods other than mechanical sieving. The particle size distribution of the fine clay particles was determined using sedimentation analysis. Gravity sedimentation with an Andreasen pipette was used for particles in the sub-sieve size range larger than 0.6 μm. Below 0.6 μm gravitational techniques are inappropriate due to Brownian motion. In this investigation the particle size distribution for particles below 0.6 μm was obtained using centrifugal sedimentation. The centrifuge accelerates the sedimentation rates and allows the determination of the finer particle sizes.

Figure 4.1 shows the particle size distribution for the kaolin clay as determined by gravitational and centrifugal Andreasen pipette sedimentation. This figure indicates that approximately 50% of the particles have an equivalent spherical diameter of less than 0.6 μm. The two gravity sedimentation trials show good agreement. The mass of the particles obtained at the lower end of the accepted particle size range for this method deviates from those obtained for the top of the centrifugal sedimentation curve. This may indicate that particles having a diameter of 0.6 microns were influenced by Brownian motion in gravity sedimentation. This discontinuity in the particle size distribution was not expected and thought to be a result of experimental error.

The density of the Dry Branch Pioneer kaolin clay was determined to be 2693 kg/m^3. The methods used to determine the density can be found in section 3.2.2. The experimental data can be found in Table 4.7. Electrophoretic mobility, supernatant

ionic composition, and pH analysis were completed for selected slurry samples and will be discussed in later sections.

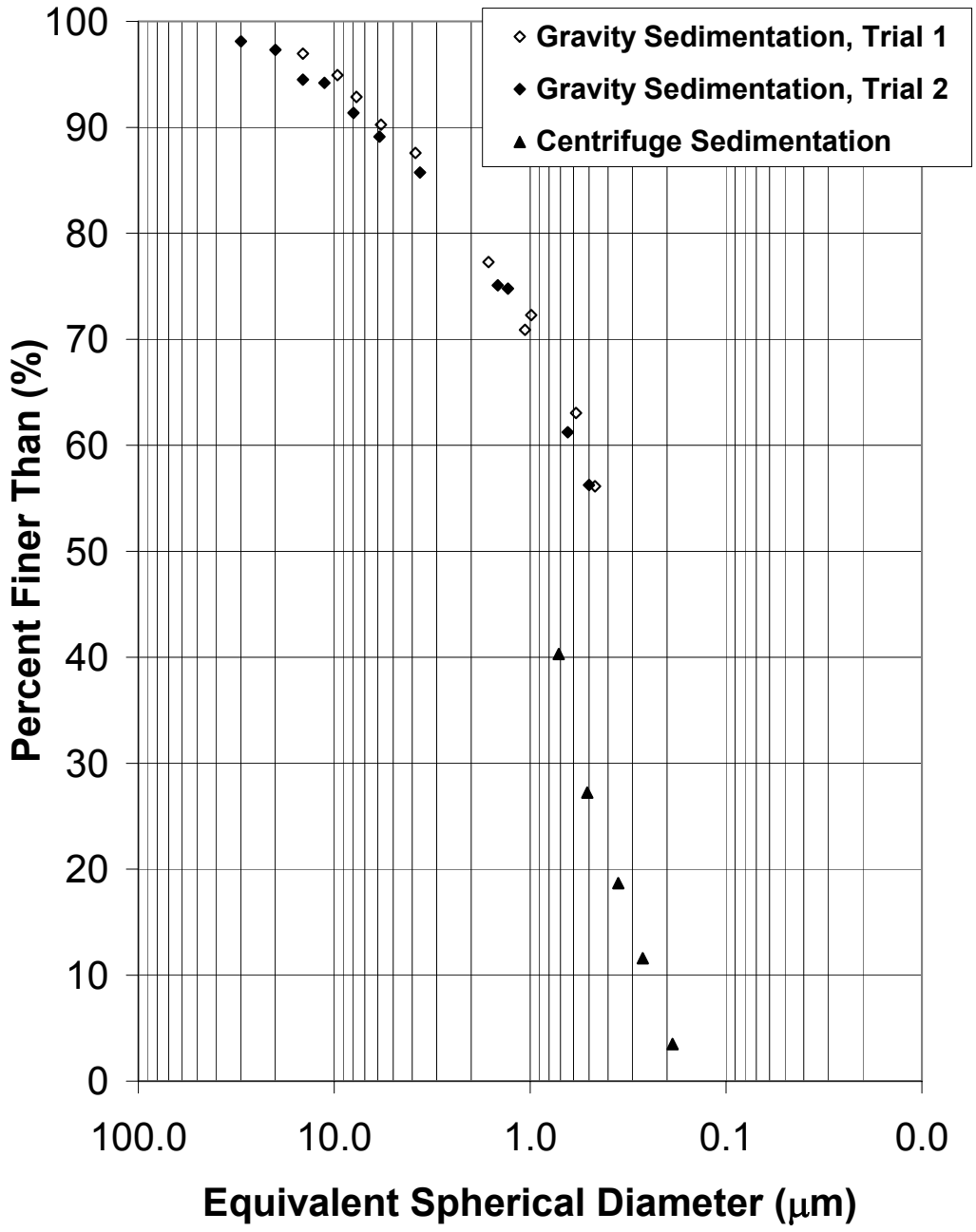

Figure 4.1: Dry Branch Pioneer kaolin clay particle size distribution as determined by Andreasen pipette experimental procedures.

Table 4.4: Particle Size Distribution Dry Branch Kaolin Clay Andreasen Pipette Gravity Sedimentation Trial 1

Sample	Total Time (s)	Target Particle Size (μm)	Wt% Kaolin Clay Sampled	Percent Finer Than
Initial	0	--	2.41	100.00
1	953	14.4	2.34	96.96
2	2104	9.6	2.29	94.91
3	3226	7.7	2.24	92.88
4	5625	5.8	2.18	90.24
5	12408	3.8	2.11	87.58
6	67808	1.6	1.86	77.29
7	156330	1.1	1.71	70.89
8	177795	1.0	1.74	72.29
9	498730	0.58	1.52	63.04
10	760800	0.47	1.35	56.13

Table 4.5: Particle Size Distribution Dry Branch Kaolin Clay Andreasen Pipette Gravity Sedimentation Trial 2

Sample	Total Time (s)	Target Particle Size (μm)	Wt% Kaolin Clay Sampled	Percent Finer Than
Initial	--	--	2.46	100.00
1	236	30.0	2.41	98.10
2	521	20.0	2.39	97.31
3	980	14.4	2.33	94.50
4	1590	11.2	2.32	94.19
5	3075	8.0	2.25	91.36
6	5575	5.9	2.19	89.12
7	14101	3.7	2.11	85.73
8	86130	1.5	1.85	75.10
9	107610	1.30	1.84	74.78
10	428600	0.64	1.51	61.22
11	690540	0.5	1.38	56.25

Table 4.6: Particle Size Distribution Dry Branch Kaolin Clay Andreasen Pipette Centrifugal Sedimentation

Sample	Total Time (s)	Centrifuge ω (RPM)	Target Particle Size (μm)	Wt% Kaolin Clay Initial	Wt% Kaolin Clay Sampled	Percent Finer Than
1	1659	872	0.51	0.0252	0.0069	27.23
2	1528	652	0.71	0.0250	0.0101	40.30
3	2476	988	0.35	0.0255	0.0048	18.67
4	2810	1231	0.27	0.0256	0.0030	11.60
5	3719	1475	0.19	0.0255	0.0009	3.50

Table 4.7: Experimental Particle Density Data. Dry Branch Kaolin Clay.

Trial	Clay Volume (ml)	Clay Mass (g)	Clay Density (Kg/m^3)
1	15.47	42.26	2731
2	18.43	49.39	2680
3	19.37	52.05	2687
4	20.65	54.84	2655
5	16.03	44.17	2755
6	16.60	44.54	2682
7	16.89	45.34	2684
8	17.17	45.78	2667
Average	--	--	**2693**

4.3. Rheological Characterization

Those kaolin clay slurries which exhibited a yield stress were fitted to either the non-Newtonian Bingham or Casson rheological models. Above the yield stress, the slurry will continually deform and behave as a fluid. Below the yield stress, particle-particle interactions are strong enough to provide a structure able to resist shear distortion and the slurry will behave as a solid.

With the addition of tetrasodium pyrophosphate it was possible to create kaolin clay slurries in which the particle-particle interactions were highly repulsive. The clay particles remained dispersed and the slurry could be characterized with the Newtonian fluid model.

Both a 25.8 mm vertical pipeline loop and a Haake Couette viscometer were used to characterize the clay slurries. Figures 4.2 and 4.3 show typical experimental data sets collected with the pipeline and viscometer and the associated agreement between the data and inferred Bingham and Casson rheological models. Figure 4.2 shows that for a given pipeline experimental set of pressure gradient and velocities, each model predicts a velocity for the experimental pressure gradient. As a measure of goodness of fit, the average percent difference between each experimental and predicted velocity data points have been calculated. The results are presented in Table 4.8. An example of this analysis, shown in Figure 4.2, indicates that for the experimental data of run G2000206 the Casson model analysis is marginally better than Bingham with an average percent difference between experimental and predicted velocities of 2.4% compared to 5%.

Figure 4.3 illustrates the corresponding analysis for data obtained with the viscometer by comparing experimental torque per length versus angular velocity data. The average percent difference between experimental and predicted angular velocities for the Casson and Bingham models was 5.0% and 9.3%. The Casson model's ability to predict the experimental time rate of shear strain was slightly better in almost all cases because of the model's non-linear relationship at low shear rates. However for practical purposes both models do a good job of predicting the laminar flow behaviour of kaolin clay slurries with yield stresses.

Table 4.8: Average difference between experimental and predicted data sets for each non-Newtonian slurry run.

Run #	Cv	Pipeline Data Analysis		Viscometer Data Analysis	
		Average velocity difference $(V_{fitted}-V_{exp})/ V_{fitted}$ x 100%		Average angular velocity difference $(\omega_{fitted}-\omega_{exp})/ \omega_{fitted}$ x 100%	
		Bingham	Casson	Bingham	Casson
G2000106	10%	3.6%	4.7%	15.3%	3.6%
G2000208	10%	1.5%	3.5%	11.1%	1.5%
G2000205	14%	4.1%	1.5%	13.2%	4.1%
G2000214	14%	4.3%	2.6%	12.2%	4.3%
G2000206	17%	5.0%	2.4%	9.3%	5.0%
G2000210	17%	5.1%	1.0%	17.1%	5.1%
G2000209	17%	2.8%	3.4%	10.3%	2.8%
G2000202	19%	5.6%	2.2%	6.2%	5.6%
G2000204	19%	9.4%	3.2%	11.8%	9.4%

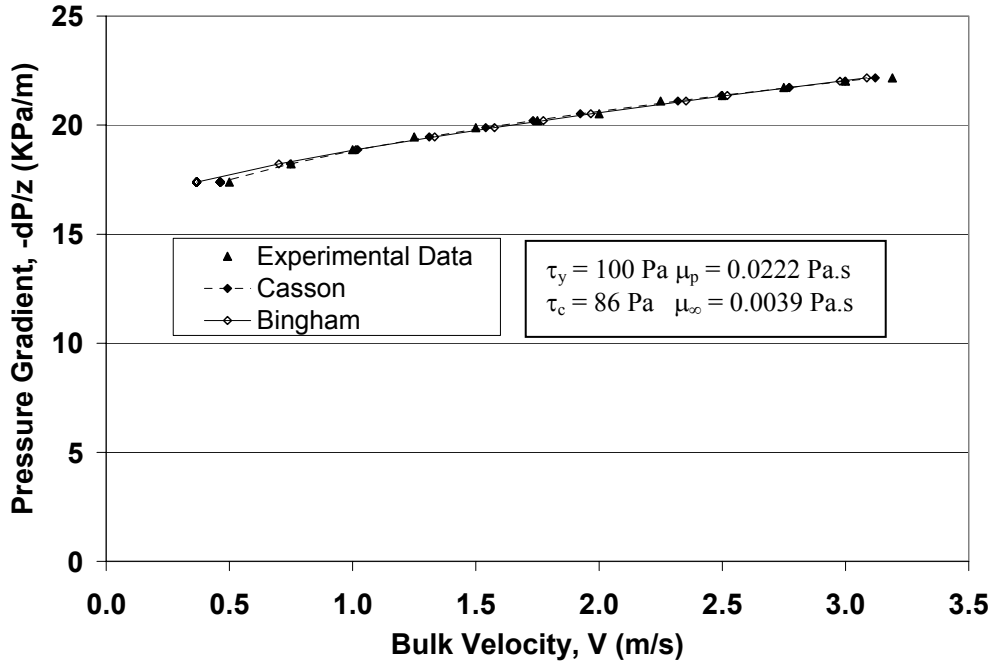

Figure 4.2: Predicted laminar flow pressure gradient using Bingham and Casson inferred model parameters for run G2000206, Cv = 0.17 Dry Branch kaolin clay slurry with no TSPP added.

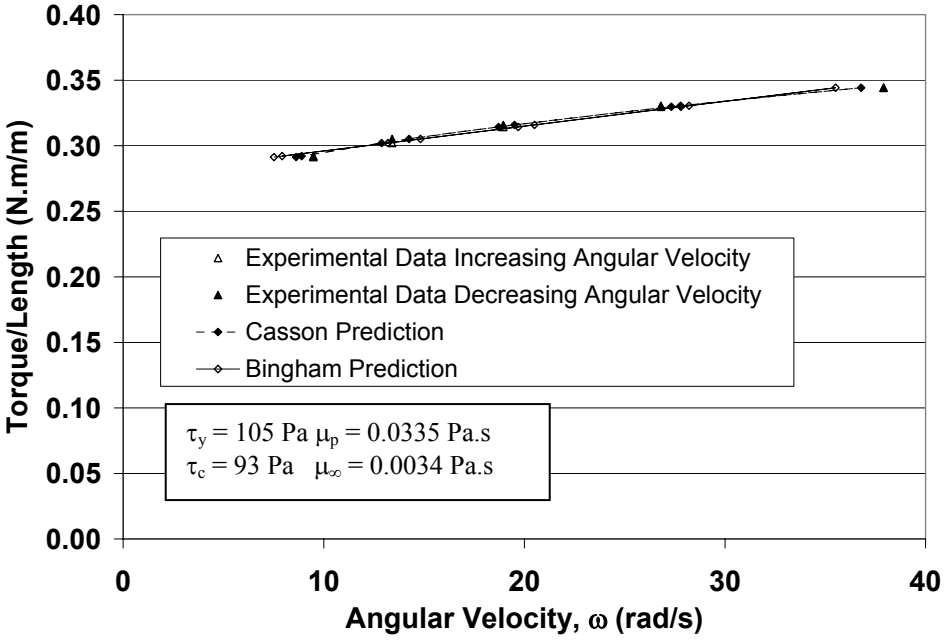

Figure 4.3: Predicted laminar flow viscometer torque per spindle length using Bingham and Casson inferred model parameters for run G2000206, Cv = 0.17 Dry Branch kaolin clay slurry with no TSPP added.

4.4. Pipeline and Viscometer Agreement

Pipeline loop and Couette viscometry testing has been used to describe the behaviour of kaolin clay slurries in this research program. It is advantageous to use a viscometer because of the relatively small sample needed to characterize the slurry behaviour and its simple flow geometry. However when using data inferred from Couette viscometry to design a pipeline it is important to ensure that the shear stresses in the viscometer are similar to those which will be encountered in the pipeline. In this research study both the Bingham and Casson model results obtained from pipeline flow and Couette viscometry experiments have been compared.

There are various methods of comparing different model parameters obtained from Couette and pipeline flow regimes. For a given model, one can compare the yield stress and viscosity parameters obtained from pipeline and Couette viscometer measurements. It is also possible to calculate an apparent viscosity term at a given shear rate using both parameters to aid in the comparison of pipeline tube and Couette viscometry data. Yet another method is to plot predicted pipeline pressure gradients with model parameters obtained from Couette viscometry and compare the predicted data set to the experimental pipeline pressure gradients. All of the above methods have been employed in the comparison of pipeline and Couette flow experimental data collected.

Figures 4.4 and 4.5 show the effects of clay concentration and TSPP on the Bingham and Casson model yield stresses that were inferred from pipeline and

viscometer methods. Figures 4.6 and 4.7 show the analogous plastic viscosity model parameters inferred for the same clay slurries.

It is apparent from these figures that there is good agreement between the yield stresses inferred from the vertical pipeline tube and concentric cylinder viscometer measurements. The Bingham yield parameters inferred from the pipeline and viscometer at the highest concentration, 19% solids by volume, with no TSPP added were 148 Pa and 158 Pa respectively. The viscometer results are 6% higher than that of the pipeline. The Casson yield parameters inferred for the same slurry were 128 Pa for the pipeline and 139 Pa for the Couette viscometer.

The Casson model yield stresses are consistently lower than those obtained with the Bingham model. The Casson model's non-linear function used to describe rheological behaviour of slurries may describe the true yield stress better. However pipeline designers are usually concerned with the prediction of wall shear stresses at velocities much greater than just above the true yield stress. At higher shear stresses, both the Bingham and Casson models provide satisfactory predictions as a function of bulk velocity.

Figures 4.4 to 4.7 also illustrate the dependence of yield stress on concentration and TSPP addition for both the pipeline and Couette viscometer data. As the concentration of clay was increased the yield stress also increased. Although the yield stress was observed to increase with increasing clay concentration, the yield stress did not vary with concentration to the third power as was predicted by Thomas (1963). However in this investigation it was found that there was a threshold concentration of approximately 14% above which the yield stress increased rapidly

because of an irreversible increase in apparent viscosity with elapsed time of shear. The nature of these behaviours will be discussed in detail in Section 4.7. It is also possible to reduce or eliminate the yield stress with the addition of TSPP. As the concentration of TSPP was increased the yield stress decreased and in all slurry concentration prepared it was possible to eliminate the yield stress.

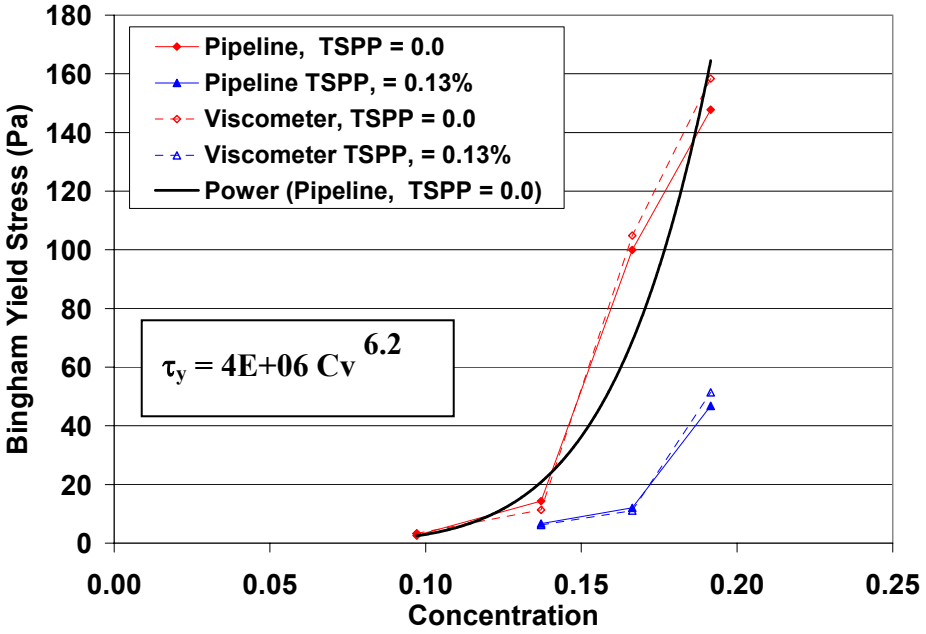

Figure 4.4: Effect of clay concentration and tetrasodium pyrophosphate addition on Bingham model inferred yield stress for Dry Branch kaolin clay slurries.

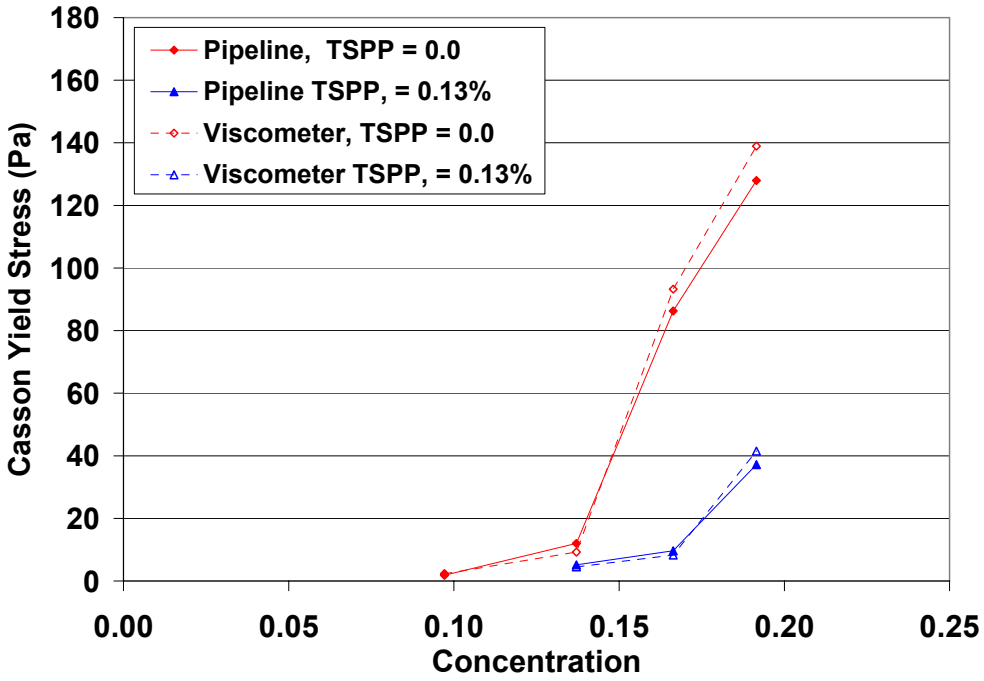

Figure 4.5: Effect of clay concentration and tetrasodium pyrophosphate addition on Casson model inferred yield stress for Dry Branch kaolin clay slurries.

The agreement between plastic viscosities inferred from pipeline and viscometer data is not as good as the agreement observed for yield stress values. Figures 4.6 and 4.7 illustrate the Bingham and Casson plastic viscosities inferred from the pipeline loop and the Couette viscometer. In some instances, there is good agreement; in others, there is a wide discrepancy between the results obtained using the two methods.

The deviation between plastic viscosity parameters inferred by the pipeline and those obtained from concentric cylinder viscometer tests could be caused by a number of factors. The sample withdrawn from the pipeline to be characterized in the viscometer represents only a small portion of the total pipeline volume and may not have been representative. The different geometries between pipeline tube and

Couette viscometer flow also contribute to different shear conditions. Also, the range of shear stresses that the viscometer can impose on the slurry sample is relatively narrow when compared to those associated with pipeline tests.

Figures 4.6 and 4.7 also illustrate the dependence of plastic viscosity on concentration and TSPP addition. Although Figure 4.6 indicates that the Bingham plastic viscosity increases with increasing clay concentration and decreasing addition of TSPP, the plastic viscosity did not vary with concentration as predicted by Thomas (1963). Thomas' suggestion that plastic viscosity increases exponentially with increasing volumetric concentration did not hold true in this experimental research program. Some of this was due to the irreversible increase in apparent viscosity with elapsed time of shear.

Figure 4.7 shows the Casson plastic viscosity dependence on concentration of solids and TSPP addition. The same trend is observed with increasing concentration but not with increasing TSPP addition. As the concentration of TSPP is increased the electrostatic repulsive forces between particles is also increased. This results in a decrease in apparent viscosity. One would think that this should also result in a decrease in the Bingham or Casson viscosity. The Bingham model's ability to describe the systematic relationship between increasing dispersant concentration and the resulting viscosity parameter gives it an advantage over the Casson model.

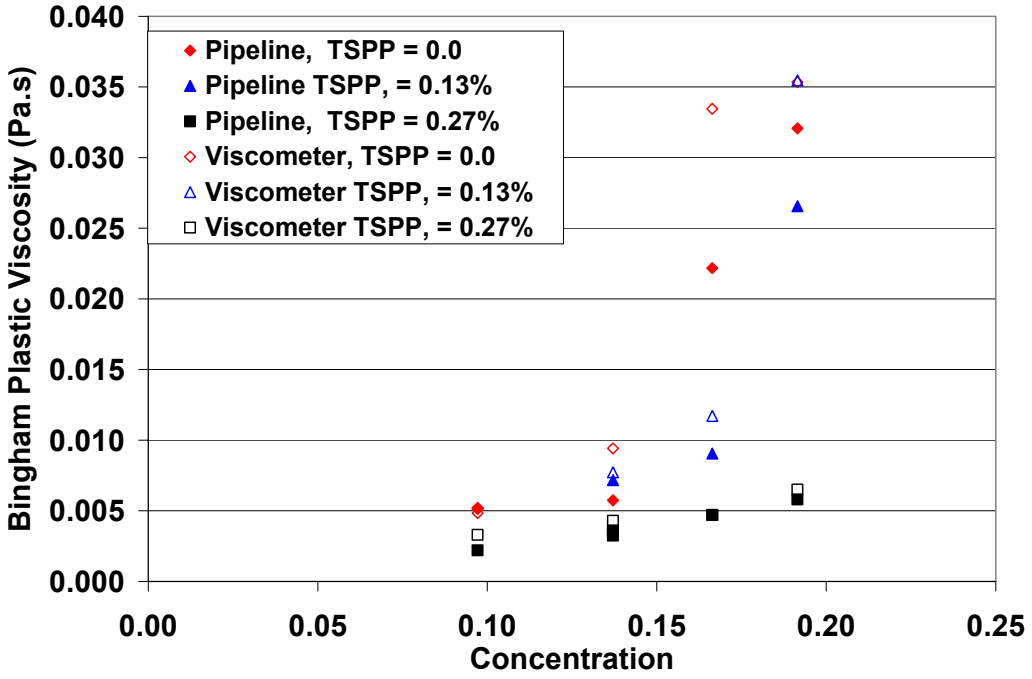

Figure 4.6: Effect of clay concentration and tetrasodium pyrophosphate addition on Bingham model inferred plastic viscosities for Dry Branch kaolin clay slurries.

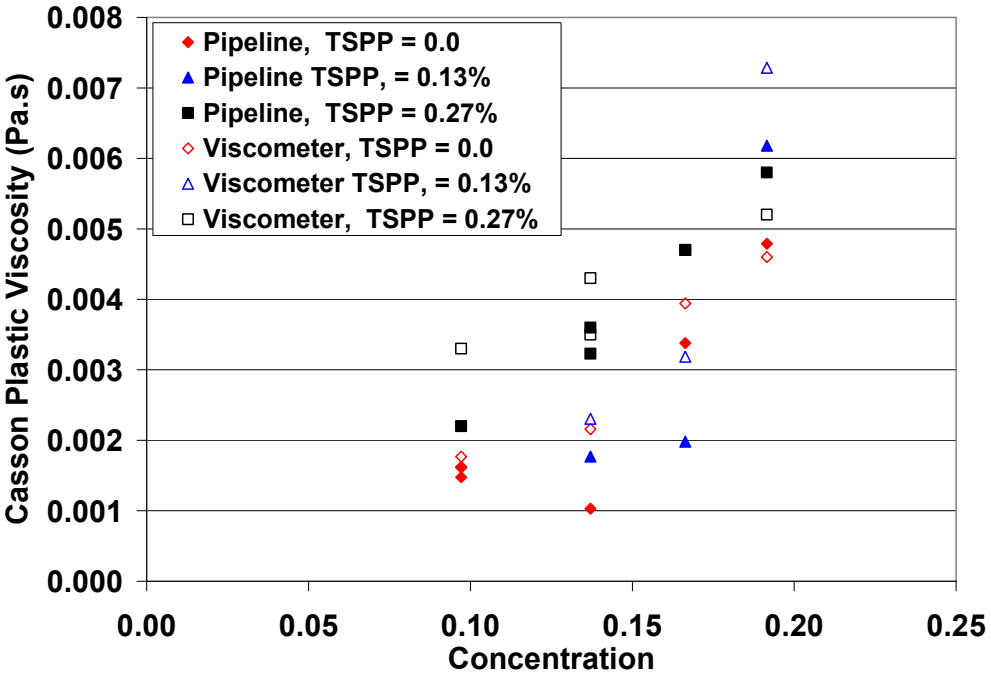

Figure 4.7: Effect of clay concentration and tetrasodium pyrophosphate addition on Casson model inferred plastic viscosities for Dry Branch kaolin clay slurries.

Hill (1996) showed that if concentric cylinder viscometer data are to be used to predict pipeline wall shear stresses the shear stresses in the viscometer must be similar to those that will be encountered in the pipeline. The same type of analysis has been used in Figures 4.8 and 4.9. The model parameters obtained with Couette viscometer data have been used to predict the laminar regime wall shear stresses observed in the 25.8 mm pipeline.

Figures 4.8, 4.9, and 4.10 show the experimental and viscometer predicted wall shear stresses for the kaolin clay slurries containing 17% by volume solids. Figure 4.8 shows that for both the Bingham and Casson models, the parameters obtained with Couette viscometer over predict the wall shear stresses by approximately 10% throughout the velocity test range although the inferred plastic viscosities from the pipeline and viscometer differ by more than 30%. It is interesting to note that the shear stress range that was used to obtain model parameters with the viscometer (105 Pa - 124 Pa) only covered the lower end of the range encountered in the pipeline loop (112 Pa – 143 Pa).

Figure 4.9 shows that, although the plastic viscosities obtained with the pipeline and viscometer differ by more than 20%, the model parameters obtained with the viscometer predicts the wall shear stresses more accurately. The shear stress range that was used in the Couette viscometer were 11 Pa -19 Pa which more accurately covers the wall shear stress encountered in the pipeline loop of 14 Pa – 21 Pa. This analysis shows the importance of using the appropriate shear environment when obtaining model parameters. These figures also show that the wall shear stress

predictions may be more sensitive to the yield stress parameter and less sensitive to the viscosity parameter obtained by the viscometer.

For the specific case where the yield stress has been eliminated using TSPP, Figure 4.10 shows that the Newtonian viscosity predicted by the viscometer was identical to that found in the pipeline loop. This analysis shows the importance of using both parameters to ascertain whether the agreement between pipeline and viscometer data is acceptable.

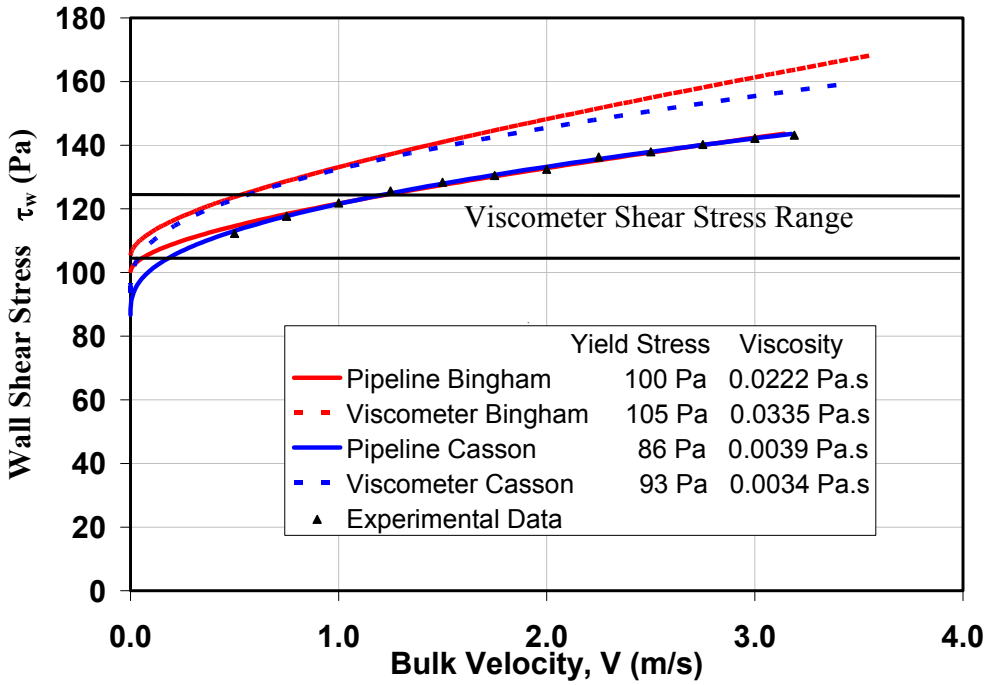

Figure 4.8: Predicted laminar flow wall shear stresses using pipeline and viscometer inferred model parameters for run G2000206, Cv = 0.17 Dry Branch kaolin clay slurry with no TSPP added.

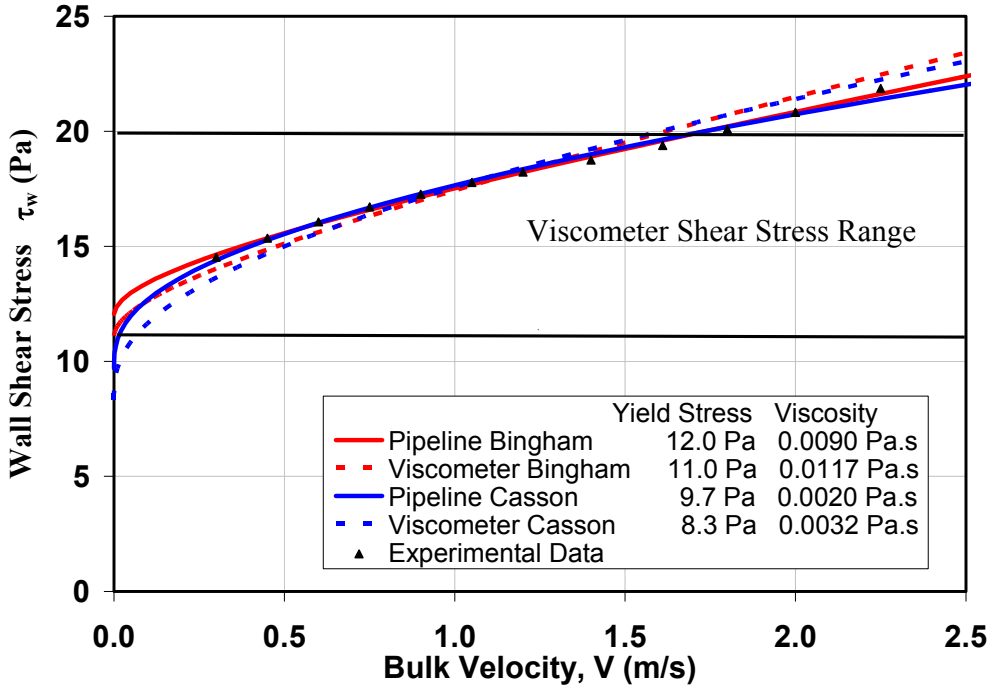

Figure 4.9: Predicted laminar flow wall shear stresses using pipeline and viscometer inferred model parameters for run G2000209 Cv = 17% Dry Branch kaolin clay slurry with 0.13% mass TSPP per mass clay added.

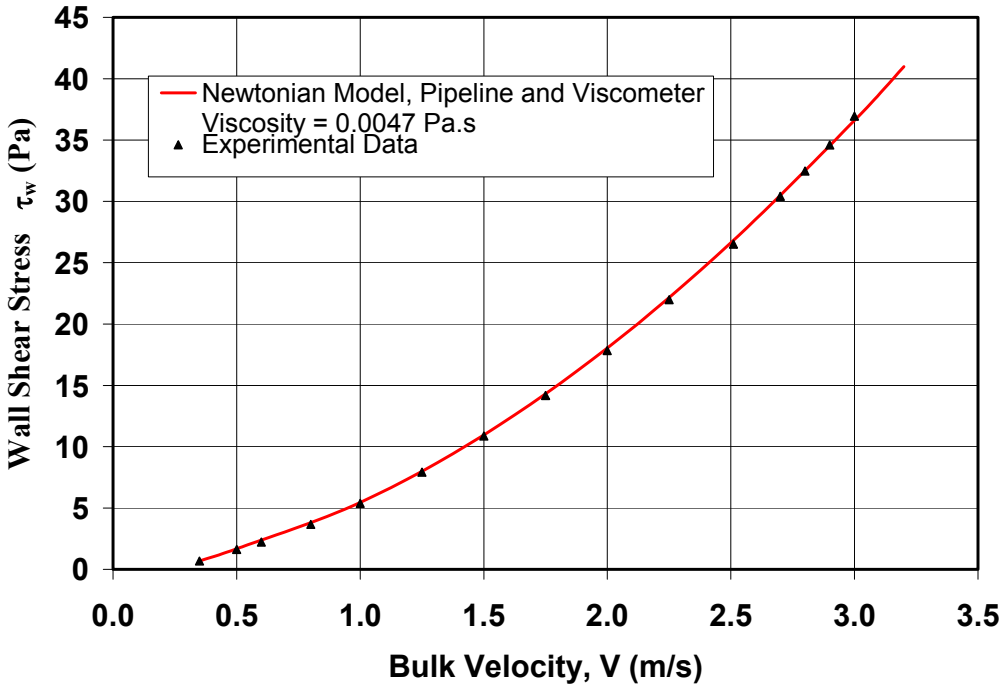

Figure 4.10: Predicted pressure gradient using pipeline and viscometer inferred model parameters for Cv = 17% Dry Branch kaolin clay slurry with 0.27% mass TSPP per mass clay added.

An alternative method used to study this agreement is to compare the apparent viscosity each model predicts at a given shear rate of interest. By using an apparent viscosity both the yield stress and viscosity parameters describe the relationship between shear stress and shear rate. This analysis shows the weight of importance that each model parameter has when comparing pipeline and Couette viscometry results. Recall that the apparent viscosity equation for the Bingham and Casson models are given by Equations 2.3 and 2.4, respectively.

Figure 4.11 shows the agreement between Bingham model apparent viscosities calculated at a shear rate of 300 s^{-1}. The shear rate value of 300 s^{-1} was chosen for analysis because it corresponds to a shear rate at the pipe wall for a Newtonian fluid at a bulk velocity of 1.0 m/s. The quantity 8V/D for Newtonian flow is called the shear rate at the pipe wall. One can see why when comparing Equations 2.11 to 2.16. The analysis was conducted for a bulk velocity of 1.0 m/s because all slurries which exhibited a yield stress would be in laminar flow condition at this velocity.

Figure 4.11 shows clearly the ability of the viscometer to describe the flow behaviour of these kaolin clay slurries accurately. The trend of these results is similar to those observed in Figures 4.4 and 4.5. This shows the importance that the yield stress value has in modelling flow behaviour of these kaolin clay slurries. The Casson models results are similar.

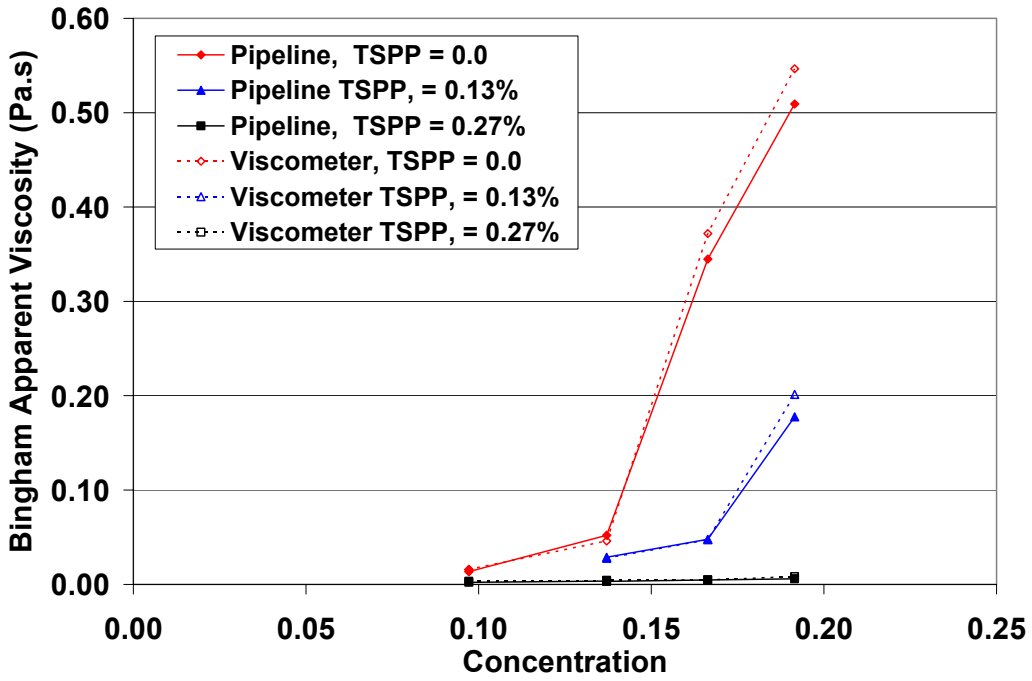

Figure 4.11: Effect of concentration and tetrasodium pyrophosphate addition on Bingham model inferred apparent viscosities for Dry Branch kaolin clay slurries.

4.5. Pipeline Turbulent Flow Predictions

The Wilson & Thomas model (1985, 1987) was used to predict turbulent flow pressure gradients for slurry runs in which a laminar to turbulent flow transition was observed. The model, described in Section 2.4, uses the yield stress and viscosity parameters inferred from the laminar flow data to predict turbulent flow pressure gradients. The transition from laminar to turbulent flow is given by the intersection between the laminar flow model prediction and the Wilson-Thomas turbulent flow prediction.

In this research program it was not possible to achieve turbulent flow for all slurries because of velocity limitations. The maximum flow rate the progressive

cavity pump delivered was 1.7 L/s. At the highest velocity attained in the pipeline loop, the transition from laminar to turbulent flow occurred only when the yield stress of the slurry was below approximately 20 Pa. Figures 4.12 and 4.13 show that it was possible to predict turbulent flow pressure gradients using both the Bingham and Casson models. The Wilson & Thomas turbulent flow pressure gradient prediction using Bingham model parameters is consistently higher than those predicted with Casson model parameters.

The author could not find a systematic reason, with the limited amount of data produced, why each model was successful in modelling some flow behaviour and provided poor predictions in others. However, in all turbulent flow situations both models were satisfactory at predicting the transition between laminar and turbulent flow regimes as shown in appendix C.

Further work could be undertaken to test the Bingham and Casson fluid turbulent flow predictions by investigating turbulent flow pressure gradients of slurries possessing higher yield stresses.

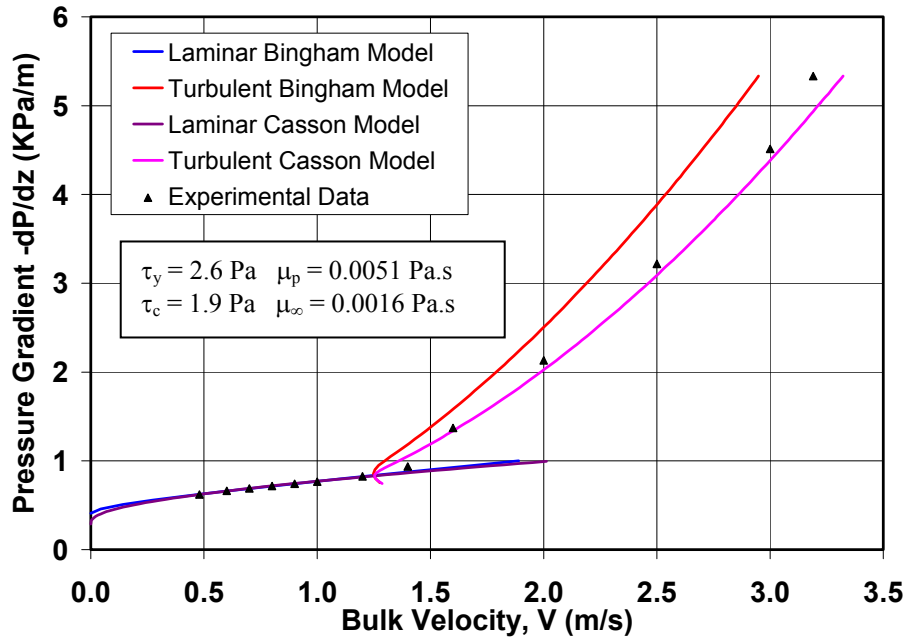

Figure 4.12: Bingham and Casson turbulent flow model comparison for run G2000106 Cv=10% kaolin with no TSPP added.

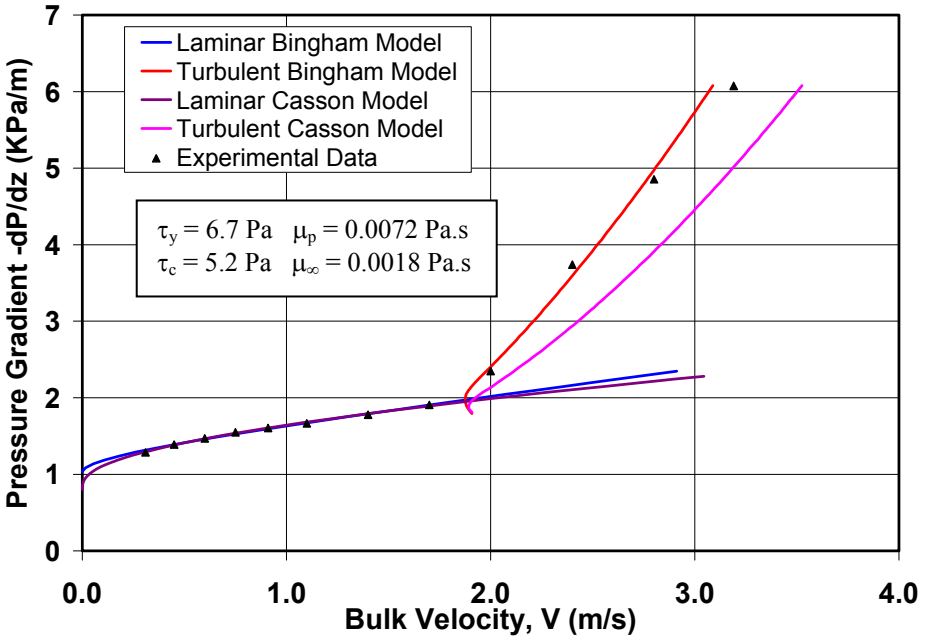

Figure 4.13: Bingham and Casson turbulent flow model comparison for run G2000214 Cv=14% Kaolin with mass ratio of TSPP/Clay = 0.13% added.

4.6. Effects of Dispersant Addition

All slurries were prepared initially with RO water and a constant mass ratio of dihydrated calcium chloride to mass of kaolin clay of 0.10% to model an industrial hard water. As discussed previously, positive ions such as calcium balance the negative charge of the particle and reduce the electric double layer thickness in an aqueous solution. The net interaction energy between particles falls into a region where particle association is dominated by van der Waals attraction and flocculation occurs. The structure created by flocculation of particles may cause the fluid to exhibit non-Newtonian yield stress characteristics. The concentration of ions at which this net particle attraction occurs is known as the flocculation value of the slurry.

TSPP, a known particle dispersant, can alter particle interactions either by chemisorption on the edge surfaces of a clay particle, producing a negative surface, or by sequestering calcium ions in solution. As a result, electrostatic repulsive forces between clay particles dominate and edge to edge and edge to face associations are weakened or eliminated. The flocculated structure in the slurry is weakened and the water originally bound in the flocculated structure is freed. The rheology of the clay slurry will thus undergo a reduction in apparent viscosity. Higher concentrations of positive ions will now be required to permit van der Waals forces to produce an increase in apparent viscosity.

In this experimental program it was possible, with the addition of small amounts of TSPP, to manipulate interactions between clay particles to target a particular slurry yield stress as shown in Figures 4.4 and 4.5. It was also possible to

eliminate non-Newtonian behaviour totally at all concentrations as illustrated in Figure 4.14. This figure also shows the increased energy losses with increasing solids concentration for the dispersed slurries.

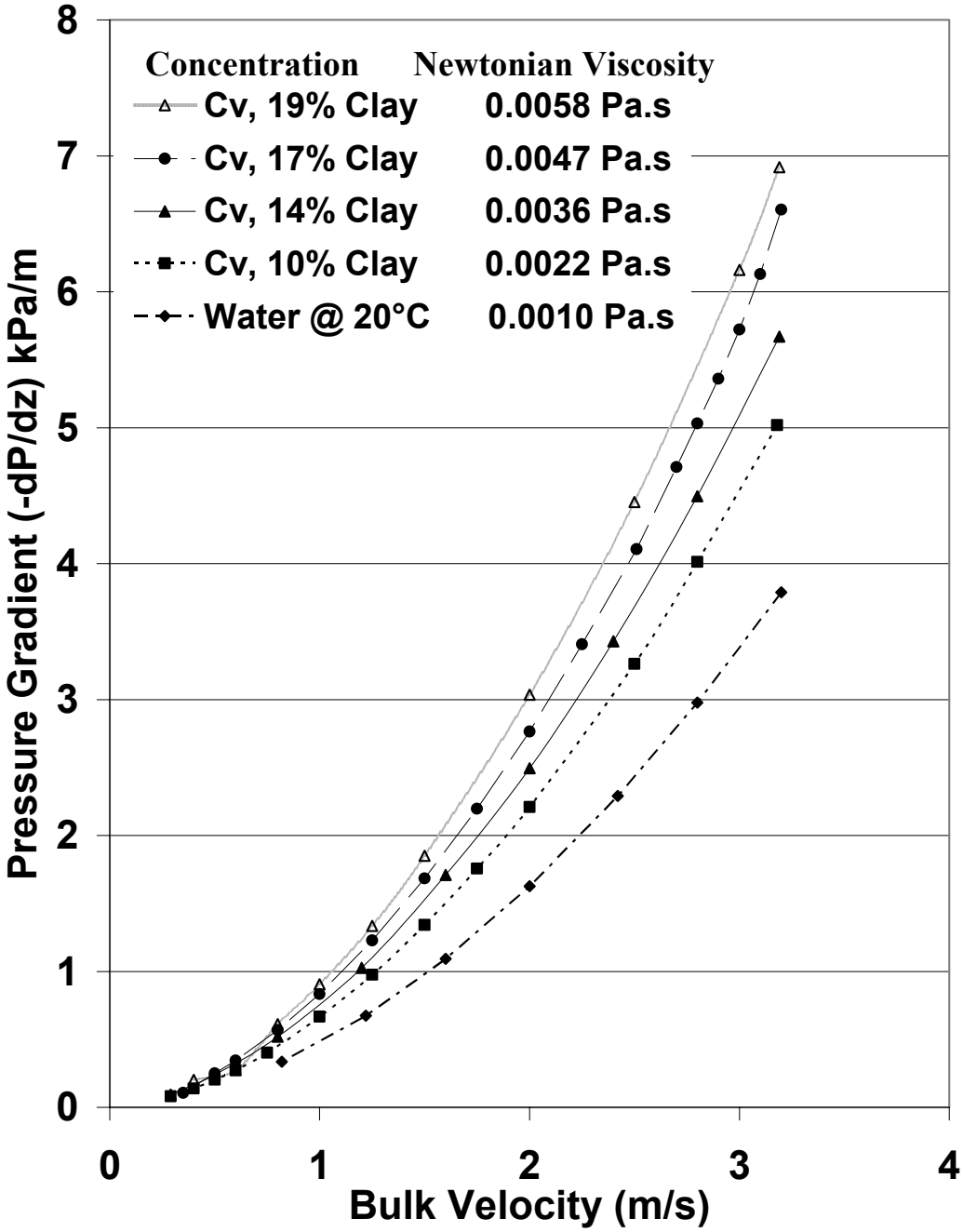

Figure 4.14: Comparison of experimental pressure gradients for all slurries having a TSPP to clay mass ratio of 0.27% to Newtonian pipe flow model.

The first photograph shown in Figure 4.15 depicts a 19% by volume solids slurry prepared with reverse osmosis water and mass ratio of dihydrated calcium chloride to clay of 0.10%. The Bingham yield stress of this slurry was measured to be 128 Pa. The second photo shows that it is possible to eliminate this yield stress by increasing the dispersant concentration of TSPP to a mass ratio of 0.27%. This caused this slurry to flow and take on the shape of its container.

Figure 4.15: Effect of adding TSPP to Dry Branch Pioneer kaolin clay slurry 19% by volume with a measured Bingham yield stress of 128 Pa.

4.7. Calcium Ion Supernatant Analysis

In an attempt to understand the nature of the effects of TSPP on the rheology of clay slurries, supernatants from samples withdrawn from the pipeline loop were tested for calcium ion concentration using an atomic absorption spectrophotometer. These results can be found in Appendix B Tables B.1 to B.4. To verify that calcium ion concentration data obtained with the atomic absorption spectrophotometer was

not altered by phosphate interference, selected samples were analysed with a mass spectrometer. These results can be found in Appendix B in Table B.5.

For samples that contained a sufficient concentration of TSPP to eliminate non-Newtonian behaviour, the calcium ion concentration was always less than 25 parts per million (ppm). Examples of the relationship between calcium ion concentration in the slurry supernatant and yield stress are shown in Figures 4.16 and 4.17. Figure 4.16 illustrates the effect of calcium concentration on yield stress for a slurry containing 14% by volume clay. Figure 4.17 shows a similar relationship for a solids concentration of 17% by volume. In all cases the yield stress increases with increasing calcium ion concentration.

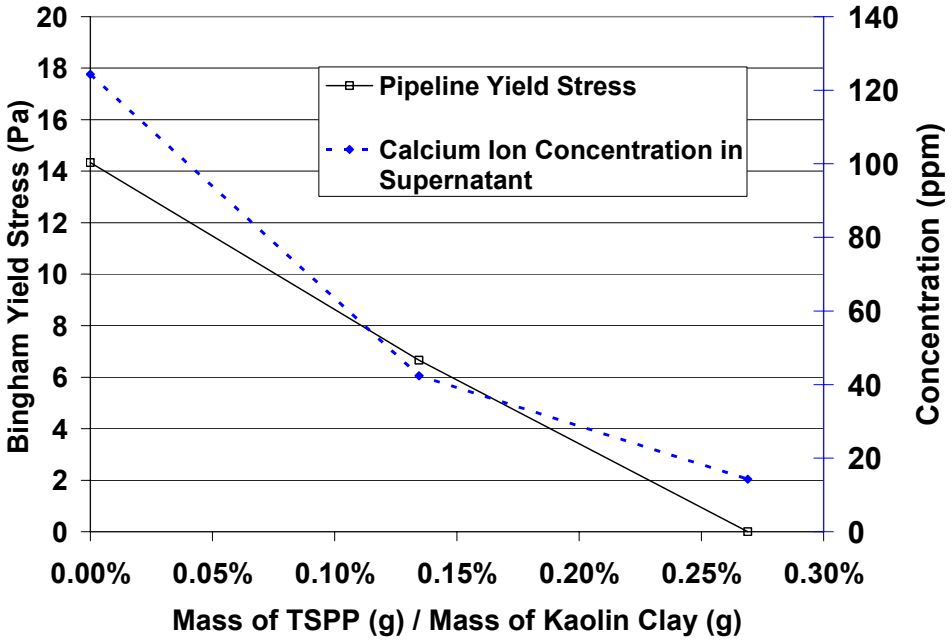

Figure 4.16: Comparison of inferred Bingham yield stress and associated supernatant calcium ion concentrations obtained for 14% by volume solids slurries.

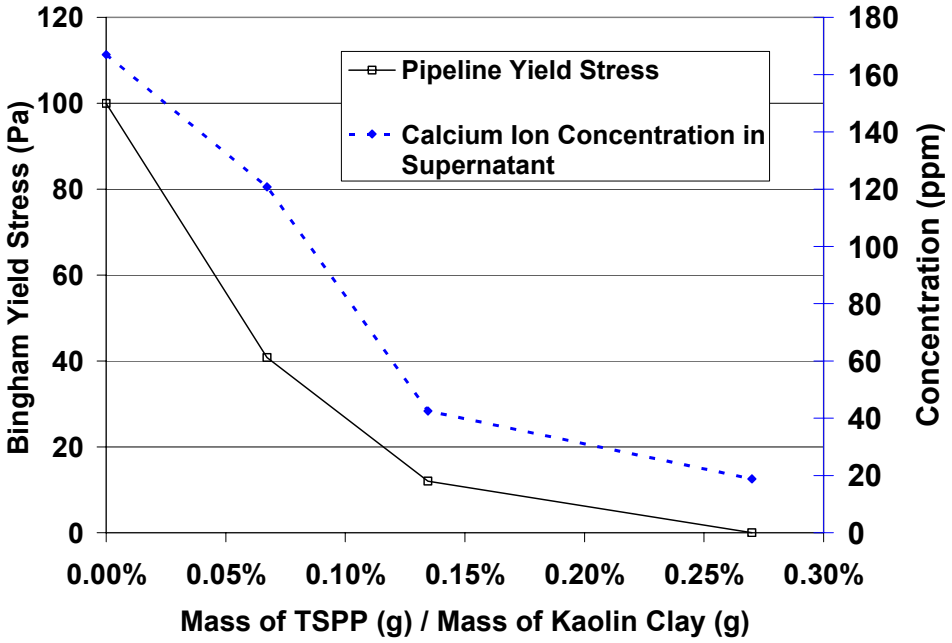

Figure 4.17: Comparison of inferred Bingham yield stress and associated supernatant calcium ion concentrations obtained for 17% by volume solids slurries.

The amount of flocculating agent needed to cause attractive particle associations increases with the addition of a dispersant i.e. the flocculation value of the slurry will increase. To verify this, an experimental slurry was prepared with 14% by volume solids and a TSPP to clay mass ratio of 0.27% to eliminate any non-Newtonian behaviour. After recording the initial pressure gradient versus velocity data set for the dispersed slurry, additional amounts of flocculant ($CaCl_2 \cdot H_2O$) were added. After each 5 grams of flocculant were added, samples were withdrawn and characterized with Couette viscometry. The data can be found in Appendix A.

Figure 4.18 shows the effects of adding 5, 10, and 15 grams of flocculant to previously dispersed slurry. This slurry had a Newtonian viscosity of 0.0032 Pa.s. After the first 5 gram addition of flocculant, there was no noticeable increase in the

viscous nature of the slurry. However, after 10 grams of flocculant was added, non-Newtonian behaviour was evident. A Bingham yield stress of 7.9 Pa and a plastic viscosity of 0.0092 Pa.s were inferred for this data set. After a total of 15 grams of flocculant had been added the non-Newtonian viscous nature of the slurry continued to rise. The yield stress and plastic viscosity increased to 15.9 Pa and 0.0096 Pa.s respectively.

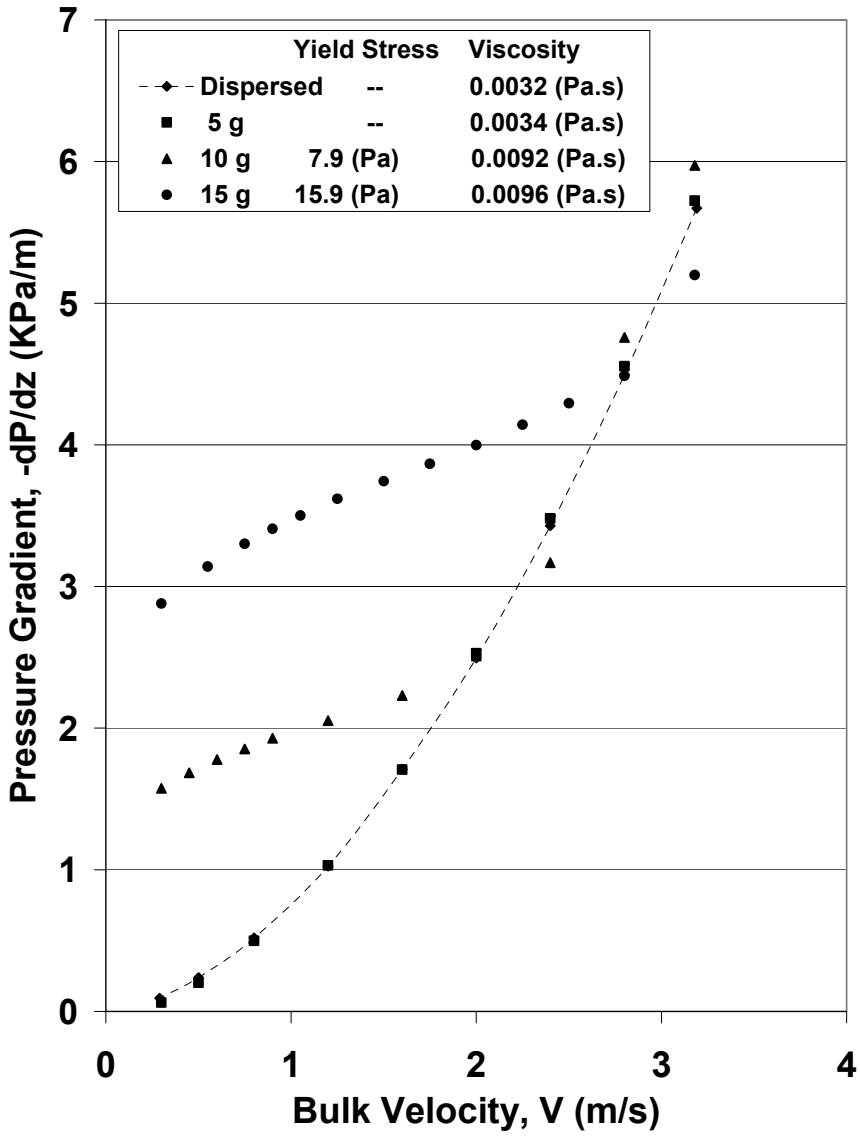

Figure 4.18: Experimental pressure gradient data for increasing amounts of flocculant added to a 17% by volume solids kaolin clay slurry.

The calcium ion concentration in the supernatant was monitored for the initially dispersed slurry and after subsequent additions of 10 and 15 grams of flocculant. Table 4.9 shows that the measured calcium ion content in the supernatant is much lower than would be expected if no dispersant had been used to alter the nature of the slurry. This also shows that TSPP is very effective at increasing the flocculation value of the slurries.

It is interesting to note that the rheological characteristics and the supernatant calcium ion concentration of runs G2000217c and G2000214 are very similar although different quantities of dispersing and flocculating agents were used. The Bingham yield stresses inferred for each data set are 7.9 Pa and 6.7 Pa and the corresponding Ca ions measured in the supernatant were 47 and 42 mg/L. Although the quantities of calcium and phosphate used in run G2000217c are higher than in G2000214 both slurries were composed of 14% by volume solids. This shows the importance of the slurry ionic environment in manipulating the nature of clay slurries and that it is the calcium ion concentration which is the dominant factor.

Table 4.9: Calcium ion analysis for supernatant

Run #	Mass of $CaCl_2 \cdot 2H_2O$ added to stand tank (grams)	$CaCl_2 \cdot 2H_2O$ / Kaolin Clay Mass Ratio	Ca ion calculated (ppm)	Ca ion measured by AASP (ppm)
G2000217a	--	0.10%	113	15
G2000217b	5	0.16%	182	Not Taken
G2000217c	10	0.22%	252	47
G2000217d	15	0.28%	322	110

4.8. Irreversible Increase in Apparent Viscosity

At volumetric concentrations of 17% and 19% solids by volume, instances of irreversible time dependent behaviour were observed. Figure 4.18 shows the behaviour of the highest concentration slurry tested, 19% by volume, in the absence of dispersant. To describe this behaviour it is necessary to explain how operations were carried out.

Slurry was initially loaded to the pipeline loop and recirculated for approximately 10 minutes at the highest bulk velocity attainable (3.2 m/s). A pressure gradient versus velocity data set was recorded starting at a high velocity. It was observed that as the velocity was decreased from 3.2 m/s to 3.0 m/s the corresponding 60 second time averaged pressure gradient actually increased from 11.1 kPa/m to 11.3 kPa/m. The nature of the slurry had evidently undergone an increase in apparent viscosity with elapsed time of shear. The stand tank was sealed, to ensure that these rheological increases were not due to increasing solids concentrations through evaporation. Isothermal operation of the pipeline was maintained throughout the experiment ensuring that changes in the viscosity were not due to temperature fluctuations.

Once the full pressure gradient versus velocity data set had been recorded the pump speed was increased to achieve a bulk velocity of 3.2 m/s. After approximately one hour of shear at this velocity, another pressure gradient scan was recorded. After these data had been gathered the pump was shut down and operations ceased until the next morning. When operations resumed, identical operating procedures were used in which the pump was operated at its maximum speed between successive data sets.

The experiment was eventually terminated due to excessive pump discharge pressures.

The data collected during the first day of operation are illustrated in Figure 4.19 (open symbols). The Bingham model parameters inferred from the first data set were τ_y = 51.7 Pa and μ_p = 0.0108 Pa.s. Over the next hour the yield stress increased to 86.7 Pa with a μ_p of 0.0198 Pa.s. The next morning, when operations resumed, it was noted that the apparent viscosity did not revert to its original value at the start of the run. In fact the apparent viscosity remained close to its value when the run had been stopped on the previous day. A continuous increase in apparent viscosity was observed throughout the day.

This behaviour was not rheopectic time dependence. Rheopexy occurs when the viscosity increases with time at a constant shear rate and when the shear is removed, the viscosity will gradually decrease with time to its original viscous state. When the run was concluded the yield stress had increases to approximately 3 times its initial value. Various samples withdrawn from the pipeline were also tested a week after storage and no change in the nature of the slurry was observed.

Table 4.1 shows a summary of slurry flow tests completed during this experimental program. Slurry runs which exhibited an irreversible increase in apparent viscosity have been marked as such. The non-Newtonian model parameters listed in this table are shown with the associated duration of shear which the slurry had undergone before characterization. Irreversible apparent viscosity increases occurred only in slurries having concentrations of 17 and 19% by volume solids. It

should again be noted that the data presented in Figures 4.4 to 4.11 illustrate the highest Bingham model parameters obtained.

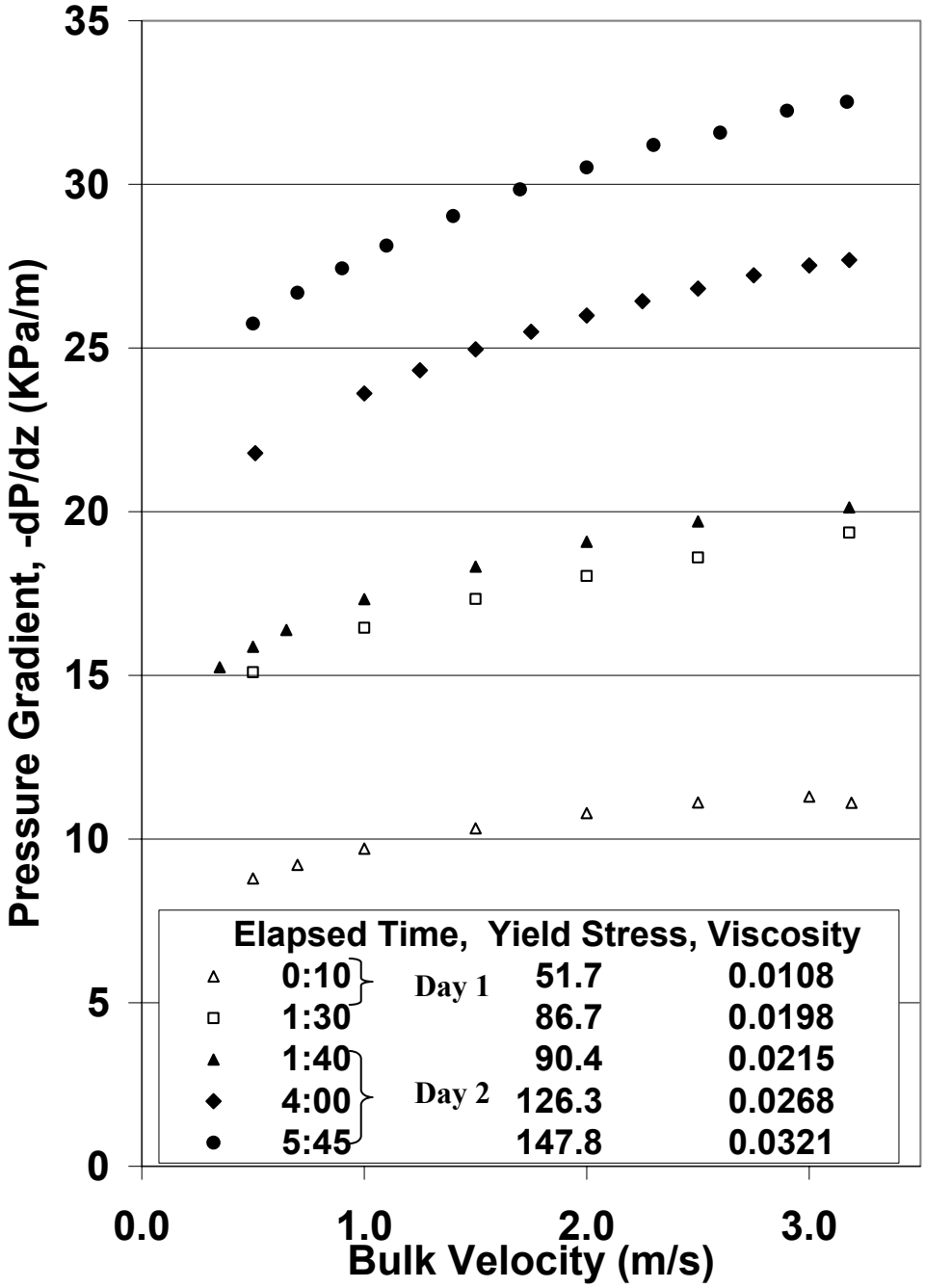

Figure 4.19: Pressure gradient versus velocity data collected for run G2000201 / 202 showing an increase in apparent viscosity with duration of shear.
Slurry composition: 19% by volume kaolin slurry with no phosphate present.

It was possible to eliminate this time dependent behaviour in the 17% by volume solids slurry with the addition of TSPP, using a dispersant to clay mass ratio of 0.27%. For the 19% by volume solids slurry, an increase in apparent viscosity was observed for every run regardless of TSPP addition. However, the magnitude of the increase was reduced with the addition of TSPP. In the absence of TSPP the yield stress increased from an initial value of 51.7 Pa to 126.3 Pa after 4 hours of shear whereas in the presence of 0.13% mass ratio TSPP/Clay the yield stress increased from an initial value of 31 Pa to 46.8 Pa after similar shear duration. Likewise the slurry run containing the highest mass ratio of TSPP / Clay (0.27%) began with no yield stress and only developed a yield stress of 0.5 Pa after 3 hours and 30 minutes.

An experimental program was conducted to further investigate the nature of these irreversible increases in apparent viscosity with time. Five 0.6 litre samples of slurries containing 19% by volume kaolin clay were prepared with RO water and a constant dihydrated calcium chloride to clay mass ratio of 0.10%. The samples were mixed initially in a low shear environment with a spatula to create a homogeneous slurry. The mixtures were then sheared with a Servodyne mixer at a rotation speed which would not entrain air. The slurries were mixed for various durations: (0, 1, 2, 4, and 8 hours) to examine any changes taking place in the slurry. 400 ml of sample were withdrawn to examine any change in viscosity, particle size, electrophoretic mobility, slurry pH, and the calcium ion content in the supernatant. The results are summarized in Table 4.10.

Table 4.10 Experimental results of shear duration tests of 19 by volume solids kaolin clay slurry containing 0.10% flocculant / clay mass ratio.

Run Number	Shear Duration (hours)	Couette Viscometry (Bingham) τ_y (Pa)	μ_p (Pa.s)	Particles wt% finer than 0.50 micron	Electrophoretic Mobility (m^2/volt sec) $x10^{-8}$	Calcium Ion Analysis (ppm)	pH
P00140	0	24.5	0.0226	19.9	--	202.1	6.60
P01140	1	28.4	0.0245	14.7	1.41	202.1	6.49
P02140	2	36.5	0.0256	16.7	1.40	202.9	6.59
P04140	4	47.0	0.0241	15.8	1.37	180.5	6.60
P08140	8	49.8	0.0200	19.7	1.41	199.7	6.58

Table 4.10 shows the associated increase in viscosity with duration of shear. After 8 hours of shear duration with the mixer, the yield stress of the 19 percent volume by solids slurry was measured to be 50 Pa. The highest yield stress measured for the same slurry makeup in the vertical pipeline loop as measured by the same viscometer was 158 Pa. If this slurry had been characterized with only the viscometer and had been prepared in a low shear environment a yield stress of 24.5 Pa would have been obtained.

This shear duration test shows the importance of using the appropriate shear environment when testing high concentration solids kaolin clay slurries. It is advisable to use similar industrial mixing procedures in the experimental test work when characterizing the slurry. It is also advisable to test the slurry using a pipeline with similar diameter and velocity at or below the design velocity when characterizing high concentration fine particle slurries in which increases in apparent viscosity are observed.

No change was noted with respect to the properties of particle size, pH, calcium ion concentration, and electrophoretic mobility. The mobility and pH results show no appreciable variation for the five samples created (duration of shear at times 0, 1, 2 ,4 ,and 8 hours). The particle size analysis results do not trend with the witnessed increase in yield stress. The results for the sample sheared with the spatula (duration of shear 0) indicate a yield stress of 24.5 Pa and a corresponding weight percent of particles finer than 0.50 microns of 19.9%. The yield stress for the sample shear for the longest duration of 8 hours increased to 49.8 Pa. However the

corresponding weight percent of particle finer than 0.50 microns remained relatively unchanged at 19.7%.

The analysis of calcium ions in the supernatant showed very little change from the spatula sheared mixture to those exposed to 1,2, and 8 hours of intense shear with the mixer. At a shear duration of 4 hours there is change from the time zero sample of 202.1 ppm of calcium ions to 180.5 ppm of calcium ions. To verify this result two additional calcium ion concentration 4 hour shear duration tests were completed. These results are summarized in Table 4.11.

Table 4.11 Replicate experimental results of 4 hour shear duration tests of 19 by volume solids kaolin clay slurry containing 0.10% flocculant / clay mass ratio.

Time of Shear (hour)	Calcium ion in supernatant (mg/L)	pH
0	166	6.86
4	164	6.89
0	170	6.23
4	173	6.28

The results found in Table 4.11 indicate that there is little variation in calcium ion concentration with elapsed time of shear. The variation in calcium ion concentration in the original test may have been due to experimental error.

A possible explanation for the observed increase in apparent viscosity was proposed by Larsen (1994). Kaolin particle agglomerates, which are initially orientated in a face to face structure, are reoriented under high shear conditions into a card house structure. The card house structure both immobilizes a finite fraction of the aqueous phase and also forms a stronger particle network. The net result is that

additional energy is required to transport the mixture and the apparent viscosity increases. It is important to note that Larsen proposed this mechanism to describe rheopectic behaviour. Rheopectic time dependence was not observed in this study since the slurries did not revert back to their original rheological behaviour after a period of time. On the other hand, the explanation of a shift from face to face to a face to edge structure is consistent with the results presented in Table 4.10

To further understand the irreversible increase in apparent viscosity in concentrated kaolin clay slurries, work could be done to interpret the change in structure that the clay slurry undergoes. It may be possible in further studies to look at this changing structure in its natural environment without altering the slurry using specialized microscopic techniques.

5. CONCLUSIONS AND RECOMMENDATIONS

An experimental research program was conducted at the Saskatchewan Research Council Pipe Flow Technology Centre to determine the nature of the effects of solids concentration and chemical species on the rheology of kaolin clay slurries. Specifically, the effect of adding a flocculant, dihydrated calcium chloride, ($CaCl_2 \bullet 2H_2O$) and a dispersing agent tetrasodium pyrophosphate (TSPP, $Na_4P_2O_7$), to the rheology of kaolin clay slurries.

To characterise these slurries, a 25.8 mm vertical pipe loop was used to gather pressure gradient measurements as a function of bulk velocity. These experimental pressure gradients were then compared to the integrated Bingham and Casson model equations to obtain yield stress and viscosity parameters. Concentric cylinder viscometry was also used to obtain torque measurements as a function of angular velocity to obtain model parameters. The calcium ion concentration in the slurry supernatant was monitored to understand its effect on clay rheology. Electrophoretic mobility, particle size, and pH measurements were also made to understand the effect of chemical species on the charged atmosphere surrounding the clay particles.

- The kaolin clay slurries exhibited yield stresses and could be characterised with either the two-parameter Bingham or Casson continuum flow models. Increasing the clay concentration in the slurry, while keeping the mass ratio of flocculant to kaolin constant, increased both the yield and viscosity parameters.
- There was generally good agreement between the rheological parameters obtained in the Couette flow viscometer and that in the pipeline loop.

- In slurries for which it was possible to obtain turbulent flow, the transition to turbulent flow was predicted accurately by the Wilson & Thomas method for both Bingham and Casson models. However, the author could not find a systematic reason why the pressure gradient predictions were modelled more accurately with the Bingham model in some instances and the Casson in others.
- It was possible to reduce or eliminate the yield stress of a slurry which has significant amount of calcium ion present with the addition of the dispersing agent TSPP.
- The calcium ion content of the supernatant extracted from the slurries proved to be an indicator of the degree of flocculation. If the Calcium ion remained below 25 mg / litre of supernatant, the particle-particle repulsion forces were dominant and the slurry exhibited Newtonian characteristics.
- When exposed to extended periods of high shear conditions in the pipeline loop, slurries with clay concentrations of 17% by volume solids or greater exhibited an irreversible increase in apparent viscosity with time.
- An attempt was made to understand this irreversible thickening characteristic. Four identical 19% by volume solids clay slurries were exposed to varying amounts of shear (0, 2, 4 and 8 hours of vigorous mixing). The rheological parameters where then determined using a Couette viscometry. All displayed an increase in yield stress with time of shear mixing. Laboratory tests did not reveal any appreciable differences in particle size, electrophoretic mobility, calcium ion concentration or pH with this irreversible change.

- It is recommended that further work be undertaken to understand the irreversible increase in apparent viscosity in concentrated kaolin clay slurries.
- It is recommended that when characterizing kaolin clay particle slurries the appropriate shear environment be used.
- It is recommended that further work be undertaken to extend the current body of knowledge regarding the Wilson & Thomas turbulent flow pressure gradient predictions for the Bingham and Casson models. Such an investigation should allow designers to determine which of the two models is more appropriate for a given slurry.

6. REFERENCES

Allen, T.A., "Particle Size Measurement – Powder Sampling and Particle Size Measurement", Chapman & Hall, Fifth Edition, New York, NY, 228-235, 296-275, 1997

Blossem, B., Personal communication, IMERYS Worldwide Paper Division, Rosswell, GA, December 2000.

Carty W.M., "Rheology and Plasticity for Ceramic Processing," Ceramic Transactions (Fundamentals of Refractory Technology), American Ceramic Society, Westerville, OH, 29-52, 2001

Carty W.M., "Rheology of Aqueous Clay Suspensions" Available at: http://www.conrad.ab.ca/yildirim/seminars/process_water/21_WCarty_Rheolgy_aqueous_clay_suspensions.pdf May 2001

Carty, W.M., "The Colloidal Nature of Kaolinite", The American Ceramic Society Bulletin, 78, No. 8, August 1999.

Casson, N., "A Flow Equation For Pigment-Oil Suspensions of The Printing Ink Type", Rheology of Disperse Systems, University College of Swansea, Sept. 1957, 84-105

Goodwin, J., Personal communication, Interfacial Dynamics Corporation, Portland, OR, July 2001

Hill, K.B., "Pipeline Flow of Particles in Fluids With Yield Stresses", Ph.D. Thesis in Chemical Engineering, University of Saskatchewan, Saskatoon, SK, 1996

Hill, K.B., and Shook. C.A., "Pipeline Transport of Coarse Particles by Water and by Fluids with Yield Stresses", Particulate Science and Technology, 16, 163-183, 1998

Holtz R.D., and W.D. Kovacs, "An introduction to Geotechnical Engineering", Prentice Hall, New Jersey, 84, 1981.

Larsen P., Wang, Z., and Xiang, W., "Rheological properties of sediment suspensions and their implications" Journal of Hydraulic Research, 32, 495-516, 1994

Loomis, G.A., "Grain Size of Whiteware Clays as Determined by the Andreasen Pipette", Journal of the American Ceramic Society, 21, 393-399, 1938

Masliyah, J., “Electrokinetic transport phenomenon”, Alberta Oil Sands Technology and Research Authority, Edmonton, AB, 35, 1994.

Michaels, A.S., and Bolger, J.C., “The Plastic Flow Behaviour of Flocculated Kaolin Suspensions”, I & EC Fundamentals, 1, No. 3, 153-162, August 1962

O’Connor and W.M. Carty, “The Effect of Ionic Concentration on the Viscosity of Clay-Based Systems”, Ceramic Engineering and Science Proceedings, 19[2], 65-76, 1998

Rossington K.R., Y. Senapati, and Carty, W.M., “A Critical Evaluation of Dispersants: Part 2, Effects on Rheology, pH, and Specific Adsorption," Ceram. Eng. Sci. Proc., 20 [2], 119-132, 1999

Shook, C.A. and Gillies, R.G., and Sanders, R. S., “Pipeline Hydrotransport with Applications in the Oil Sand Industry”, Saskatchewan Research Council, Saskatoon, SK, Publication No. 11508-1E02, 3-1 - 3-5, 2002

Shook, C.A. and Roco, M.C., “Slurry Flow: Principles and Practice”, Butterworth-Heinemann, Boston, 1-154, 1991.

Thiessen, P. A., “Wechselseitige Adsorbtion von Kolloiden”, Z. Elektrochem., 48, 675-681, 1942

Thomas, D.G., “Transport Characteristics of Suspensions - VII Relation of Hindered Settling Floc Characteristics to Rheological Parameters”, American Institute of Chemical Engineering Journal, 9, No. 3, 310-316, May 1963

Van Olphen, H., “An introduction to Clay Colloid Chemistry” Second Edition, Wiley, New York, 1977.

Wilson, K.C. and Thomas, A.D., “A New Analysis of Non-Newtonian Fluids”, Can. J. Chem. Eng., 63, 539-546, 1985

Xu, J., Gillies, R.G., Small, M.H., and Shook, C.A., “Laminar and Turbulent Flow of Kaolin Slurries”, Proc. Hydrotransport 12, BHR Group, Cranfield, U. K., 595-613, 1993

APPENDIX A

PIPELINE AND VISCOMETER FLOW DATA

Pipeline Flow Data for Clear Water

Run Number: G2000100
Date: 07/00
Pipe Diameter (m): 0.025825
Wall Roughness (μm): 2.51

Velocity (m/s)	Pressure Gradient (kPa/m)	Temperature (°C)
3.20	3.719	23.9
2.80	2.932	24.9
2.42	2.229	25.5
2.00	1.603	26.0
1.60	1.078	26.3
1.22	0.652	26.6
0.82	0.326	26.7

Pipeline and Viscometer Flow Data for Cv = 0.10 Kaolin Clay Slurries

Run Number:	G2000208	Date:	08/00
Temperature (°C):	20	Slurry Density (kg/m^3):	1161
Pipeline Diameter (m):	0.025825	Wall Roughness (μm):	2.51

Mass of $CaCl_2 \cdot 2H_2O$ added / Mass Clay: 0.10%
Mass of TSPP added / Mass Clay: No TSPP Added

Velocity (m/s)	Pressure Gradient (kPa/m)
3.19	5.182
2.86	4.229
2.35	2.947
1.75	1.735
1.60	1.454
1.46	1.071
1.30	0.859
1.15	0.794
1.00	0.754
0.84	0.716
0.70	0.681
0.55	0.641
0.40	0.597
0.29	0.562

Inferred Bingham Parameters:
Yield Stress τ_y (Pa): 2.6
Plastic Viscosity μ_p (Pa.s): 0.0055

Inferred Casson Parameters:
Yield Stress τ_c (Pa): 1.9
Plastic Viscosity μ_∞ (Pa.s): 0.0015

Viscometer:	Haake RV 3
Length of Spindle (m):	0.60
Radius of Spindle (m):	0.2001
Radius of Cup (m):	0.2004

ω (rad/s)	T/L (N.m/m)
3.35	9.25E-03
4.73	9.68E-03
6.70	1.05E-02
9.48	1.15E-02
13.40	1.23E-02
18.95	1.38E-02
26.81	1.58E-02
37.91	1.86E-02
26.81	1.58E-02
18.95	1.38E-02
13.40	1.23E-02
9.48	1.14E-02
6.70	1.02E-02
4.73	9.60E-03
3.35	9.10E-03

Inferred Bingham Parameters:
Yield Stress τ_y (Pa): 3.2
Plastic Viscosity μ_p (Pa.s): 0.0048

Inferred Casson Parameters:
Yield Stress τ_c (Pa): 2.3
Plastic Viscosity μ_∞ (Pa.s): 0.0016

Pipeline and Viscometer Flow Data for Cv = 0.10 Kaolin Clay Slurries

Run Number:	G2000106	Date:	07/00
Temperature (°C):	20	Slurry Density (kg/m^3):	1161
Pipeline Diameter (m):	0.025825	Wall Roughness (μm):	2.51

Mass of $CaCl_2 \cdot 2H_2O$ added / Mass Clay: 0.10%
Mass of TSPP added / Mass Clay: No TSPP Added

Velocity (m/s)	Pressure Gradient (kPa/m)
3.19	5.333
3.00	4.512
2.50	3.218
2.00	2.131
1.60	1.370
1.40	0.936
1.20	0.825
1.00	0.766
0.90	0.741
0.80	0.717
0.70	0.690
0.60	0.662
0.48	0.621

Inferred Bingham Parameters:
Yield Stress τ_y (Pa): 2.6
Plastic Viscosity μ_p (Pa.s): 0.0051

Inferred Casson Parameters:
Yield Stress τ_c (Pa): 1.9
Plastic Viscosity μ_∞ (Pa.s): 0.0016

Viscometer:	Haake RV 3
Length of Spindle (m):	0.60
Radius of Spindle (m):	0.2001
Radius of Cup (m):	0.2004

ω (rad/s)	T/L (N.m/m)
3.35	9.25E-03
4.73	9.89E-03
6.70	1.08E-02
9.48	1.18E-02
13.40	1.29E-02
18.95	1.44E-02
26.81	1.64E-02
37.91	1.95E-02
26.81	1.66E-02
18.95	1.47E-02
13.40	1.30E-02
9.48	1.18E-02
6.70	1.08E-02
4.73	9.96E-03
3.35	9.32E-03

Inferred Bingham Parameters:
Yield Stress τ_y (Pa): 3.3
Plastic Viscosity μ_p (Pa.s): 0.0052

Inferred Casson Parameters:
Yield Stress τ_c (Pa): 2.3
Plastic Viscosity μ_∞ (Pa.s): 0.0018

Pipeline and Viscometer Flow Data for Cv = 0.10 Kaolin Clay Slurries

Run Number:	G2000212	Date:	08/00
Temperature (°C):	20	Slurry Density (kg/m^3):	1161
Pipeline Diameter (m):	0.025825	Wall Roughness (μm):	2.51

Mass of $CaCl_2 \cdot 2H_2O$ added / Mass Clay: 0.10%
Mass of TSPP added / Mass Clay: 0.27%

Velocity (m/s)	Pressure Gradient (kPa/m)
3.18	5.019
2.80	4.013
2.50	3.263
2.00	2.210
1.75	1.756
1.50	1.341
1.25	0.975
1.00	0.667
0.75	0.403
0.60	0.274
0.50	0.204
0.40	0.140
0.29	0.082

Inferred Newtonian Viscosity:
Viscosity μ (Pa.s): 0.0022*
*Turbulent Flow Data

Viscometer:	Haake RV 3
Length of Spindle (m):	0.60
Radius of Spindle (m):	0.2001
Radius of Cup (m):	0.2004

ω (rad/s)	T/L (N.m/m)
18.95	2.37E-03
26.81	4.59E-03
37.91	8.17E-03
26.81	5.02E-03
18.95	2.72E-03

Inferred Newtonian Viscosity:
Viscosity μ (Pa.s): 0.0033

Pipeline and Viscometer Flow Data for Cv = 0.14 Kaolin Clay Slurries

Run Number:	G2000205	Date:	07/00
Temperature (°C):	20	Slurry Density (kg/m^3):	1228
Pipeline Diameter (m):	0.025825	Wall Roughness (μm):	2.51

Mass of $CaCl_2 \cdot 2H_2O$ added / Mass Clay: 0.10%
Mass of TSPP added / Mass Clay: No TSPP Added

Velocity (m/s)	Pressure Gradient (kPa/m)
3.20	5.457
3.00	4.829
2.80	3.829
2.60	3.483
2.40	3.402
2.20	3.336
2.00	3.278
1.60	3.156
1.00	2.925
0.70	2.771
0.50	2.650

Inferred Bingham Parameters:
Yield Stress τ_y (Pa): 14.3
Plastic Viscosity μ_p (Pa.s): 0.0057

Inferred Casson Parameters:
Yield Stress τ_c (Pa): 12.0
Plastic Viscosity μ_∞ (Pa.s): 0.0010

Viscometer: Haake RV 3
Length of Spindle (m): 0.60
Radius of Spindle (m): 0.2001
Radius of Cup (m): 0.2004

ω (rad/s)	T/L (N.m/m)
4.73	3.14E-02
6.70	3.29E-02
9.48	3.50E-02
13.40	3.75E-02
18.95	4.05E-02
26.81	4.41E-02
37.91	4.90E-02
26.81	4.45E-02
18.95	4.09E-02
13.40	3.79E-02
9.48	3.55E-02
6.70	3.35E-02
4.73	3.18E-02

Inferred Bingham Parameters:
Yield Stress τ_y (Pa): 11.3
Plastic Viscosity μ_p (Pa.s): 0.0094

Inferred Casson Parameters:
Yield Stress τ_c (Pa): 9.2
Plastic Viscosity μ_∞ (Pa.s): 0.0022

Pipeline and Viscometer Flow Data for Cv = 0.14 Kaolin Clay Slurries

Run Number:	G2000105	Date:	07/00
Temperature (°C):	20	Slurry Density (kg/m^3):	1228
Pipeline Diameter (m):	0.025825	Wall Roughness (μm):	2.51

Mass of $CaCl_2 \cdot 2H_2O$ added / Mass Clay: 0.10%
Mass of TSPP added / Mass Clay: 0.10%

Velocity (m/s)	Pressure Gradient (kPa/m)
3.23	5.845
3.00	5.144
2.50	3.562
2.00	2.123
1.60	1.790
1.40	1.677
1.19	1.582
1.00	1.504
0.90	1.467
0.80	1.422
0.70	1.402
0.60	1.346
0.45	1.281

Inferred Bingham Parameters:
Yield Stress τ_y (Pa): 5.9
Plastic Viscosity μ_p (Pa.s): 0.0078

Inferred Casson Parameters:
Yield Stress τ_c (Pa): 4.4
Plastic Viscosity μ_∞ (Pa.s): 0.0021

Viscometer: Haake RV 3
Length of Spindle (m): 0.60
Radius of Spindle (m): 0.2001
Radius of Cup (m): 0.2004

ω (rad/s)	T/L (N.m/m)
4.73	2.02E-02
6.70	2.17E-02
9.48	2.36E-02
13.40	2.57E-02
18.95	2.82E-02
26.81	3.15E-02
37.91	3.58E-02
26.81	3.16E-02
18.95	2.82E-02
13.40	2.55E-02
9.48	2.33E-02
6.70	2.16E-02
4.73	2.01E-02

Inferred Bingham Parameters:
Yield Stress τ_y (Pa): 7.1
Plastic Viscosity μ_p (Pa.s): 0.0084

Inferred Casson Parameters:
Yield Stress τ_c (Pa): 5.2
Plastic Viscosity μ_∞ (Pa.s): 0.0025

Pipeline and Viscometer Flow Data for Cv = 14% Kaolin Clay Slurries

Run Number:	G2000214	Date:	07/00
Temperature (°C):	20	Slurry Density (kg/m^3):	1228
Pipeline Diameter (m):	0.025825	Wall Roughness (μm):	2.51

Mass of $CaCl_2 \cdot 2H_2O$ added / Mass Clay: 0.10%
Mass of TSPP added / Mass Clay: 0.13%

Velocity (m/s)	Pressure Gradient (kPa/m)
3.19	6.075
2.80	4.856
2.40	3.739
2.00	2.350
1.70	1.909
1.40	1.779
1.10	1.666
0.91	1.606
0.75	1.549
0.60	1.471
0.45	1.389
0.31	1.287

Inferred Bingham Parameters:
Yield Stress τ_y (Pa): 6.7
Plastic Viscosity μ_p (Pa.s): 0.0072

Inferred Casson Parameters:
Yield Stress τ_c (Pa): 5.2
Plastic Viscosity μ_∞ (Pa.s): 0.0018

Viscometer:	Haake RV 3
Length of Spindle (m):	0.60
Radius of Spindle (m):	0.2001
Radius of Cup (m):	0.2004

ω (rad/s)	T/L (N.m/m)
4.73	1.78E-02
6.70	1.89E-02
9.48	2.04E-02
13.40	2.24E-02
18.95	2.50E-02
26.81	2.80E-02
37.91	3.20E-02
26.81	2.84E-02
18.95	2.52E-02
13.40	2.29E-02
9.48	2.08E-02
6.70	1.94E-02
4.73	1.83E-02
3.35	1.72E-02

Inferred Bingham Parameters:
Yield Stress τ_y (Pa): 6.2
Plastic Viscosity μ_p (Pa.s): 0.0077

Inferred Casson Parameters:
Yield Stress τ_c (Pa): 4.5
Plastic Viscosity μ_∞ (Pa.s): 0.0023

Pipeline and Viscometer Flow Data for Cv = 14% Kaolin Clay Slurries

Run Number:	G2000215	Date:	07/00
Temperature (°C):	20	Slurry Density (kg/m^3):	1228
Pipeline Diameter (m):	0.025825	Wall Roughness (μm):	2.51

Mass of $CaCl_2 \cdot 2H_2O$ added / Mass Clay: 0.10%
Mass of TSPP added / Mass Clay: 0.27%

Velocity (m/s)	Pressure Gradient (kPa/m)
3.18	5.774
2.80	4.588
2.40	3.493
2.00	2.537
1.60	1.702
1.20	1.029
0.90	0.615
0.75	0.442
0.60	0.294
0.45	0.170
0.30	0.053

Inferred Newtonian Viscosity:
Viscosity μ (Pa.s): 0.0035*
*Turbulent Flow Data

Viscometer:	Haake RV 3
Length of Spindle (m):	0.60
Radius of Spindle (m):	0.2001
Radius of Cup (m):	0.2004

ω (rad/s)	T/L (N.m/m)
13.40	2.29E-03
18.95	3.51E-03
26.81	5.52E-03
37.91	9.96E-03
26.81	5.59E-03
18.95	3.37E-03
13.40	2.22E-03

Inferred Newtonian Viscosity:
Viscosity μ (Pa.s): 0.0040

Pipeline and Viscometer Flow Data for Cv = 14% Kaolin Clay Slurries

Run Number:	G2000217	Date:	07/00
Temperature (°C):	20	Slurry Density (kg/m^3):	1228
Pipeline Diameter (m):	0.025825	Wall Roughness (μm):	2.51

Mass of $CaCl_2 \cdot 2H_2O$ added / Mass Clay: 0.10%
Mass of TSPP added / Mass Clay: 0.27%

Velocity (m/s)	Pressure Gradient (kPa/m)
3.19	5.671
2.80	4.496
2.40	3.429
2.00	2.495
1.60	1.710
1.20	1.026
0.80	0.519
0.50	0.240
0.29	0.093

Inferred Newtonian Viscosity:
Viscosity μ (Pa.s): 0.0032*
*Turbulent Flow Data

Viscometer: Haake RV 3
Length of Spindle (m): 0.60
Radius of Spindle (m): 0.2001
Radius of Cup (m): 0.2004

ω (rad/s)	T/L (N.m/m)
13.40	2.94E-03
18.95	4.30E-03
26.81	6.24E-03
37.91	1.02E-02
26.81	6.09E-03
18.95	4.30E-03
13.40	3.01E-03

Inferred Newtonian Viscosity:
Viscosity μ (Pa.s): 0.0043

Pipeline Flow Data for $CaCl_2 \cdot 2H_2O$ Recirculation Addition to Cv = 0.14 Kaolin Clay Slurry Run G2000217

Cumulative mass of $CaCl_2 \cdot 2H_2O$ added to recirculation stream: 5.0 grams

Velocity (m/s)	Pressure Gradient (kPa/m)
3.18	5.723
2.80	4.554
2.40	3.481
2.00	2.528
1.60	1.707
1.20	1.032
0.80	0.499
0.50	0.203
0.30	0.064

Inferred Newtonian Viscosity:
Viscosity μ (Pa.s): 0.0034*
*Turbulent Flow Data

Cumulative mass of $CaCl_2 \cdot 2H_2O$ added to recirculation stream: 10.0 grams

Velocity (m/s)	Pressure Gradient (kPa/m)
3.18	5.972
2.80	4.759
2.40	3.169
2.00	2.509
1.60	2.231
0.90	1.928
0.60	1.778
0.30	1.575

Inferred Bingham Parameters:
Yield Stress τ_y (Pa): 7.9
Plastic Viscosity μ_p (Pa.s): 0.0092

Inferred Casson Parameters:
Yield Stress τ_c (Pa): 6.1
Plastic Viscosity μ_∞ (Pa.s): 0.0023

Cumulative mass of $CaCl_2 \cdot 2H_2O$ added to recirculation stream: 15.0 grams

Velocity (m/s)	Pressure Gradient (kPa/m)
3.18	5.200
2.80	4.487
2.50	4.295
2.00	3.999
1.50	3.744
1.05	3.501
0.75	3.302
0.30	2.880

Inferred Bingham Parameters:
Yield Stress τ_y (Pa): 15.9
Plastic Viscosity μ_p (Pa.s): 0.0096

Inferred Casson Parameters:
Yield Stress τ_c (Pa): 12.9
Plastic Viscosity μ_∞ (Pa.s): 0.0020

Viscometer Flow Data for $CaCl_2 \cdot 2H_2O$ Recirculation Addition to Cv=14% Kaolin Clay Slurry Run G2000217

Cumulative mass of $CaCl_2 \cdot 2H_2O$ added to recirculation stream: 5.0 grams

Viscometer: Haake RV 3
Length of Spindle (m): 0.60
Radius of Spindle (m): 0.2001
Radius of Cup (m): 0.2004

ω (rad/s)	T/L (N.m/m)
13.40	3.66E-03
18.95	5.09E-03
26.81	7.67E-03
37.91	1.04E-02
26.81	7.24E-03
18.95	5.16E-03
13.40	3.87E-03

Inferred Newtonian Viscosity:
Viscosity μ (Pa.s): 0.0049

Cumulative mass of $CaCl_2 \cdot 2H_2O$ added to recirculation stream: 10.0 grams

Viscometer: Haake RV 3
Length of Spindle (m): 0.60
Radius of Spindle (m): 0.2001
Radius of Cup (m): 0.2004

ω (rad/s)	T/L (N.m/m)
4.73	2.34E-02
6.70	2.51E-02
9.48	2.71E-02
13.40	2.94E-02
18.95	3.25E-02
26.81	3.65E-02
37.91	4.14E-02
26.81	3.66E-02
18.95	3.26E-02
13.40	2.94E-02
9.48	2.71E-02
6.70	2.51E-02
4.73	2.33E-02

Inferred Bingham Parameters:
Yield Stress τ_y (Pa): 8.2
Plastic Viscosity μ_p (Pa.s): 0.0097

Inferred Casson Parameters:
Yield Stress τ_c (Pa): 6.0
Plastic Viscosity μ_∞ (Pa.s): 0.0028

Cumulative mass of $CaCl_2 \cdot 2H_2O$ added to recirculation stream: 15.0 grams

Viscometer: Haake RV 3
Length of Spindle (m): 0.60
Radius of Spindle (m): 0.2001
Radius of Cup (m): 0.2004

ω (rad/s)	T/L (N.m/m)
3.18	5.200
2.80	4.487
2.50	4.295
2.00	3.999
1.50	3.744
1.05	3.501
0.75	3.302
0.30	2.880

Inferred Bingham Parameters:
Yield Stress τ_y (Pa): 15.6
Plastic Viscosity μ_p (Pa.s): 0.0119

Inferred Casson Parameters:
Yield Stress τ_c (Pa): 12.5
Plastic Viscosity μ_∞ (Pa.s): 0.0025

Pipeline and Viscometer Flow Data for Cv = 0.17 Kaolin Clay Slurries

Run Number:	G2000206	Date:	08/00
Temperature (°C):	20	Slurry Density (kg/m^3):	1278
Pipeline Diameter (m):	0.025825	Wall Roughness (μm):	2.51

Mass of $CaCl_2 \cdot 2H_2O$ added / Mass Clay: 0.10%
Mass of TSPP added / Mass Clay: No TSPP Added

This Slurry Exhibited an Increase in apparent viscosity with time.
Pressure Drop vs. Velocity Data Recorded after Slurry Sheared at 3.2 m/s for and Elapsed Time of 2hours 20 min

Velocity (m/s)	Pressure Gradient (kPa/m)
3.19	12.817
3.00	12.715
2.80	12.592
2.60	12.456
2.25	12.151
1.75	11.734
1.25	11.220
0.75	10.483
0.50	9.976

Inferred Bingham Parameters:
Yield Stress τ_y (Pa): 57.2
Plastic Viscosity μ_p (Pa.s): 0.0134

Inferred Casson Parameters:
Yield Stress τ_c (Pa): 49.1
Plastic Viscosity μ_∞ (Pa.s): 0.0021

Elapsed Time of Shear: 8hours 40min

Velocity (m/s)	Pressure Gradient (kPa/m)
3.19	20.796
3.00	20.716
2.50	20.081
2.00	19.368
1.50	18.735
1.00	17.796
0.75	17.008
0.50	16.231

Inferred Bingham Parameters:
Yield Stress τ_y (Pa): 93.9
Plastic Viscosity μ_p (Pa.s): 0.0210

Inferred Casson Parameters:
Yield Stress τ_c (Pa): 80.5
Plastic Viscosity μ_∞ (Pa.s): 0.0033

Elapsed Time of Shear: 9hours

Velocity (m/s)	Pressure Gradient (kPa/m)
3.19	22.169
3.00	22.016
2.50	21.358
2.00	20.518
1.50	19.883
1.00	18.871
0.50	17.393

Inferred Bingham Parameters:
Yield Stress τ_y (Pa): 100.0
Plastic Viscosity μ_p (Pa.s): 0.0222

Inferred Casson Parameters:
Yield Stress τ_c (Pa): 86.3
Plastic Viscosity μ_∞ (Pa.s): 0.0034

Viscometry performed on slurry before loading pipeline loop and after discharge.

Viscometer:	Haake RV 3
Length of Spindle (m):	0.60
Radius of Spindle (m):	0.2001
Radius of Cup (m):	0.2004

Before Loading Pipeline Loop

ω (rad/s)	T/L (N.m/m)
9.48	6.98E-02
13.40	7.51E-02
18.95	7.82E-02
26.81	8.59E-02
37.91	9.28E-02
26.81	9.05E-02
18.95	8.36E-02
13.40	7.82E-02
9.48	7.44E-02

Inferred Bingham Parameters:

Yield Stress τ_y (Pa):	24.8
Plastic Viscosity μ_p (Pa.s):	0.0139

Inferred Casson Parameters:

Yield Stress τ_c (Pa):	20.6
Plastic Viscosity μ_∞ (Pa.s):	0.0025

After Discharging Pipeline Loop

ω (rad/s)	T/L (N.m/m)
9.48	2.91E-01
13.40	3.02E-01
18.95	3.14E-01
26.81	3.30E-01
37.91	3.44E-01
26.81	3.30E-01
18.95	3.16E-01
13.40	3.05E-01
9.48	2.92E-01

Inferred Bingham Parameters:

Yield Stress τ_y (Pa):	104.8
Plastic Viscosity μ_p (Pa.s):	0.0335

Inferred Casson Parameters:

Yield Stress τ_c (Pa):	93.3
Plastic Viscosity μ_∞ (Pa.s):	0.0039

Pipeline and Viscometer Flow Data for Cv = 0.17 Kaolin Clay Slurries

Run Number:	G2000210	Date:	08/00
Temperature (°C):	20	Slurry Density (kg/m^3):	1278
Pipeline Diameter (m):	0.025825	Wall Roughness (μm):	2.51

Mass of $CaCl_2 \cdot 2H_2O$ added / Mass Clay: 0.10%
Mass of TSPP added / Mass Clay: 0.07%

This Slurry Exhibited an Increase in apparent viscosity with time.
Pressure Drop vs. Velocity Data Recorded after Slurry Sheared at 3.2 m/s for and Elapsed Time of:

3hours 25 min

Velocity (m/s)	Pressure Gradient (kPa/m)
3.19	10.099
3.00	10.001
2.80	9.871
2.25	9.465
1.75	9.042
1.25	8.540
0.60	7.610
0.30	6.959

Inferred Bingham Parameters:
Yield Stress τ_y (Pa): 40.8
Plastic Viscosity μ_p (Pa.s): 0.0149

Inferred Casson Parameters:
Yield Stress τ_c (Pa): 33.8
Plastic Viscosity μ_∞ (Pa.s): 0.0029

Elapsed Time of Shear: 10hours 45min

Velocity (m/s)	Pressure Gradient (kPa/m)
3.19	16.253
2.99	16.220
2.50	15.810
2.00	15.230
1.50	14.602
1.20	14.134
0.90	13.527
0.60	12.795
0.29	11.824

Inferred Bingham Parameters:
Yield Stress τ_y (Pa): 71.1
Plastic Viscosity μ_p (Pa.s): 0.0192

Inferred Casson Parameters:
Yield Stress τ_c (Pa): 60.2
Plastic Viscosity μ_∞ (Pa.s): 0.0033

Elapsed Time of Shear: 17hours

Velocity (m/s)	Pressure Gradient (kPa/m)
3.19	21.395
3.00	21.147
2.50	20.657
2.00	19.948
1.50	19.129
1.00	18.127
0.60	16.819
0.30	15.831

Inferred Bingham Parameters:
Yield Stress τ_y (Pa): 93.8
Plastic Viscosity μ_p (Pa.s): 0.0243

Inferred Casson Parameters:
Yield Stress τ_c (Pa): 80.1
Plastic Viscosity μ_∞ (Pa.s): 0.0040

Viscometry performed on slurry before loading pipeline loop and after discharge.

Viscometer: Haake RV 3
Length of Spindle (m): 0.60
Radius of Spindle (m): 0.2001
Radius of Cup (m): 0.2004

Before Loading Pipeline Loop

ω (rad/s)	T/L (N.m/m)
9.48	5.44E-02
13.40	5.98E-02
18.95	6.52E-02
26.81	7.13E-02
37.91	7.74E-02
26.81	7.36E-02
18.95	6.90E-02
13.40	6.36E-02
9.48	6.06E-02
6.70	5.52E-02
9.48	5.44E-02

Inferred Bingham Parameters:
Yield Stress τ_y (Pa): 19.4
Plastic Viscosity μ_p (Pa.s): 0.0133

Inferred Casson Parameters:
Yield Stress τ_c (Pa): 15.8
Plastic Viscosity μ_∞ (Pa.s): 0.0027

After Discharging Pipeline Loop

ω (rad/s)	T/L (N.m/m)
9.48	2.72E-01
13.40	2.84E-01
18.95	2.97E-01
26.81	3.12E-01
37.91	3.29E-01
26.81	3.14E-01
18.95	3.01E-01
13.40	2.89E-01
9.48	2.76E-01

Inferred Bingham Parameters:
Yield Stress τ_y (Pa): 98.1
Plastic Viscosity μ_p (Pa.s): 0.0345

Inferred Casson Parameters:
Yield Stress τ_c (Pa): 86.3
Plastic Viscosity μ_∞ (Pa.s): 0.0044

Pipeline and Viscometer Flow Data for Cv = 0.17 Kaolin Clay Slurries

Run Number:	G2000209	Date:	08/00
Temperature (°C):	20	Slurry Density (kg/m^3):	1278
Pipeline Diameter (m):	0.025825	Wall Roughness (μm):	2.51

Mass of $CaCl_2 \cdot 2H_2O$ added / Mass Clay: 0.10%
Mass of TSPP added / Mass Clay: 0.13%

Velocity (m/s)	Pressure Gradient (kPa/m)
3.20	6.545
2.75	4.349
2.51	3.894
2.25	3.386
2.00	3.225
1.61	3.003
1.20	2.824
0.90	2.674
0.60	2.489
0.30	2.250

Inferred Bingham Parameters:
Yield Stress τ_y (Pa): 12.0
Plastic Viscosity μ_p (Pa.s): 0.0090

Inferred Casson Parameters:
Yield Stress τ_c (Pa): 9.6
Plastic Viscosity μ_∞ (Pa.s): 0.0020

Viscometer:	Haake RV 3
Length of Spindle (m):	0.60
Radius of Spindle (m):	0.2001
Radius of Cup (m):	0.2004

ω (rad/s)	T/L (N.m/m)
4.73	3.15E-02
6.70	3.32E-02
9.48	3.58E-02
13.40	3.88E-02
18.95	4.25E-02
26.81	4.72E-02
37.91	5.30E-02
26.81	4.72E-02
18.95	4.24E-02
13.40	3.87E-02
9.48	3.58E-02
6.70	3.33E-02
4.73	3.16E-02

Inferred Bingham Parameters:
Yield Stress τ_y (Pa): 11.1
Plastic Viscosity μ_p (Pa.s): 0.0117

Inferred Casson Parameters:
Yield Stress τ_c (Pa): 8.3
Plastic Viscosity μ_∞ (Pa.s): 0.0032

Pipeline and Viscometer Flow Data for Cv = 0.17 Kaolin Clay Slurries

Run Number:	G2000207	Date:	07/00
Temperature (°C):	20	Slurry Density (kg/m^3):	1278
Pipeline Diameter (m):	0.025825	Wall Roughness (μm):	2.51

Mass of $CaCl_2 \cdot 2H_2O$ added / Mass Clay: 0.10%
Mass of TSPP added / Mass Clay: 0.27%

Velocity (m/s)	Pressure Gradient (kPa/m)
3.00	5.722
2.90	5.359
2.80	5.031
2.70	4.710
2.51	4.107
2.25	3.406
2.00	2.764
1.75	2.197
1.50	1.684
1.25	1.229
1.00	0.833
0.80	0.568
0.60	0.345
0.50	0.251
0.35	0.106

Inferred Newtonian Viscosity:
Viscosity μ (Pa.s): 0.0047*
*Turbulent Flow Data

Viscometer: Haake RV 3
Length of Spindle (m): 0.60
Radius of Spindle (m): 0.2001
Radius of Cup (m): 0.2004

ω (rad/s)	T/L (N.m/m)
13.40	3.23E-03
18.95	4.66E-03
26.81	6.59E-03
37.91	1.08E-02
26.81	6.67E-03
18.95	4.87E-03
13.40	3.23E-03

Inferred Newtonian Viscosity:
Viscosity μ (Pa.s): 0.0047

Pipeline and Viscometer Flow Data for Cv = 0.19 Kaolin Clay Slurries

Run Number:	G2000201 / G2000202	Date:	07/00
Temperature (°C):	20	Slurry Density (kg/m^3):	1321
Pipeline Diameter (m):	0.025825	Wall Roughness (μm):	2.51

Mass of $CaCl_2 \cdot 2H_2O$ added / Mass Clay: 0.10%
Mass of TSPP added / Mass Clay: No TSPP added

This Slurry Exhibited an Increase in apparent viscosity with time.
Pressure Drop vs. Velocity Data Recorded after Slurry Sheared at 3.2 m/s for and Elapsed Time of:

0hours 10 min

Velocity (m/s)	Pressure Gradient (kPa/m)
3.19	11.112
3.00	11.301
2.50	11.114
2.00	10.796
1.50	10.322
1.00	9.707
0.70	9.209
0.50	8.793

Inferred Bingham Parameters:
Yield Stress τ_y (Pa): 51.7
Plastic Viscosity μ_p (Pa.s): 0.0108

Inferred Casson Parameters:
Yield Stress τ_c (Pa): 44.0
Plastic Viscosity μ_∞ (Pa.s): 0.0018

Elapsed Time of Shear: 1hour 30 min

Velocity (m/s)	Pressure Gradient (kPa/m)
3.18	19.363
2.50	18.598
2.00	18.036
1.50	17.332
1.00	16.451
0.50	15.099

Inferred Bingham Parameters:
Yield Stress τ_y (Pa): 86.7
Plastic Viscosity μ_p (Pa.s): 0.0198

Inferred Casson Parameters:
Yield Stress τ_c (Pa): 75.5
Plastic Viscosity μ_∞ (Pa.s): 0.0031

Day 2
Elapsed Time of Shear: 1hours 40 min

Velocity (m/s)	Pressure Gradient (kPa/m)
3.18	20.133
2.50	19.701
2.00	19.081
1.50	18.322
1.00	17.330
0.65	16.388
0.50	15.874
0.35	15.250

Inferred Bingham Parameters:
Yield Stress τ_y (Pa): 90.4
Plastic Viscosity μ_p (Pa.s): 0.0215

Inferred Casson Parameters:
Yield Stress τ_c (Pa): 77.8
Plastic Viscosity μ_∞ (Pa.s): 0.0034

Elapsed Time of Shear: 4hours

Velocity (m/s)	Pressure Gradient (kPa/m)
3.18	27.693
3.00	27.522
2.75	27.223
2.50	26.814
2.25	26.434
2.00	25.993
1.75	25.500
1.50	24.965
1.25	24.321
1.00	23.611
0.51	21.791

Inferred Bingham Parameters:
Yield Stress τ_y (Pa): 126.3
Plastic Viscosity μ_p (Pa.s): 0.0268

Inferred Casson Parameters:
Yield Stress τ_c (Pa): 108.3
Plastic Viscosity μ_∞ (Pa.s): 0.0042

Elapsed Time of Shear: 5hours 45min

Velocity (m/s)	Pressure Gradient (kPa/m)
3.17	32.518
2.90	32.251
2.60	31.581
2.30	31.201
2.00	30.517
1.70	29.845
1.40	29.030
1.10	28.128
0.90	27.436
0.70	26.690
0.50	25.742

Inferred Bingham Parameters:
Yield Stress τ_y (Pa): 147.8
Plastic Viscosity μ_p (Pa.s): 0.0321

Inferred Casson Parameters:
Yield Stress τ_c (Pa): 128.0
Plastic Viscosity μ_∞ (Pa.s): 0.0048

Viscometry performed on slurry before loading pipeline loop and after discharge.

Viscometer:	Haake RV 3
Length of Spindle (m):	0.60
Radius of Spindle (m):	0.2001
Radius of Cup (m):	0.2004

Before Loading Pipeline Loop

ω (rad/s)	T/L (N.m/m)
9.48	1.46E-01
13.40	1.55E-01
18.95	1.64E-01
26.81	1.76E-01
37.91	1.89E-01
26.81	1.78E-01
18.95	1.69E-01
13.40	1.59E-01
9.48	1.53E-01

Inferred Bingham Parameters:

Yield Stress τ_y (Pa):	51.9
Plastic Viscosity μ_p (Pa.s):	0.0255

Inferred Casson Parameters:

Yield Stress τ_c (Pa):	44.0
Plastic Viscosity μ_∞ (Pa.s):	0.0042

After Discharging Pipeline Loop

ω (rad/s)	T/L (N.m/m)
13.40	4.42E-01
18.95	4.58E-01
26.81	4.76E-01
37.91	4.98E-01
53.62	5.23E-01
53.62	5.23E-01
37.91	4.98E-01
26.81	4.72E-01
18.95	4.52E-01
13.40	4.42E-01

Inferred Bingham Parameters:

Yield Stress τ_y (Pa):	158.4
Plastic Viscosity μ_p (Pa.s):	0.0353

Inferred Casson Parameters:

Yield Stress τ_c (Pa):	138.9
Plastic Viscosity μ_∞ (Pa.s):	0.0046

Pipeline and Viscometer Flow Data for Cv = 0.19 Kaolin Clay Slurries

Run Number:	G2000204	Date:	07/00
Temperature (°C):	20	Slurry Density (kg/m^3):	1321
Pipeline Diameter (m):	0.025825	Wall Roughness (μm):	2.51

Mass of $CaCl_2 \cdot 2H_2O$ added / Mass Clay: 0.10%
Mass of TSPP added / Mass Clay: 0.13%

This Slurry Exhibited an Increase in apparent viscosity with time.
Pressure Drop vs. Velocity Data Recorded after Slurry Sheared at 3.2 m/s for and Elapsed Time of: 3hours

Velocity (m/s)	Pressure Gradient (kPa/m)
3.19	11.100
3.00	10.914
2.80	10.733
2.40	10.357
2.00	9.943
1.60	9.490
1.20	8.953
0.80	8.288
0.40	7.345

Inferred Bingham Parameters:
Yield Stress τ_y (Pa): 40.9
Plastic Viscosity μ_p (Pa.s): 0.0205

Inferred Casson Parameters:
Yield Stress τ_c (Pa): 32.5
Plastic Viscosity μ_∞ (Pa.s): 0.0047

Elapsed Time of Shear: 3hours 30min

Velocity (m/s)	Pressure Gradient (kPa/m)
3.19	13.187
3.00	12.978
2.75	12.731
2.25	12.162
1.75	11.479
1.25	10.677
0.60	9.253
0.40	8.622

Inferred Bingham Parameters:
Yield Stress τ_y (Pa): 46.8
Plastic Viscosity μ_p (Pa.s): 0.0266

Inferred Casson Parameters:
Yield Stress τ_c (Pa): 37.2
Plastic Viscosity μ_∞ (Pa.s): 0.0062

Viscometry performed on slurry before loading pipeline loop and after discharge.

Viscometer:	Haake RV 3
Length of Spindle (m):	0.60
Radius of Spindle (m):	0.2001
Radius of Cup (m):	0.2004

Before Loading Pipeline Loop

ω (rad/s)	T/L (N.m/m)
6.70	8.66E-02
9.48	9.12E-02
13.40	9.74E-02
18.95	1.04E-01
26.81	1.14E-01
37.91	1.23E-01
26.81	1.15E-01
18.95	1.07E-01
13.40	9.97E-02
9.48	9.28E-02
6.70	8.97E-02

Inferred Bingham Parameters:

Yield Stress τ_y (Pa):	31.0
Plastic Viscosity μ_p (Pa.s):	0.0207

Inferred Casson Parameters:

Yield Stress τ_c (Pa):	25.2
Plastic Viscosity μ_∞ (Pa.s):	0.0041

After Discharging Pipeline Loop

ω (rad/s)	T/L (N.m/m)
6.70	1.45E-01
9.48	1.54E-01
13.40	1.65E-01
18.95	1.76E-01
26.81	1.90E-01
37.91	2.07E-01
26.81	1.91E-01
18.95	1.77E-01
13.40	1.66E-01
9.48	1.55E-01
6.70	1.46E-01

Inferred Bingham Parameters:

Yield Stress τ_y (Pa):	51.4
Plastic Viscosity μ_p (Pa.s):	0.0355

Inferred Casson Parameters:

Yield Stress τ_c (Pa):	41.5
Plastic Viscosity μ_∞ (Pa.s):	0.0073

Pipeline and Viscometer Flow Data for Cv = 0.19 Kaolin Clay Slurries

Run Number:	G2000203	Date:	08/00
Temperature (°C):	20	Slurry Density (kg/m^3):	1321
Pipeline Diameter (m):	0.025825	Wall Roughness (μm):	2.51

Mass of $CaCl_2 \cdot 2H_2O$ added / Mass Clay: 0.10%
Mass of TSPP added / Mass Clay: 0.27%

This Slurry Exhibited an Increase in apparent viscosity with time.
Pressure Drop vs. Velocity Data Recorded after Slurry Sheared at 3.2 m/s for and Elapsed Time of: 0 min

Velocity (m/s)	Pressure Gradient (kPa/m)
3.19	6.917
3.00	6.161
2.50	4.453
2.00	3.035
1.50	1.850
1.25	1.335
1.00	0.906
0.80	0.611
0.60	0.275
0.40	0.202

Inferred Newtonian Viscosity:
Viscosity μ (Pa.s): 0.0058

Elapsed Time of Shear: 30min

Velocity (m/s)	Pressure Gradient (kPa/m)
3.19	6.914
3.00	6.130
2.50	4.453
2.00	3.021
1.75	2.377
1.25	1.323
0.80	0.634
0.75	0.474
0.70	0.398
0.65	0.326
0.60	0.308
0.55	0.297
0.50	0.274
0.45	0.253
0.40	0.242
0.35	0.227

Inferred Bingham Parameters:
Yield Stress τ_y (Pa): 0.52
Plastic Viscosity μ_p (Pa.s): 0.0070

Inferred Casson Parameters:
Yield Stress τ_c (Pa): 0.21
Plastic Viscosity μ_∞ (Pa.s): 0.0042

Viscometry performed on slurry before loading pipeline loop and after discharge.

Viscometer:	Haake RV 3
Length of Spindle (m):	0.60
Radius of Spindle (m):	0.2001
Radius of Cup (m):	0.2004

Before Loading Pipeline Loop

ω (rad/s)	T/L (N.m/m)
26.81	1.13E-02
18.95	8.53E-03
13.40	6.38E-03
9.48	5.09E-03
6.70	3.80E-03

Inferred Bingham Parameters:

Yield Stress τ_y (Pa):	0.56
Plastic Viscosity μ_p (Pa.s):	0.0065

Inferred Casson Parameters:

Yield Stress τ_c (Pa):	0.13
Plastic Viscosity μ_∞ (Pa.s):	0.0052

After Discharging Pipeline Loop

ω (rad/s)	T/L (N.m/m)
26.81	1.58E-02
18.95	1.23E-02
13.40	9.46E-03
9.48	7.53E-03
6.70	5.88E-03

Inferred Bingham Parameters:

Yield Stress τ_y (Pa):	1.05
Plastic Viscosity μ_p (Pa.s):	0.0087

Inferred Casson Parameters:

Yield Stress τ_c (Pa):	0.30
Plastic Viscosity μ_∞ (Pa.s):	0.0064

APPENDIX B

SLURRY SUPERNATANT CALCIUM ION ANALYSIS

WITH AN ATOMIC ABSORPTION SPECTROPHOTOMETER

Table B.1 Kaolin Clay Slurry Cv = 0.19 Calcium ion supernatant data.

Run #	Mass of TSPP / Mass Clay	Mass of $CaCl_2 \cdot 2H_2O$ / Mass Clay	Ca^{++} ion calculated (ppm)	Ca^{++} ion measured by AASP (ppm)
G2000201/2	0.00%	0.10%	168	198
G2000204	0.13%	0.10%	168	57
G2000203	0.27%	0.10%	168	21

Table B.2 Kaolin Clay Slurry Cv = 17% by volume solids Calcium ion supernatant data.

Run #	Mass of TSPP / Mass Clay	Mass of $CaCl_2 \cdot 2H_2O$ / Mass Clay	Ca^{++} ion calculated (ppm)	Ca^{++} ion measured by AASP (ppm)
G2000206	0.00%	0.10%	142	136
G2000210	0.07%	0.10%	142	Not Taken
G2000209	0.13%	0.10%	142	40
G2000207	0.27%	0.10%	142	4

Table B.3 Kaolin Clay Slurry Cv = 0.14 Calcium ion supernatant data.

Run #	Mass of TSPP / Mass Clay	Mass of $CaCl_2 \cdot 2H_2O$ / Mass Clay	Ca^{++} ion calculated (ppm)	Ca^{++} ion measured by AASP (ppm)
G2000205	0.00%	0.10%	113	124
G2000214	0.13%	0.10%	113	42
G2000217a	0.27%	0.10%	113	15
G2000217b	0.27%	0.16%	182	Not Taken
G2000217c	0.27%	0.22%	252	47
G2000217d	0.27%	0.28%	322	110
G2000215	0.27%	0.10%	113	14

* $CaCl_2 \cdot 2H_2O$ was added stepwise during run G2000217 through recirculation into the stand tank in an attempt to increase the viscosity of this slurry. G2000217b,c,d each underwent 5 gram additions of $CaCl_2 \cdot 2H_2O$ for a total of 15 additional grams added.

Table B.4 Kaolin Clay Slurry Cv = 0.10 Calcium ion supernatant data.

Run #	Mass of TSPP / Mass Clay	Mass of $CaCl_2 \cdot 2H_2O$ / Mass Clay	Ca^{++} ion calculated (ppm)	Ca^{++} ion measured by AASP (ppm)
G2000106a	--	0.10%	76	79
G2000208	--	0.10%	77	82
G2000212	0.27%	0.10%	76	14

Table B.5 Kaolin Clay Slurry Cv = 10% by volume solids total ion mass spectrometer supernatant data (mg of analyte/ L of solution).

Sample Description: Analogous Pipeline Run:

1564: R/O Water
1565: Clay Slurry Cv: 13%, (No Chemicals Added)
1566: Clay Slurry Cv: 13%, Flocculant Mass Ratio: 0.10%, Deflocculant Mass Ratio: N/A
1567: Clay Slurry Cv: 13%, Flocculant Mass Ratio: 0.10%, Deflocculant Mass Ratio: 0.13%
1568: Clay Slurry Cv: 13%, Flocculant Mass Ratio: 0.10%, Deflocculant Mass Ratio: 0.27%
1569*: Clay Slurry Cv: 13%, Flocculant Mass Ratio: 0.10%, Deflocculant Mass Ratio: 0.27%
*Supernatant filtered with 0.22 mm filter paper

Analyte	1564	1565	1566	1567	1568	1569
Aluminum	0.14	0.12	0.11	0.09	4.1	2.9
Barium	0.004	0.01	0.039	0.005	0.021	0.006
Beryllium	<0.001	<0.001	<0.001	<0.001	<0.001	<0.001
Boron	0.007	0.02	0.02	0.021	0.033	0.042
Cadmium	<0.001	<0.001	<0.001	<0.001	<0.001	<0.001
Calcium	1.4	24	130	27	15	12
Chromium	<0.001	0.002	0.002	0.003	0.006	0.006
Cobalt	<0.001	<0.001	<0.001	<0.001	<0.001	<0.001
Copper	<0.001	0.004	0.003	0.005	0.012	0.011
Iron	0.005	0.014	0.01	0.004	0.37	0.29
Lead	<0.002	<0.002	<0.002	<0.002	0.007	0.009
Magnesium	<0.1	0.6	2	0.7	1.3	1.4
Manganese	<0.001	<0.001	<0.001	<0.001	0.053	0.1
Molybdenum	<0.001	<0.001	<0.001	0.002	0.004	0.003
Nickel	<0.001	<0.001	<0.001	<0.001	0.003	0.002
Phosphorus	<0.01	0.02	0.01	5.4	16	17
Potassium	<0.2	0.8	1.7	1.5	1.3	1.4
Silicon, Soluble	0.93	11	11	15	15	14
Silver	<0.001	<0.001	<0.001	<0.001	<0.001	<0.001
Sodium	3.9	5.2	7.4	86	150	160
Strontium	0.007	0.089	0.34	0.065	0.038	0.022
Titanium	<0.001	<0.001	<0.001	<0.001	0.01	0.008
Vanadium	<0.001	0.003	0.001	0.032	0.068	0.07
Zinc	<0.005	<0.005	<0.005	<0.005	0.055	0.046
Zirconium	<0.001	<0.001	<0.001	<0.001	0.007	0.005

APPENDIX C

TURBULENT PIPELINE FLOW LOOP EXPERIMENTAL DATA WITH WILSON & THOMAS TURBULENT FLOW PREDICTIONS

Run#:	G2000106
Cv:	0.10
Mass $CaCl_2 \cdot H_2O$ / Mass Clay:	0.10%
Mass TSPP / Mass Clay:	0.00%

Inferred Parameters from Laminar Flow Experimental Data

Bingham:	τ_y (Pa): 2.6	μ_p (Pa.s): 0.0051
Casson:	τ_c (Pa): 1.9	μ_∞(Pa.s): 0.0016

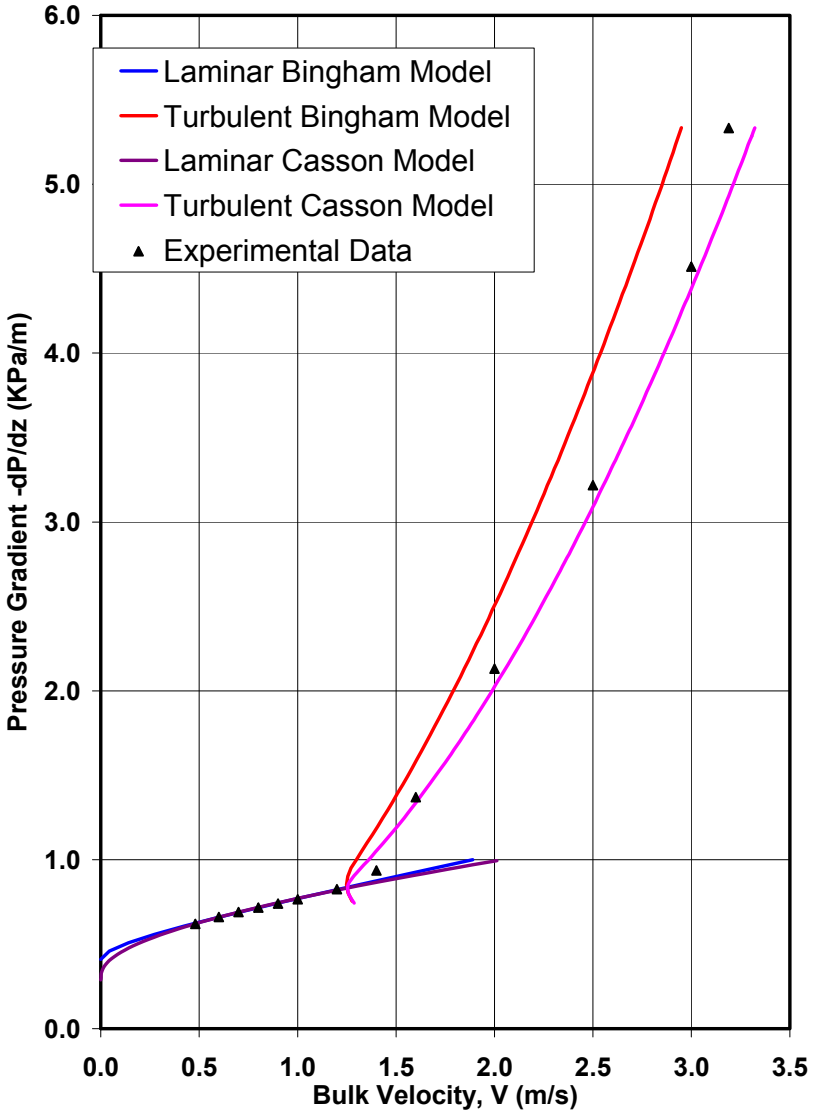

Figure D.1: Comparison of the experimental frictional head loss with Bingham and Casson fluid model predictions for Cv = 0.10 Kaolin Clay Slurry in 25.8 mm vertical pipeline loop. The model parameters were chosen to fit the laminar flow data.

Run#: G2000208
Cv: 0.10
Mass $CaCl_2 \cdot H_2O$ / Mass Clay: 0.10%
Mass TSPP / Mass Clay: 0.00%

Inferred Parameters from Laminar Flow Experimental Data
Bingham: τ_y (Pa): 2.6 μ_p (Pa.s): 0.0051
Casson: τ_c (Pa): 1.9 μ_∞(Pa.s): 0.0015

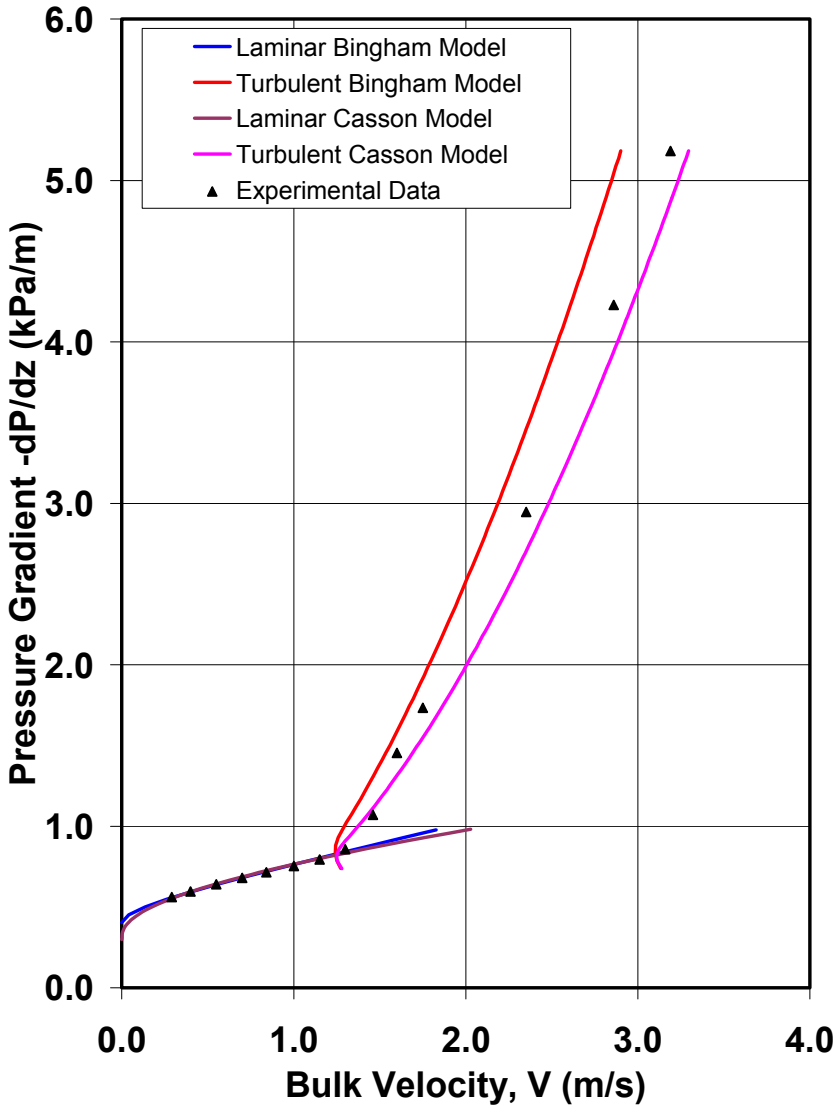

Figure D.2: Comparison of the experimental frictional head loss with Bingham and Casson fluid model predictions for Cv = 0.10 Kaolin Clay Slurry in 25.8 mm vertical pipeline loop. The model parameters were chosen to fit the laminar flow data.

Run#:	G2000205
Cv:	0.14
Mass $CaCl_2 \cdot H_2O$ / Mass Clay:	0.10%
Mass TSPP / Mass Clay:	0.00%

Inferred Parameters from Laminar Flow Experimental Data

Bingham:	τ_y (Pa): 14.3	μ_p (Pa.s): 0.0057
Casson:	τ_c (Pa): 12.0	μ_∞(Pa.s): 0.0010

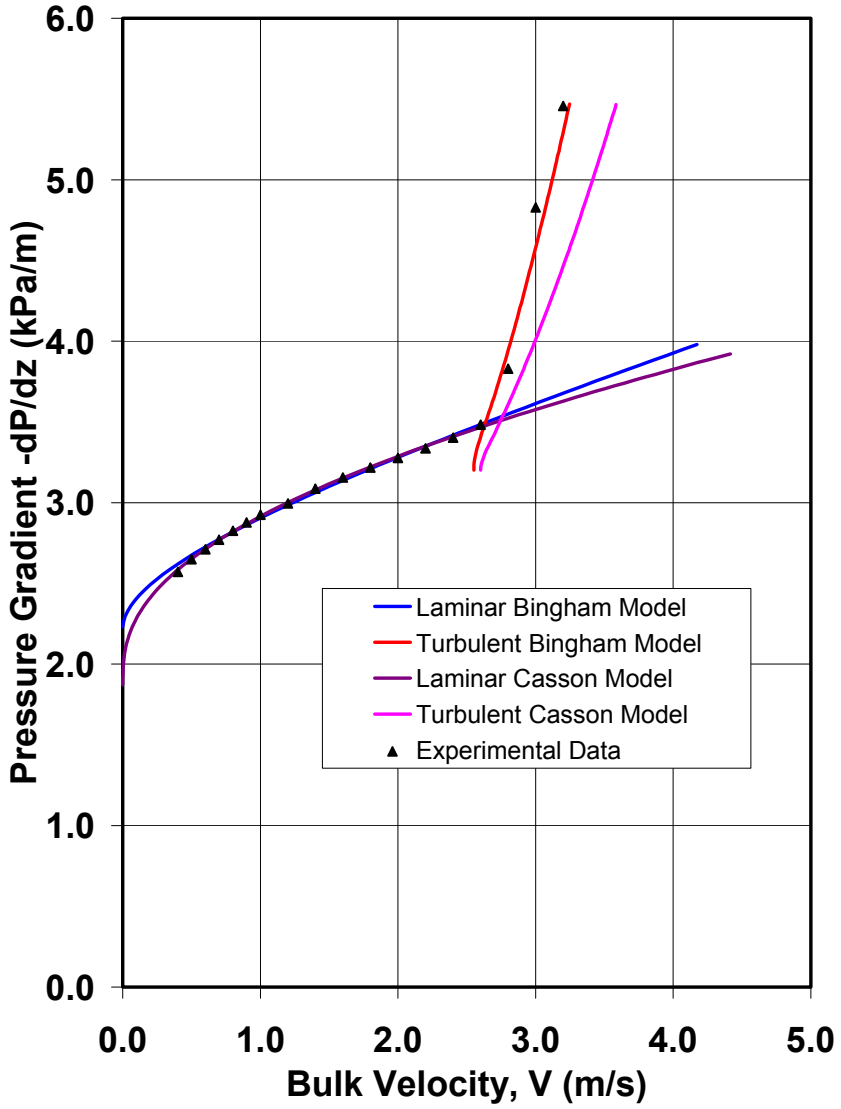

Figure D.3: Comparison of the experimental frictional head loss with Bingham and Casson fluid model predictions for Cv = 0.14 Kaolin Clay Slurry in 25.8 mm vertical pipeline loop. The model parameters were chosen to fit the laminar flow data.

Run#:	G2000105
Cv:	0.14
Mass $CaCl_2 \cdot H_2O$ / Mass Clay:	0.10%
Mass TSPP / Mass Clay:	0.10%

Inferred Parameters from Laminar Flow Experimental Data

Bingham: τ_y (Pa): 5.9 μ_p (Pa.s): 0.0078

Casson: τ_c (Pa):4.4 μ_∞(Pa.s): 0.0021

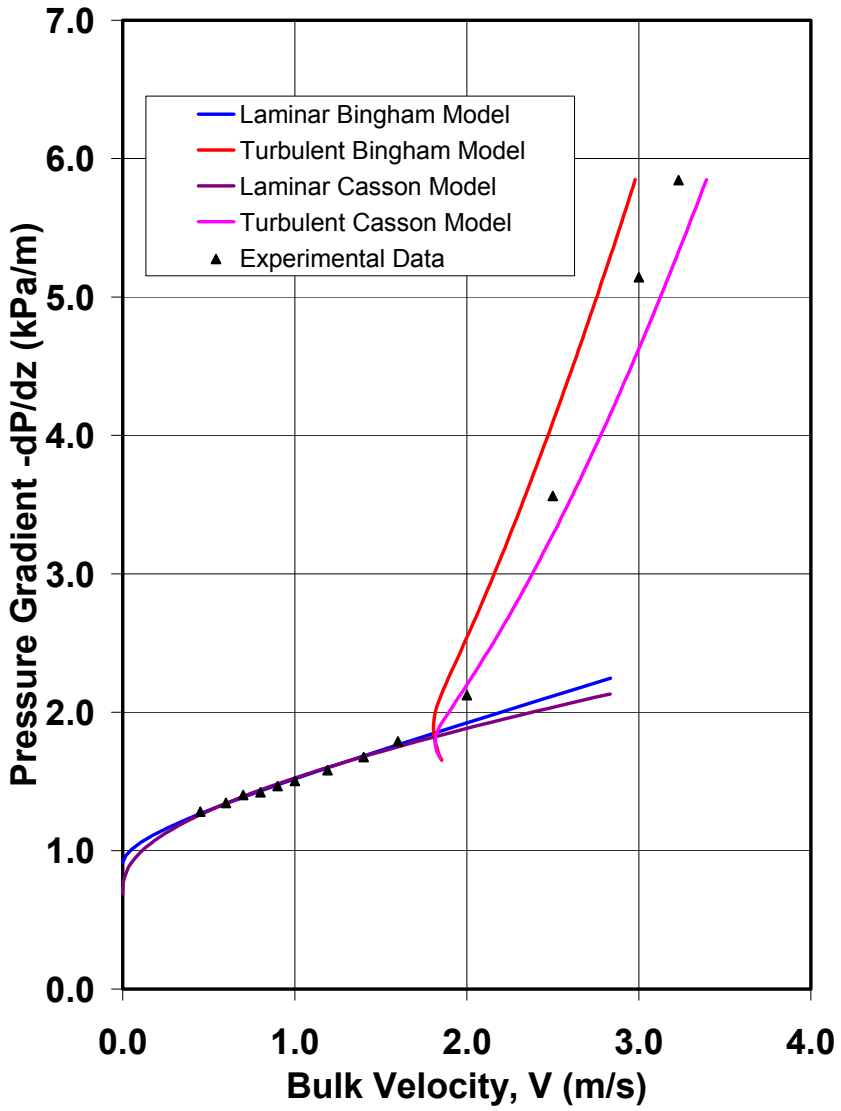

Figure D.4: Comparison of the experimental frictional head loss with Bingham and Casson fluid model predictions for Cv = 0.14 Kaolin Clay Slurry in 25.8 mm vertical pipeline loop. The model parameters were chosen to fit the laminar flow data.

Run#: G2000217
Cv: 0.14
Mass $CaCl_2 \cdot H_2O$ / Mass Clay: 0.10%
Mass TSPP / Mass Clay: 0.13%
10 grams of $CaCl_2 \cdot H_2O$ has been re-circulated into the system to increase the inter particle attraction.

Inferred Parameters from Laminar Flow Experimental Data
Bingham: τ_y (Pa): 7.9 μ_p (Pa.s): 0.0092
Casson: τ_c (Pa):6.1 μ_∞(Pa.s): 0.0023

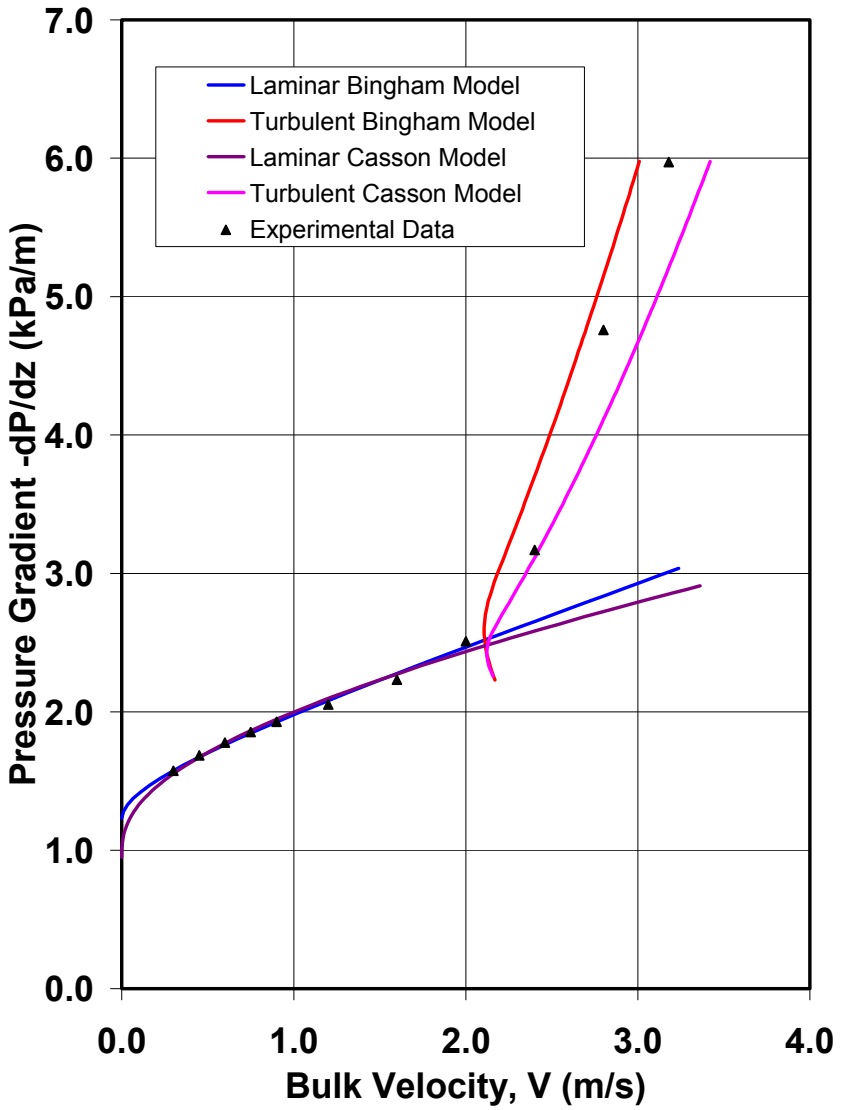

Figure D.5: Comparison of the experimental frictional head loss with Bingham and Casson fluid model predictions for Cv = 0.14 Kaolin Clay Slurry in 25.8 mm vertical pipeline loop. The model parameters were chosen to fit the laminar flow data.

Run#:	G2000214
Cv:	0.14
Mass $CaCl_2 \cdot H_2O$ / Mass Clay:	0.10%
Mass TSPP / Mass Clay:	0.13%

Inferred Parameters from Laminar Flow Experimental Data

Bingham:	τ_y (Pa): 6.7	μ_p (Pa.s): 0.0072
Casson:	τ_c (Pa): 5.2	μ_∞(Pa.s): 0.0018

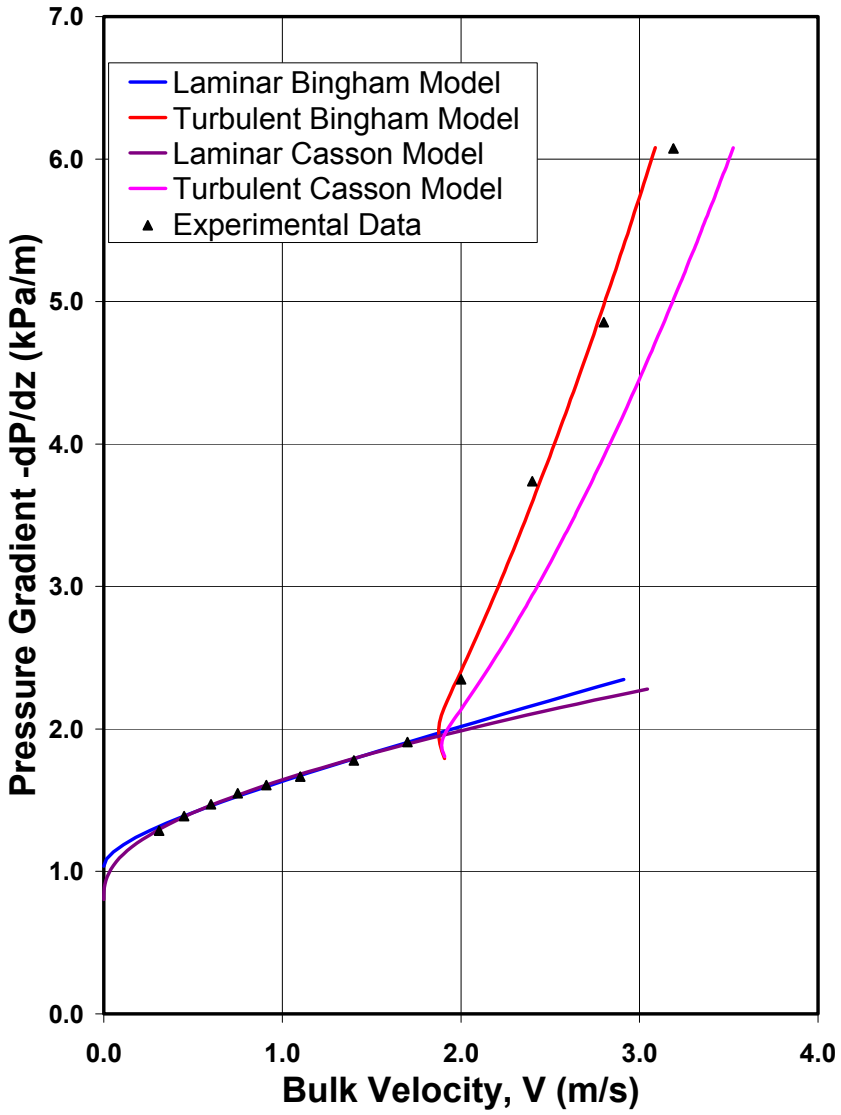

Figure D.6: Comparison of the experimental frictional head loss with Bingham and Casson fluid model predictions for Cv = 0.14 Kaolin Clay Slurry in 25.8 mm vertical pipeline loop. The model parameters were chosen to fit the laminar flow data.

Run#:	G2000209
Cv:	0.17
Mass $CaCl_2 \cdot H_2O$ / Mass Clay:	0.10%
Mass TSPP / Mass Clay:	0.13%

Inferred Parameters from Laminar Flow Experimental Data

Bingham: τ_y (Pa): 12.0 μ_p (Pa.s): 0.0090

Casson: τ_c (Pa): 9.7 μ_∞(Pa.s): 0.0020

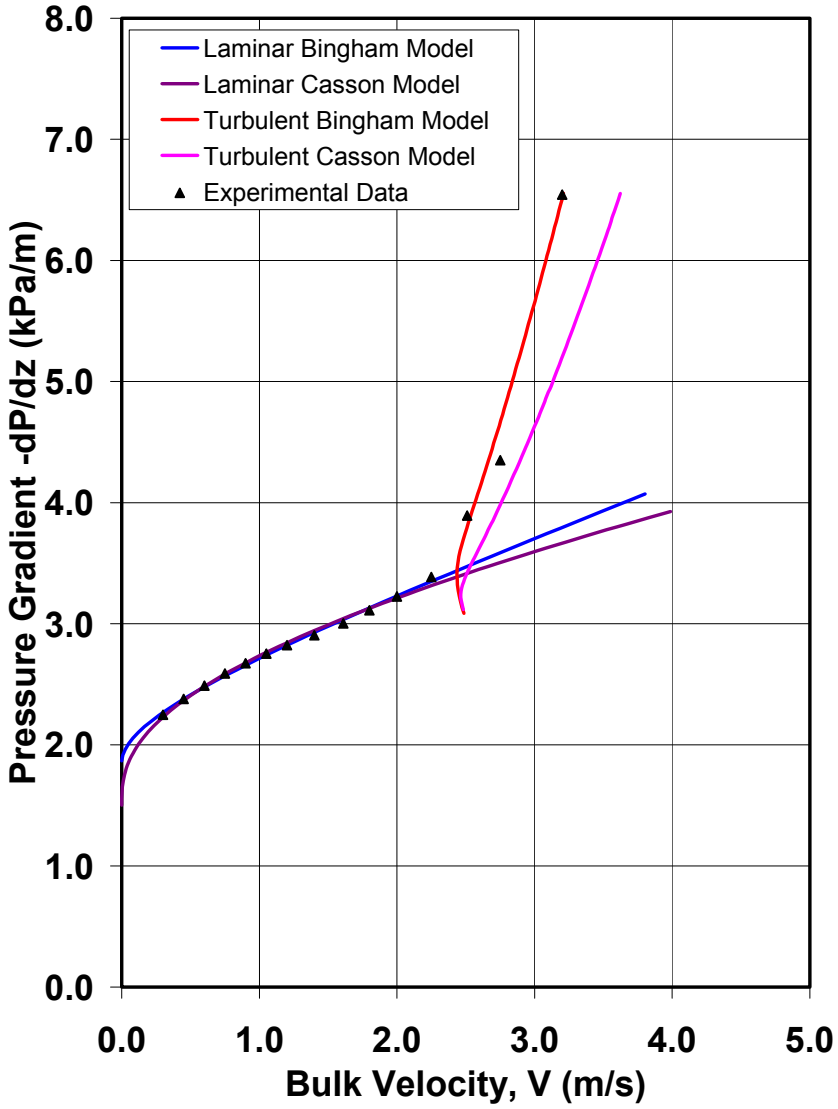

Figure D.7: Comparison of the experimental frictional head loss with Bingham and Casson fluid model predictions for Cv = 0.14 Kaolin Clay Slurry in 25.8 mm vertical pipeline loop. The model parameters were chosen to fit the laminar flow data.

APPENDIX D

Particle Diameter Derivation From Centrifugal Andreasen Pipette Methods

Ryan Spelay 2000

In order to determine the settling velocity of a particle one must perform a force balance on a single particle settling in infinite dilution. In this derivation it is assumed that the particle reaches terminal settling velocity immediately. The gravitational term can also be neglected since it was previously shown that the centrifugal force is so much greater than the gravitational force. Therefore, accounting for the centrifugal, buoyancy and drag forces on the settling particle it is known that at the terminal velocity:

$$\sum F_{particle} = 0$$

$$F_{drag} = F_{centrifugal}$$

$$\frac{C_D \rho_f V_s^2 A_p}{2} = (\rho_s - \rho_f) V_P \omega^2 r$$

Where: C_D = Coefficient of drag {Dimensionless}
A_p = Projected area of a settling particle {m^2}
V_P = Volume of a particle {m^3}

In order for Stokes Law to be applicable for a centrifuging situation many simplifying assumptions have to be made. One such assumption is that the particles are perfectly rigid, smooth and spherical. Another assumption is that the flow is in the Stokes region. This means that the Reynolds Number must be less than 0.1. The Reynolds Number for a settling particle is a dimensionless quantity defined as:

$$N_{\mathrm{Re}} = \frac{\rho_f D_P V_s}{\mu_f}$$

Where: N_{Re} = the Reynolds Number {dimensionless}
ρ_f = the density of the fluid {kg/m^3}
D_p = particle diameter {m}
V_s = particle settling velocity {m/s}
μ_f = fluid viscosity {Pa·s}

In the Stokes region of settling for a spherical rigid particle the coefficient of drag can be related to the Reynolds number by the equation:

$$C_D = \frac{24}{N_{\mathrm{Re}}} = \frac{24\mu_f}{\rho_f D_P V_s}$$

Substitution of this equation into the force balance along with the formulas for the projected area and volume of a sphere yields:

$$\frac{12\mu_f V_s}{D_P}\left(\frac{\pi}{4} D_P^2\right) = (\rho_s - \rho_f)\left(\frac{\pi}{6} D_P^3\right)\omega^2 r$$

Upon further simplification, Stokes Law for gravitational sedimentation can be rewritten for a particle travelling in a circular path as:

$$v_{settle} = \frac{\omega^2 r(\rho_s - \rho_f)D_P^2}{18\mu}$$

Where: v_{settle} = the particles settling velocity {m/s}
ω = the angular velocity of the centrifuge {rad/s}
r = the radial position in the centrifuge {m}
ρ_s = the density of the solid particles {kg/m^3}
ρ_f = the density of the fluid {kg/m^3}
D_p = the spherical diameter of the settling particle {m}
μ = the viscosity of the fluid {Pa·s}

One can see by Stokes Law that the settling velocity is not only dependent on many of the same factors as in gravitational sedimentation but it is also dependent on radial position. This radial dependence makes a straightforward solution impossible and thus a more involved approach must be taken. This involved approach treats each individual particle as rigid body. It is also assumed that after dispersion and mixing, each of the particles has an initial velocity of zero but attains its terminal velocity instantly. It is also assumed that particle flow is only in the radial direction of the centrifuge (azimuthal/axial direction of the pipette) and that the wall and interparticle effects are negligible.

From the basic kinematic equations it is known that for a rigid body travelling at a constant velocity:

$$v = \frac{dr}{dt}$$

Where: v = terminal velocity of particle {m/s}
r = radial displacement of the particle {m}
t = time of displacement {s}

It should be noted that in the Stokes equation the terminal velocity is a function of radial distance and it is not constant but rather it changes instantaneously with increasing radial displacement. However, if the particle's motion is only in the radial direction the differential term of the above equation can be equated to the Stokes terminal settling velocity by:

$$v_{settle} = \frac{dr}{dt} = \frac{w^2 r(\rho_s - \rho_f) D_P^2}{18\mu}$$

Manipulating the above equation into a solvable form and applying the boundary conditions yields:

$$\int_S^R \frac{dr}{r} = \int_0^t \frac{w^2(\rho_s - \rho_f) D_P^2}{18\mu} dt$$

Where: R = the final radial displacement of a particle with D_P {m}
S = the initial radial displacement of a particle with D_P {m}

Solving the above integral and noting that all of the terms on the right hand side are independent of time yields:

$$\ln\left(\frac{R}{S}\right) = \frac{w^2(\rho_s - \rho_f) D_P^2}{18\mu} t$$

Solving for D_P, the particles equivalent spherical diameter, yields:

$$D_P = \left[\frac{18\mu}{w^2 t(\rho_s - \rho_f)} \ln\left(\frac{R}{S}\right)\right]^{1/2}$$

When working with a centrifuge the desired angular velocity is not achieved instantaneously but rather it takes a finite period of time to be reached. This is also true for the stopping of the centrifuge in that it also takes a finite period of time for the centrifuge to come to rest. These acceleration and de-acceleration times are not accounted for in the original derivation and thus if they become significant compared to the actual run time, a sizeable error will be incorporated into the particle sizes calculated.

To overcome the possibility of introducing this error, a derivation incorporating ramp times has been created. In this derivation linear ramping functions are assumed for the acceleration and de-acceleration periods of the centrifuge. A schematic graph of angular velocity versus time is shown below.

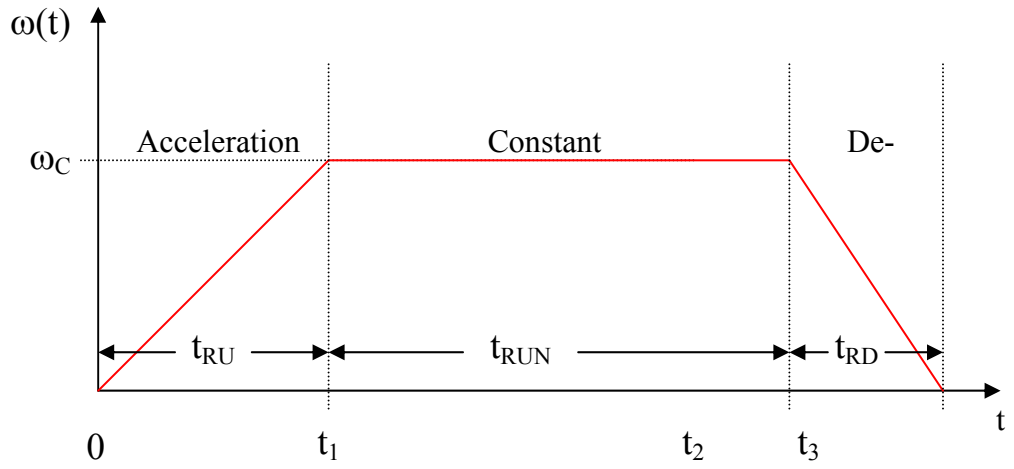

Figure D.1: Idealized plot of centrifuge angular velocities in the ramping regions

From the plot above it can be seen that:

$$t_{RU} = t_1$$

$$t_{RUN} = t_2 - t_1$$

$$t_{RD} = t_3 - t_2$$

The angular velocity can also be expressed as a function of t for the 3 time regions:

$$\omega(t) = \frac{\omega_C}{t_1} t \qquad ; 0 < t < t_1$$

$$\omega(t) = \omega_C \qquad ; t_1 < t < t_2$$

$$\omega(t) = \frac{\omega_C}{t_3 - t_2}(t3 - t) \qquad ; t_2 < t < t_3$$

Therefore if one follows the same derivation that was performed when the ramping times were ignored the following equations are obtained for each of the three time regions.

For ($0 < t < t_1$):

$$\int_S^{R_1} \frac{dr}{r} = \int_0^{t_1} \frac{w^2(\rho_s - \rho_f)D_P^2}{18\mu} dt$$

$$\int_S^{R_1} \frac{dr}{r} = \int_0^{t_1} \frac{w_C{}^2(\rho_s - \rho_f)D_P^2}{18\mu t_1^2} t^2 dt$$

$$\ln\left(\frac{R_1}{S}\right) = \frac{w_C{}^2(\rho_s - \rho_f)D_P^2}{54\mu} t_1$$

$$\ln\left(\frac{R_1}{S}\right) = \frac{w_C{}^2(\rho_s - \rho_f)D_P^2}{54\mu} t_{RU}$$

For ($t_1 < t < t_2$):

$$\int_{R_1}^{R_2} \frac{dr}{r} = \int_{t_1}^{t_2} \frac{w^2(\rho_s - \rho_f)D_P^2}{18\mu} dt$$

$$\int_{R_1}^{R_2} \frac{dr}{r} = \int_{t_1}^{t_2} \frac{w_C{}^2(\rho_s - \rho_f)D_P^2}{18\mu} dt$$

$$\ln\left(\frac{R_2}{R_1}\right) = \frac{w_C{}^2(\rho_s - \rho_f)D_P^2}{18\mu}(t_2 - t_1)$$

$$\ln\left(\frac{R_2}{R_1}\right) = \frac{w_C{}^2(\rho_s - \rho_f)D_P^2}{18\mu} t_{RUN}$$

For ($t_2 < t < t_3$):

$$\int_{R_2}^{R} \frac{dr}{r} = \int_{t_2}^{t_3} \frac{w^2(\rho_s - \rho_f)D_P^2}{18\mu} dt$$

$$\int_{R_2}^{R} \frac{dr}{r} = \int_{t_2}^{t_3} \frac{w_C{}^2(\rho_s - \rho_f)D_P^2}{18\mu(t_3 - t_2)^2}(t_3 - t)^2 dt$$

$$\ln\left(\frac{R}{R_2}\right) = \frac{w_C{}^2(\rho_s - \rho_f)D_P^2}{54\mu}(t_3 - t_2)$$

$$\ln\left(\frac{R}{R_2}\right) = \frac{w_C{}^2(\rho_s - \rho_f)D_P^2}{54\mu} t_{RD}$$

Summing the resulting equations for each of the three time periods yields:

$$\ln\left(\frac{R}{S}\right) = \frac{w_C{}^2(\rho_s - \rho_f)D_P^2}{\mu}\left(\frac{t_{RU}}{54} + \frac{t_{RUN}}{18} + \frac{t_{RD}}{54}\right)$$

$$D_P = \left[\frac{\mu \ln\left(\frac{R}{S}\right)}{w_C{}^2(\rho_s - \rho_f)\left(\frac{t_{RU}}{54} + \frac{t_{RUN}}{18} + \frac{t_{RD}}{54}\right)}\right]^{1/2}$$

Now particle diameters can be calculated based on not only the constant run time of the centrifuge but also on the ramping times. However, it should be noted that in this derivation it is assumed that the tubes are always oriented horizontally and in the radial direction. In some centrifuges when the acceleration and de-acceleration phases are occurring, the tube may be oriented at some angle to the horizontal. This may introduce some error (be it small), to the final particle diameter calculated. However, the error resulting from the tubes not being horizontal is smaller than the error resulting from ignoring the ramping times completely.

APPENDIX E

Instrument Calibrations

Pressure Transducer (Upstream Pressure Gradient Test Section)

Validyne differential pressure transducer calibrated against pressure measured by a manometer containing merium fluid with a density of 2.950 kg/m^3

High Side (cm)	Low Side (cm)	Reading (volts)	Pressure (kPa)
189.9	16.1	2.503	50.25
179.9	25.9	2.225	44.52
170.2	35.9	1.942	38.83
159.7	46.6	1.636	32.70
149.6	56.7	1.356	26.86
139.3	67.0	1.049	20.90
129.1	77.2	0.754	15.00
119.3	86.9	0.473	9.37
103.0	103.0	0.006	0.00

Slope (kPa/volt)	20.094
Zero (volts)	0.0085
Correlation coefficient	0.99999

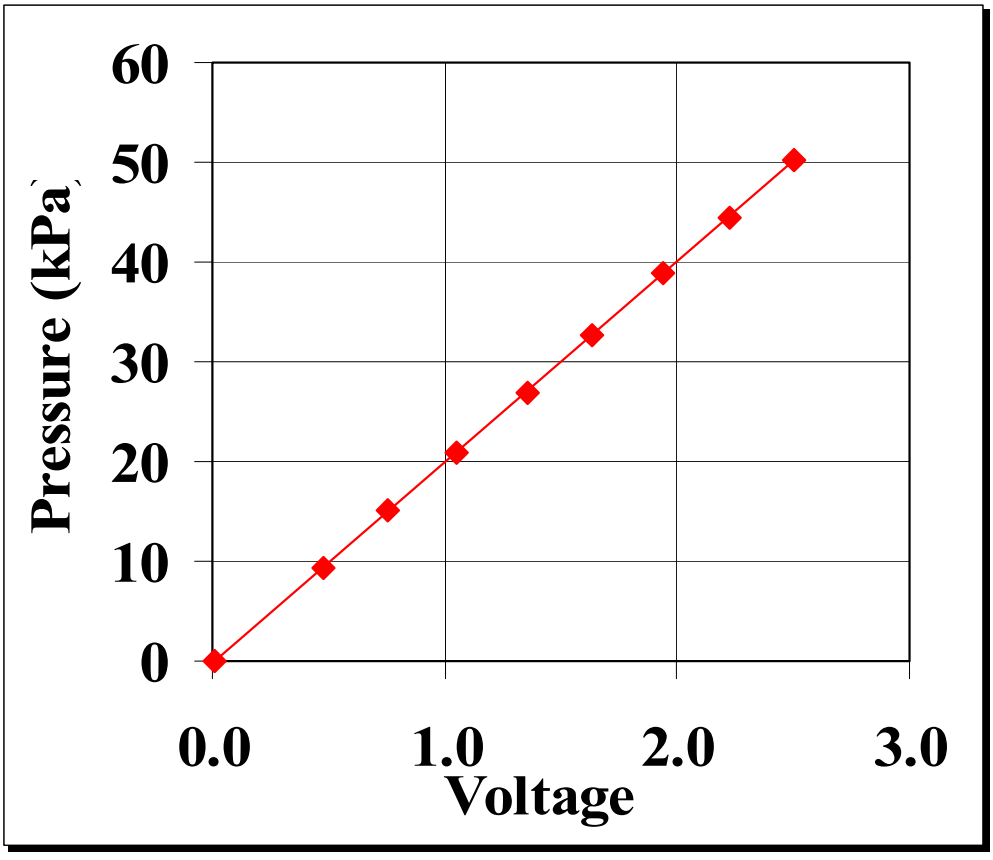

Pressure Transducer (Downstream Pressure Gradient Test Section)

Validyne differential pressure transducer calibrated against pressure measured by a manometer containing merium fluid with a density of 2.950 kg/m^3

High Side (cm)	Low Side (cm)	Reading (volts)	Pressure (kPa)
189.5	16.4	2.495	50.04
175.4	30.7	2.086	41.83
160.8	45.3	1.666	33.39
144.8	61.2	1.208	24.17
130.0	76.0	0.782	15.61
119.7	86.2	0.487	9.68
111.1	94.8	0.240	4.71
102.9	102.9	0.006	0.00

Slope (kPa/volt)	20.109
Zero (volts)	0.0058
Correlation coefficient	1.0000

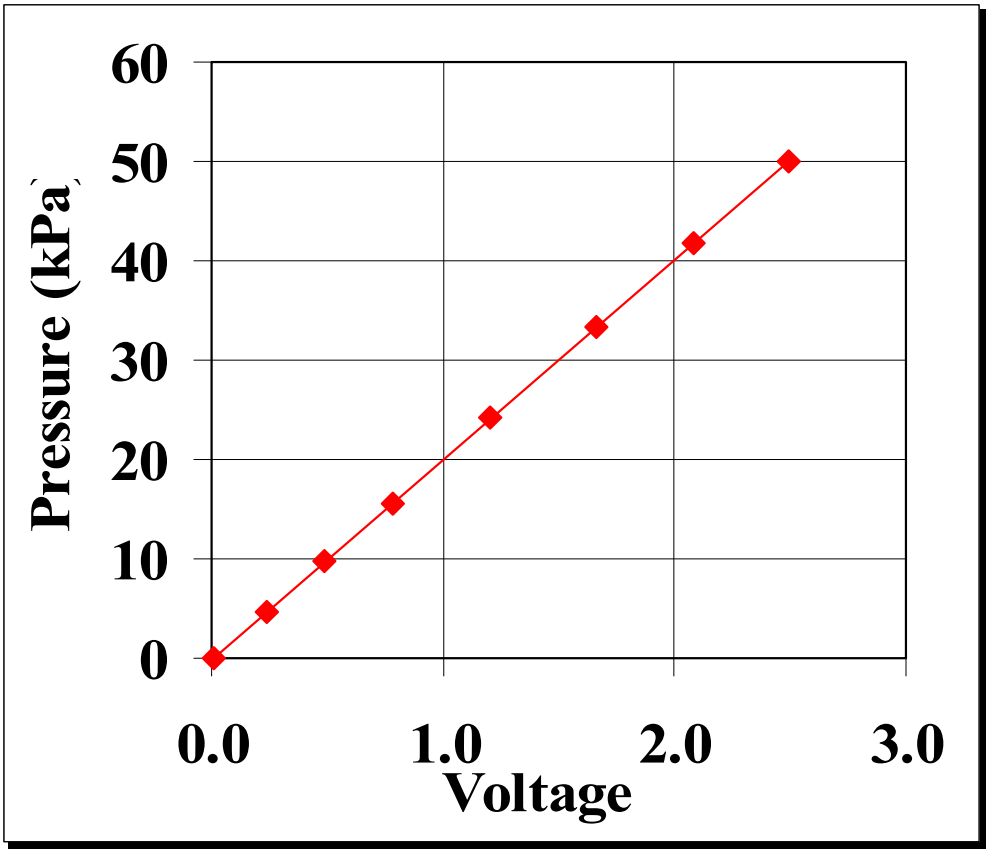

Bucket and Stopwatch Flow Calibration for 3L6 progressive cavity pump

Elapsed Time (s)	Weight (kg)	Density (kg/m3)	Reading (volts)	Flow Rate (L/s)
0.00	0.00	997.3	0.989	0.000
41.34	19.50	998.5	1.621	0.472
23.40	18.12	998.4	2.007	0.776
16.06	18.78	998.4	2.542	1.171
11.97	18.14	998.3	2.975	1.518

Slope (L/s/volt)	0.763
Zero (volts)	0.995
Correlation coefficient	0.99992

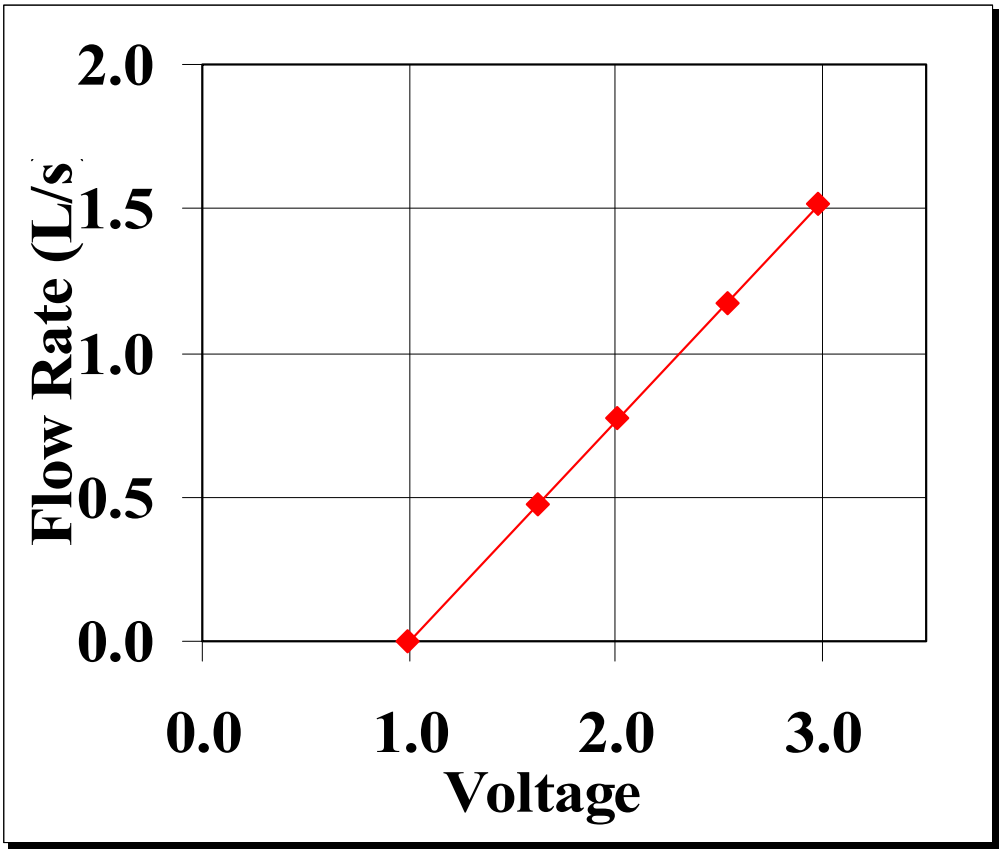

Viscometer Calibration (Measuring Head MK500)

Viscosity Standard	Cannon S200 oil
Temperature (°C)	25
Standard Viscosity (Pa.s)	0.4078
Spindle	MV1
R1 (m)	0.02004
R2 (m)	0.02100
L (m)	0.0600
Full Scale T. (N.m)	0.045
Slope (T/L vs. w)	0.0231
Viscosity	0.4089
Percent Error	0.26%

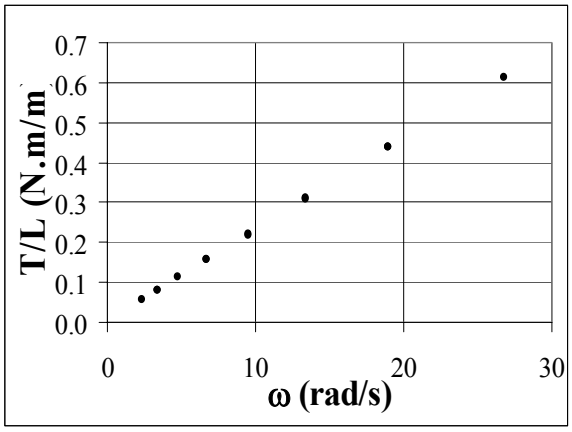

Experimental Data

RPM	TORQUE (% OF FS)	ω (rad/s)	T/L (N.m/m)
32.0	10.6	3.35	0.080
64.0	21.0	6.70	0.158
90.5	29.6	9.48	0.222
128.0	41.6	13.40	0.312
181.0	58.5	18.95	0.439
256.0	81.6	26.81	0.612
181.0	58.7	18.95	0.440
128.0	41.2	13.40	0.309
90.5	28.9	9.48	0.217
64.0	21.1	6.70	0.158
45.2	15.3	4.73	0.115
32.0	10.8	3.35	0.081
22.6	7.8	2.37	0.059

Viscometer Calibration (Measuring Head MK50)

Viscosity Standard	Cannon S200 oil
Temperature (°C)	25
Standard Viscosity (Pa.s)	0.4078
Spindle	MV1
R1 (m)	0.02004
R2 (m)	0.02100
L (m)	0.0600
Full Scale T. (N.m)	0.0043
Slope (T/L vs. w)	0.0228
Viscosity	0.4035
Percent Error	1.05%

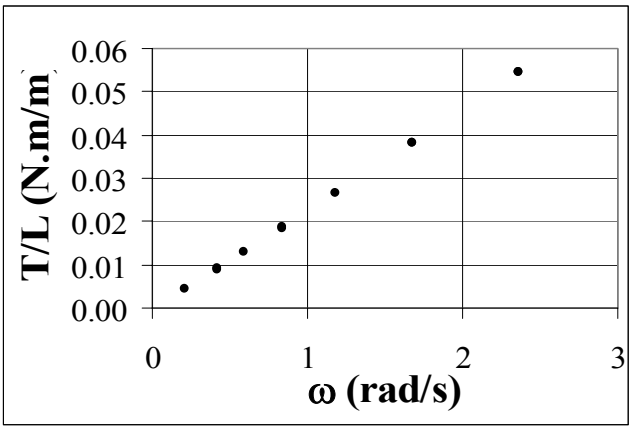

Experimental Data

RPM	TORQUE (% OF FS)	ω (rad/s)	T/L (N.m/m)
4.0	12.7	0.42	0.0092
8.0	25.8	0.84	0.0187
16.0	52.7	1.68	0.0382
22.6	75.3	2.37	0.0545
22.6	75.2	2.37	0.0544
16.0	52.7	1.68	0.0382
11.3	36.6	1.18	0.0265
8.0	25.4	0.84	0.0184
5.7	17.8	0.59	0.0129
4.0	12.3	0.42	0.0089
2.0	6.0	0.21	0.0043